12

AD A124276

AFGL-TR-82-0328

DEVELOPMENT OF AN AIRBORNE VISIBILITY METER

D. F. Hansen

HSS Inc
2 Alfred Circle
Bedford, Mass. 01730

Final Report
20 February 1981 - 30 Sept 1982

15 November 1982

Approved for public release; distribution unlimited

DTIC FILE COPY

AIR FORCE GEOPHYSICS LABORATORY
AIR FORCE SYSTEMS COMMAND
UNITED STATES AIR FORCE
HANSCOM AFB, MASSACHUSETTS

DTIC
ELECTE
FEB 0 9 1983
S D
E

Qualified requestors may obtain additional copies from the Defense Technical Information Center. All others should apply to the National Technical Information Service.

UNCLASSIFIED
SECURITY CLASSIFICATION OF THIS PAGE (When Data Entered)

REPORT DOCUMENTATION PAGE		READ INSTRUCTIONS BEFORE COMPLETING FORM
1. REPORT NUMBER AFGL-TR-82-0328	2. GOVT ACCESSION NO. AD-A124 226	3. RECIPIENT'S CATALOG NUMBER
4. TITLE (and Subtitle) DEVELOPMENT OF AN AIRBORNE VISIBILITY METER		5. TYPE OF REPORT & PERIOD COVERED Final, Feb 20, 1981-30 Sept 1982 6. PERFORMING ORG. REPORT NUMBER HSS-B-092
7. AUTHOR(s) D. F. Hansen		8. CONTRACT OR GRANT NUMBER(s) F19628-81-C-0005
9. PERFORMING ORGANIZATION NAME AND ADDRESS HSS Inc 2 Alfred Circle Bedford, Mass. 01730		10. PROGRAM ELEMENT, PROJECT, TASK AREA & WORK UNIT NUMBERS 63707F 268801AA
11. CONTROLLING OFFICE NAME AND ADDRESS Air Force Geophysics Laboratory Hanscom AFB Ma 01731 Monitor: Frederick Brousaides/ LYS		12. REPORT DATE 15 November 1982 13. NUMBER OF PAGES 168
14. MONITORING AGENCY NAME & ADDRESS(if different from Controlling Office)		15. SECURITY CLASS. (of this report) UNCLASSIFIED 15a. DECLASSIFICATION DOWNGRADING SCHEDULE

16. DISTRIBUTION STATEMENT (of this Report)

Approved for public release; distribution unlimited

17. DISTRIBUTION STATEMENT (of the abstract entered in Block 20, if different from Report)

18. SUPPLEMENTARY NOTES

19. KEY WORDS (Continue on reverse side if necessary and identify by block number)

Nephelometer
Scatter-meter
Visibility meter
Cloud detector

20. ABSTRACT (Continue on reverse side if necessary and identify by block number)

A light-weight, compact nephelometer for the detection of cloud presence and the estimation of visual range was designed, fabricated, and tested. The device is intended for airborne deployment for use in a tactical weather observation system and in support of precision guided munition missions. The sensor is a fixed angle nephelometer utilizing an infrared emitting diode at 0.88 micrometers and a silicon photovoltaic detector. The sensor was calibrated in an environmental fog chamber over a wide range of fog and haze

DD FORM 1 JAN 73 1473 EDITION OF 1 NOV 65 IS OBSOLETE

UNCLASSIFIED
SECURITY CLASSIFICATION OF THIS PAGE (When Data Entered)

conditions. The sensor was found to have a very wide dynamic range of sensitivity (over three decades of attenuation coefficient) and, within operational requirements for accuracy, its performance can be described by a universal algorithm. The nephelometer was field tested at AFGL's Weather Test Facility at Otis AFB; high correlations were observed with transmissometers and other forward-scatter meters.

Accession For
NTIS GRA&I X
DTIC TAB
Unannounced
Justification
By
Distribution/
Availability Codes
Dist Avail and/or Special
A

DTIC COPY INSPECTED 2

PREFACE

This report documents the development, calibration and testing of a new airborne meteorological sensor, a visibility meter based on the principles of nephelometry. The instrument, called the AVM (Airborne Visibility Meter), is intended for use on remote piloted vehicles (RPV's); for that reason its design goals are very demanding. The AVM must be small, compact, lightweight, have low power consumption, and have a measuring capability equal to that of any ground-based visibility meter.

The successful completion of this instrument development program can be attributable to the people who made important contributions to the program: V. Logiudice, A.H. Pierson, W. Shubert, M.P. Shuler, A.H. Tuttle and J.M. Young.

Development of the AVM is one part of a larger Air Force program named PRESSURS, an acronym for Pre-Strike Surveillance and Reconnaissance System. Mr. Fred Brousaides of AFGL was the technical monitor for the HSS Inc contract. Mr. Brousaides provided the necessary liaison between HSS Inc and other elements of the PRESSURS program which resulted in the successful development of an instrument specific to the needs of that program.

The PRESSURS program is still in its formative phase. Deployment vehicles and operational tactics are still under investigation. Decisions on these matters will in turn impact some of the AVM physical features and measurement parameters. Meanwhile, Mr. Brousaides and the author have attempted to determine the optimum measurement parameters for the AVM based on one possible deployment vehicle and hypothetical operational tactics. This optimization process has been in the form of lengthly discussions in which a healthy interchange of ideas and results of analytical investigations some of which are contained in this report. In addition to these contributions Mr.

Brousaides should be acknowledged for many other contributions to the AVM development program in particular his participation in and direction of the two week long calibration and test program at CALSPAN.

CONTENTS

CONTENTS (Cont)

CONTENTS (Cont)

LIST OF ILLUSTRATIONS

LIST OF ILLUSTRATIONS (Cont)

LIST OF TABLES

LIST OF TABLES (Cont)

1. BACKGROUND

Precision guided munitions are now well established in the Air Force weapon inventory and more sophisticated precision guided munitions are constantly being developed. These systems have the potential for providing highly precise bombing on the one hand; on the other hand the ability to deploy them and their performance is very sensitive to the environment. Air Force support organizations which provide environmental information to the users of these systems must therefore develop support concepts and programs to minimize the effects of adverse weather on the employment of these munitions systems. The development of instruments for monitoring the environment to obtain the basic input data for those support programs is an essential part of that support. This report concerns the development of one such instrument --- an Airborne Visibility Meter (AVM).

The most common target acquisition sensor is still the human eye. Any restrictions on visibility in an operational area is important information to a forecaster who must provide forecasts on target acquisition and lock-on ranges. Visibility restrictions also provide broader implications to the forecaster. Restrictions which occur in the visible region infer the possibility of restrictions, or if not restrictions then degradation of performance, of IR guided munitions systems.

The AVM developed by HSS under this contract is intended for use on pre-strike surveillance missions to be flown by Remote Piloted Vehicles (RPVs).

The Air Force program under which the AVM was developed is named PRESSURS, an acronym for Pre-Strike Surveillance Reconnaisance Systems.

Figure 1.1 describes the relative influence of adverse weather elements on visible and infrared precision guided munitions systems. (The chart in Figure 1.1 was duplicated without alteration from Reference 1).

WAVELENGTH CATEGORIES	MICROWAVE	MILLIMETER	INFRARED				VISIBLE
			FAR FAR	FAR	MIDDLE	NEAR	
WAVELENGTH/ FREQUENCIES	10cm - 1cm 3GHz - 30GHz	1cm-0.1mm	0.1mm-15μm	15μm-6μm	6μm-2μm	2μm-0.74μm	0.74μm-0.4μm
RESOLUTION	USUALLY INCREASES WITH DECREASING WAVELENGTH						
WEATHER SENSITIVITY	GENERALLY INCREASES WITH DECREASING WAVELENGTH						
CLOUDS & FOGS	SIGNIFICANT			EXTREMELY SIGNIFICANT			
DRY AEROSOLS	INSIGNIFICANT			SIGNIFICANT		EXTREMELY SIGNIFICANT	
PRECIPITATION	SIGNIFICANT		EXTREMELY SIGNIFICANT				
ABSORPTION	SIGNIFICANT		CAN BE EXTREMELY SIGNIFICANT			EXTREMELY SIGNIFICANT	
SCATTERING	SIGNIFICANT			EXTREMELY SIGNIFICANT			

Figure 1.1. Significance of adverse weather elements and sensor resolution as a function of sensor wavelength categories (From Ref. 1).

The chart in Figure 1.1 indicates that, without exception, adverse weather elements are most significant in the visible spectral region and that the general sensitivity to weather is also greatest in the visible. The importance of the weather elements which effect visibility (i.e. 1. clouds and fog, 2. dry aerosols, 3. precipitation, 4. absorption (molecular and/or aerosol), and 5. scattering) depends, in varying degrees upon the mission and the forecasts which are intended in support of that mission.

In the case of the AVM there are two primary support functions: (1) to enable a forecaster to determine if the Slant Visual Range (SVR) is less than or greater than 10 km --- if less than 10 km then to enable the forecaster to make a determination of the SVR, and (2) to continuously monitor whether the RPV is in or out of clouds --- from this information percent cloud cover, cloud base height and cloud thickness can be established.

In an examination of the five weather elements which effect visibility, in light of the two primary support functions of the AVM, it will later be shown that dry aerosols and aerosol absorption are relatively unimportant in most environments. (Molecular absorption bands due to water vapor are present in weak amounts in the visible spectral region, but are unimportant when a wide-band sensor such as the eye is employed). Thus, in the absence of clouds, fog or precipitation, the scattering of light due to haze aerosols is the greatest single influence on visibility in all environments.

The Airborne Visibility Meter is a fixed-angle nephelometer; i.e., it measures the amount of light scattered at one angle from a beam of light that is directed through a sample volume and, from the amount of scattered light, determines the scattering coefficient due to the airborne particles present in the sample volume. Because absorption effects can be neglected, the scattering and extinction coefficients of air become identical in the visible spectral region.

The capability of measuring the aerosol scattering coefficients at slant visual ranges up to 10 km makes the AVM a very sensitive visibility meter. When the AVM is enveloped in a cloud or fog, the presence of fog particles in the sample volume induces very strong signals in the electronics. Thus, the dual capability requires the AVM to have an extremely large response dynamic range.

There is no requirement that the AVM be capable of detecting or measuring precipitation. The instrument design is, therefore, optimized for its two primary functions. However it is obvious that precipitation will induce some response from the AVM; at question is any possible correlation between that response and the type and amount of precipitation. It remained for the field tests of the instrument to provide answers to questions regarding the behavior of the AVM to one or more forms of precipitation.

We should note here that whereas the location of the AVM aboard an RPV is important for proper sampling of the ambient atmosphere we believe that the location becomes much more critical if monitoring of precipitation were to be a consideration. This could happen if monitoring precipitation were to become another measurement function of the instrument.

The program for development and testing of a prototype AVM had four major phases as follows:

(1) Design and fabrication of a laboratory model EVM (Expendable Visibility Meter).

(2) Tests of the laboratory model EVM in an environmental test chamber.

(3) Design and fabrication of a prototype EVM incorporating any improvements or modifications found to be necessary as a result of the testing and evaluation of the laboratory model.

(4) Tests of the prototype EVM in a field environment at Otis AFB.

The present concept for the deployment of an ultimate instrument revolves around RPVs as carrier vehicles. A secondary means of deploying the instrument would be by an expendable drop-package wherein the visibility meter is housed with several meteorological instruments. In the early phase of the procurement, an expendable drop-sonde was considered to be the primary means of deployment, and the RPV was considered to be a secondary mode. At that time the instrument acquired the name of Expendable Visibility Meter, or EVM in abbreviated form. Now that the priority on deployment modes has reversed we have taken the liberty of renaming the instrument an Airborne Visibility Meter, or AVM.

2. OPERATIONAL CONSTRAINTS AND CONSIDERATIONS

Many of the operational constraints which could influence the design of the AVM had yet to be defined at the outset of the program. The lack of information on these constraints resulted primarily from the fact that the deployment vehicle (i.e. the particular type of RPV) had yet to be selected, and is still uncertain at the time of this writing. Limitations on size, weight, and configuration will ultimately and unavoidably be imposed on the AVM by the particular RPV which is chosen. Location of the AVM aboard the RPV will influence the aerodynamic features and sampling configuration of the AVM. The speed and altitude ranges of the RPV combined with the flight profile tactics will impact sampling rates, measurement accuracy and the electronic output time constant.

The electrical power demand of the AVM will be small; hence it is unlikely to be influenced by any usage constraint on RPV power. The type of power available (400 cycle or 28 VDC) and the stability of that power will ultimately be of concern.

The AVM, in turn, will impact the data handling systems aboard the RPV. The telemetry or recording system, for example, must be capable of handling the data rate and the measurement precision of the AVM.

At the outset of the program, in the absence of knowledge of many of the physical and operational constraints which would be imposed on the AVM by the RPV characteristics and tactics, two guidelines were followed in arriving at a design for the Laboratory Model version of the instrument: (1) it was agreed with the AFGL program technical monitors that the laboratory model and prototype instrument demonstrate that they could perform the physical measurements required to satisfy the two primary functions of the instrument, all other concerns being secondary to that objective, and (2) to compel the AVM design into some degree of compatibility with the real world of RPVs, a "best guess" list of constraints was drawn up. This list of constraints is given in Table 2.1. As the program developed, it was recognized that higher performance RPVs were required as delivery vehicles. Thus, RPVs having speeds up to 500 mph and ascent/descent rates approaching 10,000 ft/min had to be considered.

Table 2.1. Constraints Imposed on the Design of the Laboratory and Prototype Model of the Airborne Visibility Meter.

OPERATIONAL CONSTRAINTS	
A. RPV Deployment Mode	
Altitude Range	0 to 10,000 ft.
RPV Speed	100 to 300 mph
Flight Pattern	to cover all altitudes from 100 ft. to 10,000 ft.
B. Drop-Sonde Mode	
Altitude Range	0 to 10,000 ft.
Speed	1000 ft/min.
PHYSICAL CONSTRAINTS	
Size and Weight	Minimal
Aerodynamic Configuration	Uncertain
Ambient Temperature Range	Uncertain
Internal Instrument Temp. Range	-35°C to +50°C
Power Source	28 V DC
Output Signal (Analog)	0 to 10 V
PERFORMANCE REQUIREMENTS	
A. Cloud Forecasts	(1) Report RPV is in or out of clouds; (2) 10 meter resolution; (3) extinction coefficient not required
B. Slant Visual Range Forecasts	(1) SVR >10 km or ≤ 10 km; (2) if ≤ 10 km then SVR ± 20 percent

3. PHYSICAL MEASUREMENT CONSIDERATIONS

3.1 Visibility

Visibility is a generic term concerning the ability to see distant objects. Visibility depends upon properties of the object, its background, the quality of air along the sight path, the length and illumination of the path and the observation angle with respect to the path.

Traditionally, visibility has been defined in terms of visual range, i.e. the distance from an object that corresponds to a minimum or threshold contrast between an object and its background. Threshold contrast refers to the smallest difference between two stimuli that the human eye can distinguish.

3.2 Horizontal Visual Range

The simplest visibility situation which can be treated by physical measurements concerns objects seen in a horizontal direction, against the horizon sky. This case, first treated by Koschmieder, requires uniformity of both light and atmosphere between the observer and object, and between the observer and horizon. The angular distribution of light does not matter as long as each elemental volume of air is illuminated in the same manner. The atmosphere being uniform, the extinction coefficient γ is the same along the entire path to the object or to the horizon.

If the object is the theoretical "black object" i.e. an object with zero reflectance (the closest approximation is a large black box with a small hole in it) then the visual range V is given by a relation first put forth by Koschmieder:

$$V = \frac{3.912}{\gamma} \qquad (3.1)$$

where Koschmieder took for the contrast threshold of the eye the value of $\epsilon = 0.02$.

A contrast threshold of $\epsilon = 0.02$ implies large objects as the targets of observation against the horizon sky. For small objects, or for purposes of recognition rather than detection, a contrast threshold of $\epsilon = 0.05$ is more appropriate. Equation 3.1 then becomes

$$V = \frac{3.00}{\gamma} \tag{3.2}$$

This latter equation appears to have gained wide acceptance in the Air Force; hence, we adopted its usage for this effort.

Duntley, in his extension of Koschmieder's theory (see Middleton-Reference 2), developed the theory of contrast reduction of the atmosphere and applied it to more general situations of slant paths with the observer looking upwards from the ground or downwards from an aircraft.

In the case of horizontal situations the theory of contrast reduction states that

$$C = C_o e^{-\gamma R} \tag{3.3}$$

where R is the horizontal range from the observer to the object, C_o is the inherent contrast of the object as seen against the horizon sky and C is the apparent contrast as seen by the observer. This is the simplest expression of Duntley's theory. It is adequate for the solution of problems of contrast reduction over horizontal lines-of-sight, provided the underlying assumptions are fulfilled. Its great usefulness lies in the fact that it expresses the attenuation of contrast for objects of any inherent contrast, not only for black objects.

The Koschmieder expression, Equation 3.1, can be derived from Duntley's expression for contrast reduction, Equation 3.3, by setting the contrast transmission $C/C_o = 0.02$ and taking for the range R that value V

which is given by

$$0.02 = e^{-\gamma V} \tag{3.4}$$

or

$$V = \frac{\ln 50}{\gamma} = \frac{3.912}{\gamma} \tag{3.5}$$

3.3 Slant Visual Range

The most general expression for the law of contrast reduction by the atmosphere is:

$$C = C_o(B_o'/B') \, e^{-\int_o^R \gamma(r)\, dr} \tag{3.6}$$

where R is the actual range from the observer to the object along a slant path through the atmosphere and where the extinction coefficient $\gamma(r)$ varies with position along the path.

We shall adopt as the definition of inherent contrast C_o of an object (i.e. the contrast as seen if the observer were up close to the object),

$$C_o = \frac{B_o' - B_o}{B_o'} \tag{3.7}$$

where B_o is the brightness of the object and B_o' is the brightness of its surrounding background. (Note: this definition is more convenient when the background brightness is greater than the object brightness. Middleton's definition (Reference 2) in this case always leads to negative contrast values).

Similarly the apparent contrast C of the object as seen by the observer viewing along a slant path of length R_s is

$$C = \frac{B' - B}{B'} \tag{3.8}$$

where B is the brightness of the object as modified by the addition of air light and B' is the brightness of the background, again as modified by the addition of air light.

To arrive at Equation 3.6, however, Duntley had to make certain simplifying assumptions which we enumerate here for the sake of completeness.

(1) The extinction coefficient $\gamma(r)$ which is composed of the scattering coefficient $\sigma(r)$ and absorption coefficient $\alpha(r)$, i.e. $\gamma(r) = \sigma(r) + \alpha(r)$ is dominated by the scattering term. Thus $\alpha(r) \ll \sigma(r)$ and $\gamma(r) \cong \sigma(r)$.

(2) The angular phase function $\Phi(r)$ for aerosol scattering is constant along the entire path of observation.

(3) The illumination from sun and sky is constant along the path of observation.

We now wish to obtain an expression for the Slant Visual Range looking in the downward direction as depicted in Figure 3.1.

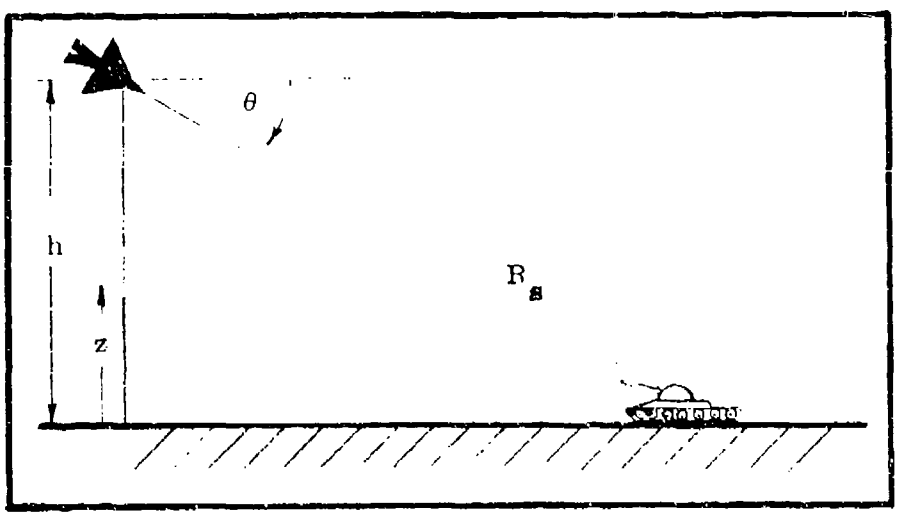

Figure 3.1. Illustration of a downward Slant Visual Range situation.

The problem of downward visual range has been dealt with more or less elaborately by several authors according to Middleton (Reference 2), but with only limited to moderate success. Our present approach to determination of the Slant Visual Range will have one distinct advantage over all previous approaches: by means of the RPV flight profile the scattering coefficient will be measured as a function of altitude. In other treatments of the problem assumptions had to be made about the altitude profile of the aerosol distribution.

Duntley defined a quantity $\bar{R}$ which he called the optical slant range. It "represents the horizontal distance in a homogeneous atmosphere for which the attenuation is the same as that actually encountered along the true path of length R".

Applying this definition to Equation (3.6) gives

$$C = C_o (B_o' / B') e^{-\sigma_o \bar{R}} \qquad (3.9)$$

where

$$\bar{R} = \frac{1}{\sigma_o} \int_o^R \sigma(r)\, dr \qquad (3.10)$$

and σ_o is the scattering coefficient at the lower end of the path (i.e at ground level for most applications).

The quantity $\bar{R}$ is unfortunately not the slant visual range because of the way in which it is defined. In most cases the Slant Visual Range, which we shall define as the quantity R_s will be greater than Duntley's Optical Slant Range, $\bar{R}$.

The Downward Slant Visual Range, R_s, is hereby defined for purposes of this report as the actual range, R_s, for which the contrast transmittance (C/C_o) has been reduced to a value of 0.05 for a "black" object viewed against a Lambertian background, with the solar zenith angle and downward observational angle chosen such that the apparent and inherent brightness of the background are equal (see Appendix A).

This definition of Slant Visual Range follows the tradition established in defining Horizontal Visual Range; i.e., by defining a physically possible although, on a practical basis, highly improbable observational situation. As defined here R_s represents the actual downward slant range for a specific, albeit improbable, situation.

For an observer up close, a white or gray Lambertian surface will take on some average brightness due to the illumination from the sun and sky. As the observer moves away from the surface, the brightness of the surface is diminished by atmospheric attenuation. However, because of the phenomenon called "optical equilibrium" an amount of brightness due to air light is added back (i.e. light scattered into the observer's line of sight by atmospheric aerosols) which under certain conditions of illumination in an amount exactly equal to that which was lost by attenuation. Thus the brightness of the background Lambertian surface remains constant for an observer at any distance. We may thus set $B_o' = B$ and Equation 3.6 reduces to

$$C = C_o e^{-\int_o^{R_s} \sigma(r)\, dr} \qquad (3.11)$$

From the AVM measurements made during the RPV flight, a forecaster can determine the altitude profile of the aerosol coefficient i.e. $\sigma(z)$ vs z. The slant visual range $R_s = h \csc \theta$ for an aircraft at an altitude h can then be determined from the following equations which are arrived at by substitutions into Equation 3.11.

$$C = C_o e^{-\csc\theta \int_o^h \sigma(z)\, dz} \qquad (3.12)$$

$$\ln (C_o/C) = \frac{R_s}{h} \int_o^h \sigma(z)\, dz \qquad (3.13)$$

$$R_s = \frac{\ln (C_o/C)}{\frac{1}{h} \int_o^h \sigma(z)\, dz} \qquad (3.14)$$

These equations apply only under the conditions of a more or less uniform horizontal stratification of the aerosols in the atmosphere. For a contrast threshold of $\epsilon = 0.05$ Equation 3.14 becomes

$$R_s = \frac{3.00}{\frac{1}{h}\int_0^h \sigma(z)\, dz} \; ; \; R_s \geq h \qquad (3.15)$$

It must be emphasized that Equation 3.15 defines the Slant Visual Range for a highly improbable situation. It is, however, a convenient means for characterizing the clarity of the atmosphere just as Horizontal Visual Range does for surface observations. A forecaster may be concerned more with Target Acquisition Range and Lock-On Sensor Range for EO systems than with Slant Visual Range, although the latter quantity will be an indicator for the other two quantities.

To determine the Target Acquisition Range, the forecaster must apply the general expression for contrast reduction (Equation 3.6). In applying that equation, he must specify the remaining parameters which enter into the solution. These are: (1) the inherent contrast, C_o, of the target vs background, (2) the apparent contrast, C, required for target acquisition, and (3) the ratio (B'/B_o') which is the ratio of the apparent brightness of the background to the inherent brightness of the background. This latter quantity creates the most difficulty for a forecaster for it obviously depends on the conditions of illumination of the air path between an aircraft and a target.

Equation 3.6 can be rearranged to give a general expression for the Slant Visual Range which is,

$$R_s = \frac{[\ln (C_o/C) - \ln (B'/B_o')]}{\frac{1}{h}\int_o^h \sigma(z)\, dz} \qquad (3.16)$$

where it is understood that the parameters in the RHS of Equation 3.16 must be chosen such that $R_s \geq h$.

It is not the purpose of this instrument development program to explore the methodology for generating fast accurate forecasts of Target Acquisition Range and Lock-On Sensor Ranges from the AVM measurements. It was necessary, however, to clearly establish a definition of Slant Visual Range to aid in determining the range of scattering coefficients which must be measured by the AVM. Having accomplished that we can move on to put that definition to use.

3.4 Aerosol Scattering Coefficients

To establish the range of scattering coefficients which must be measured by the AVM, it is also necessary to resort to models for the aerosols present in the lower atmosphere.

The maximum possible range of aerosol extinction coefficients for ground level environments is illustrated in Figure 3.2. The curves which show the wavelength variation of the extinction coefficients in this figure were taken from aerosol models of Shettle and Fenn (Reference 4). The curve for Rayleigh scattering from atmospheric molecules was from another source.

The largest ground-level extinction coefficients will accompany advection and radiation fogs. We have chosen to show only the advection fog models of Shettle and Fenn because the extinction coefficients for advection fog are somewhat greater than those of radiation fog and the purpose here is to define the limits on the extinction coefficient.

Table 3.1 is a necessary companion to Figure 3.2. This table provides the single scatter albedo for the various aerosol models of Shettle and Fenn. For example, we see that for fogs the single scatter albedo is unity at the two wavelengths of interest in the AVM program. Thus, the scattering and extinction coefficients are identical.

We have selected the Shettle and Fenn Rural Aerosol Model as being most typical of the environment in which the AVM will probably operate. The single scatter albedo for rural aerosols is very high so that particle absorbtion can

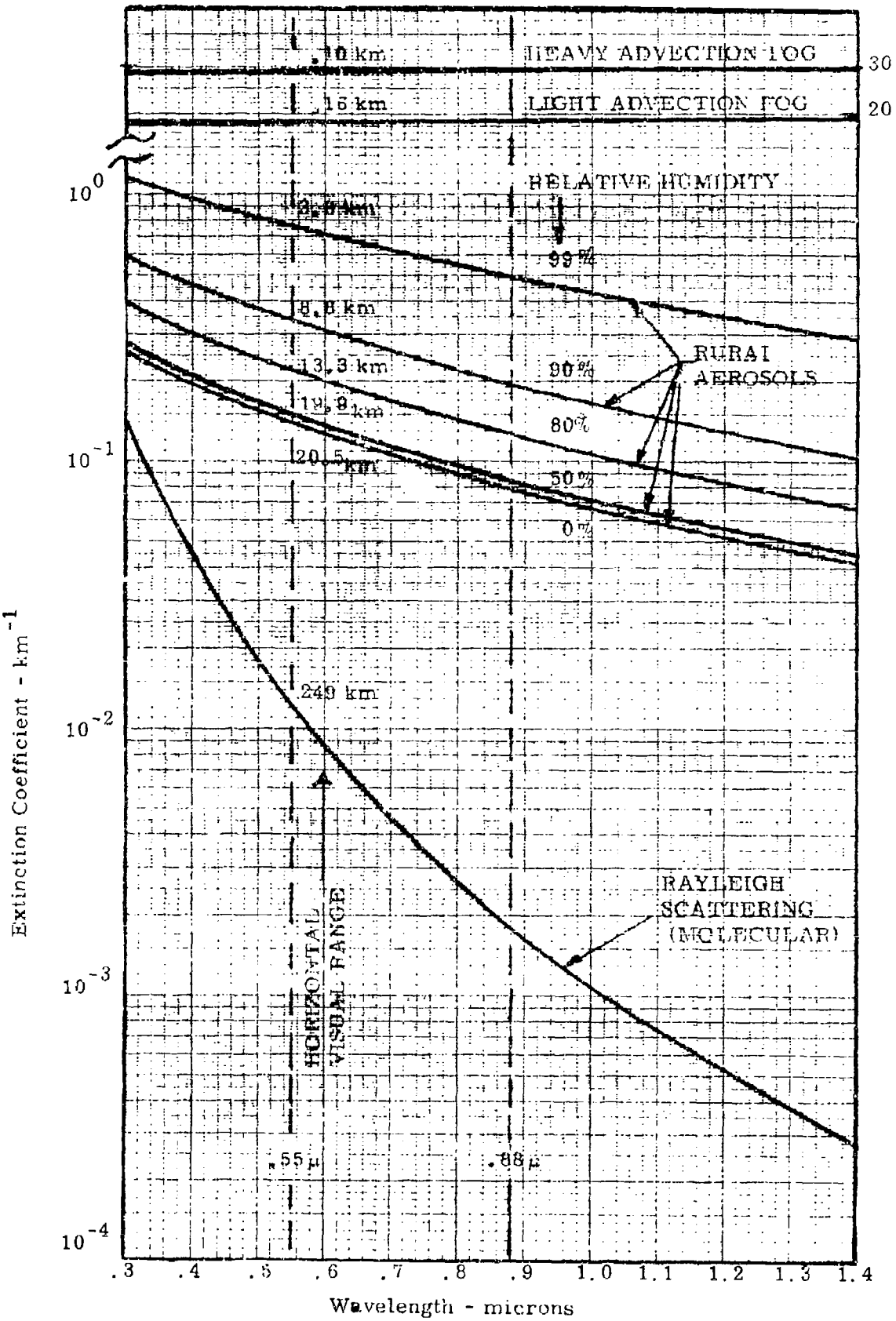

Figure 3.2. Extinction coefficients vs wavelength for various attenuators of visibility.

Table 3.1. Single Scatter Albedo for Various Aerosol Models (From Shettle and Fenn Reference 4).

ATTENUATOR		SINGLE SCATTER ALBEDO	
		$\lambda = 0.55\mu$	$\lambda = 0.88\mu$
RURAL AEROSOLS - R.H. =	0%	0.941	0.896
	50	.943	.899
	70	.946	.906
	80	.959	.929
	90	.972	.951
	95	.977	.961
	98	.983	.972
	99	.987	.979
URBAN AEROSOLS - R.H. =	0%	0.638	0.590
	50	.648	.601
	70	.703	.659
	80	.781	.745
	90	.842	.818
	95	.886	.871
	98	.924	.918
	99	.942	.940
MARITIME AEROSOLS - R.H. =	0%	0.982	0.979
	50	.984	.981
	70	.987	.985
	80	.994	.993
	90	.996	.995
	95	.997	.996
	98	.998	.997
	99	.999	.998
TROPOSPHERIC AEROSOLS-R.H.=	0%	0.959	0.856
	50	.961	.862
	70	.964	.923
	80	.974	.951
	90	.983	.969
	95	.986	.972
	98	.990	.982
	99	.992	.987
HEAVY ADVECTION FOG		1.000	1.000
LIGHT TO MOD. ADVECTION FOG		1.000	1.000
HEAVY RADIATION FOG		1.000	1.000
LIGHT TO MOD. RADIATION FOG		1.000	1.000

be neglected and the scattering and extinction coefficients can be equated. For maritime and tropospheric aerosols the particle albedo is also very high as is demonstrated in the table. Urban aerosols, on the other hand, show the absorption effects of smoke and exhaust fumes. Even in the latter case, when the relative humidity is high, the albedo is also high.

The two wavelengths of interest to the AVM program are 0.55μ and 0.88μ. The first of these wavelengths is, of course, the wavelength of maximum response of the human eye. Most visibility measurements are referenced to the 0.55μ wavelength. The second wavelength, 0.88μ, is the central operating wavelength for the AVM.

If the ratio of the scattering coefficients at the two wavelengths is a constant, then this constant will automatically be included in the calibration constant for the instrument. Table 3.2 gives an indication of how constant the ratio is for a rural aerosols. Given a mean value of 1.66 for the ratio, the maximum potential error due to the wavelength difference is $\pm$ 13 percent.

Table 3.2. Rural Aerosol Scattering Coefficients at the Wavelength of Interest to the AVM.

RELATIVE HUMIDITY (percent)	Scattering Coefficient (km^{-1})		$\frac{\sigma(.55\mu)}{\sigma(.88\mu)}$
	$\lambda = 0.55\mu$	$\lambda = 0.88\mu$	
0	.138	.0776	1.78
50	.143	.0807	1.77
70	.154	.0877	1.76
80	.215	.125	1.72
90	.331	.197	1.68
95	.417	.253	1.65
98	.589	.373	1.58
99	.772	.504	1.53

Figure 3.3 is a plot of Equation 3.15 and shows the slant visual range which is achievable as a function of the mean aerosol scattering coefficient over the altitude range 0 to h. The mean aerosol scattering coefficient, $\bar{\sigma}$, is defined by the relation

$$\bar{\sigma} = \frac{1}{h} \int_0^h \sigma(z)\, dz \qquad (3.17)$$

A primary performance requirement for the AVM is that it perform scattering coefficient measurements over a range of altitudes from which slant visual ranges up to and including 10 km can be determined with an accuracy of $\pm$ 20 per cent. We see from Figure 3.3 that the mean aerosol scattering coefficient corresponding to a slant visual range of 10 km is $\bar{\sigma} = 0.3$.

Knowing the mean aerosol scattering coefficient is not sufficient information from which to determine the smallest scattering coefficient that must be measured by the AVM. The smallest scattering coefficient will be that value which occurs at the highest flight altitude of the RPV. The maximum flight altitude of the RPV is assumed to be 10,000 ft (3.05 km).

To predict the smallest scattering coefficient, we must again resort to aerosol models for the lower atmosphere. Figure 3.4 shows several of the Shettle and Fenn (Reference 5) vertical distribution aerosol models and Elterman's 1968 Model (Reference 6). To fully utilize the information provided in Figure 3.4, we must refer to the description provided by Shettle and Fenn (Reference 5).

> In the boundary layer the shape of the aerosol size distribution and composition for the 3 surface models are assumed to be invariant with altitude. Therefore only the total particle number is being varied. Although the number density of air molecules decreases always more or less exponentially with altitude, there is considerable experimental

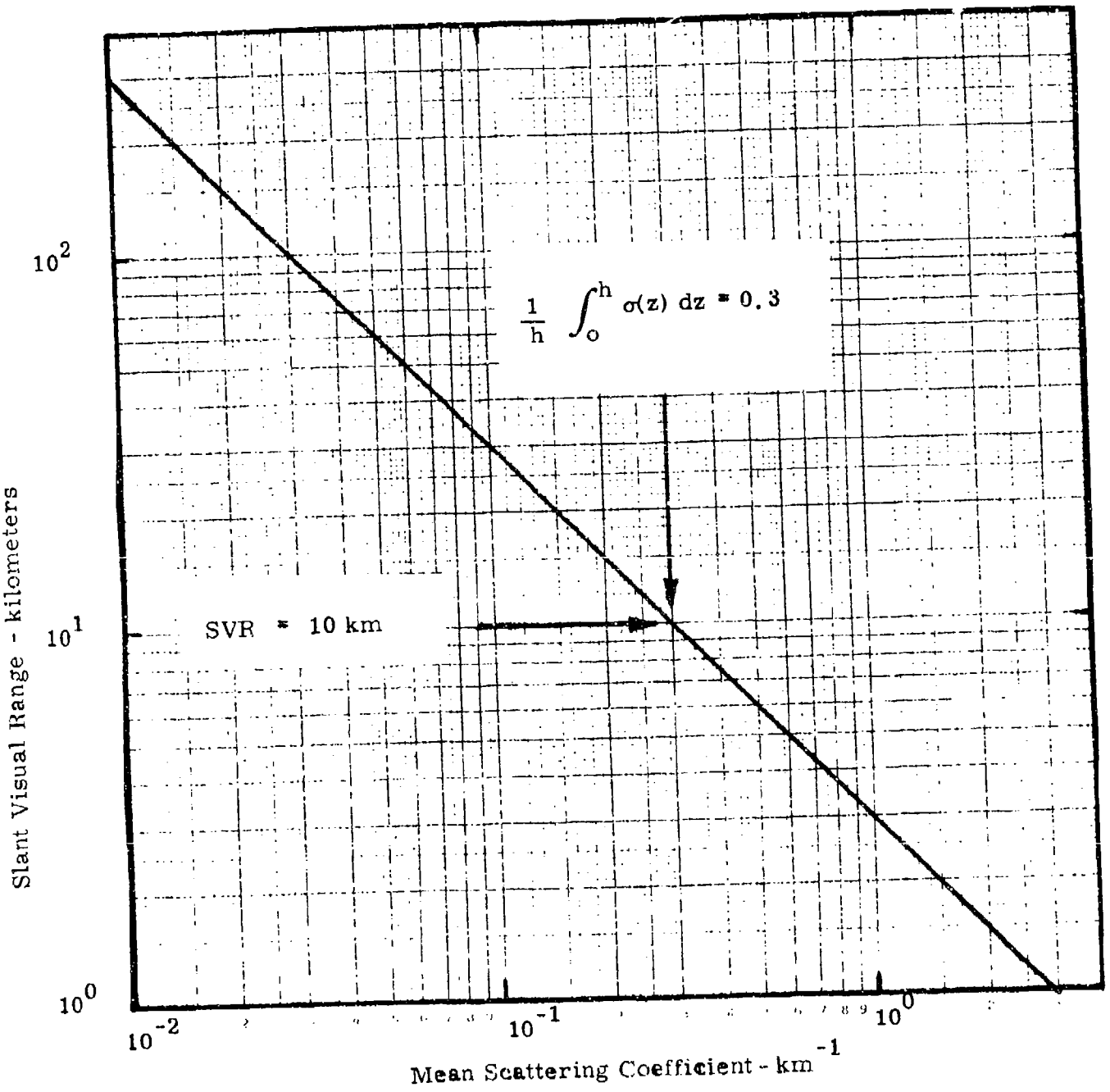

Figure 3.3 . Slant Visual Range vs Mean Aerosol Scattering Coefficient.

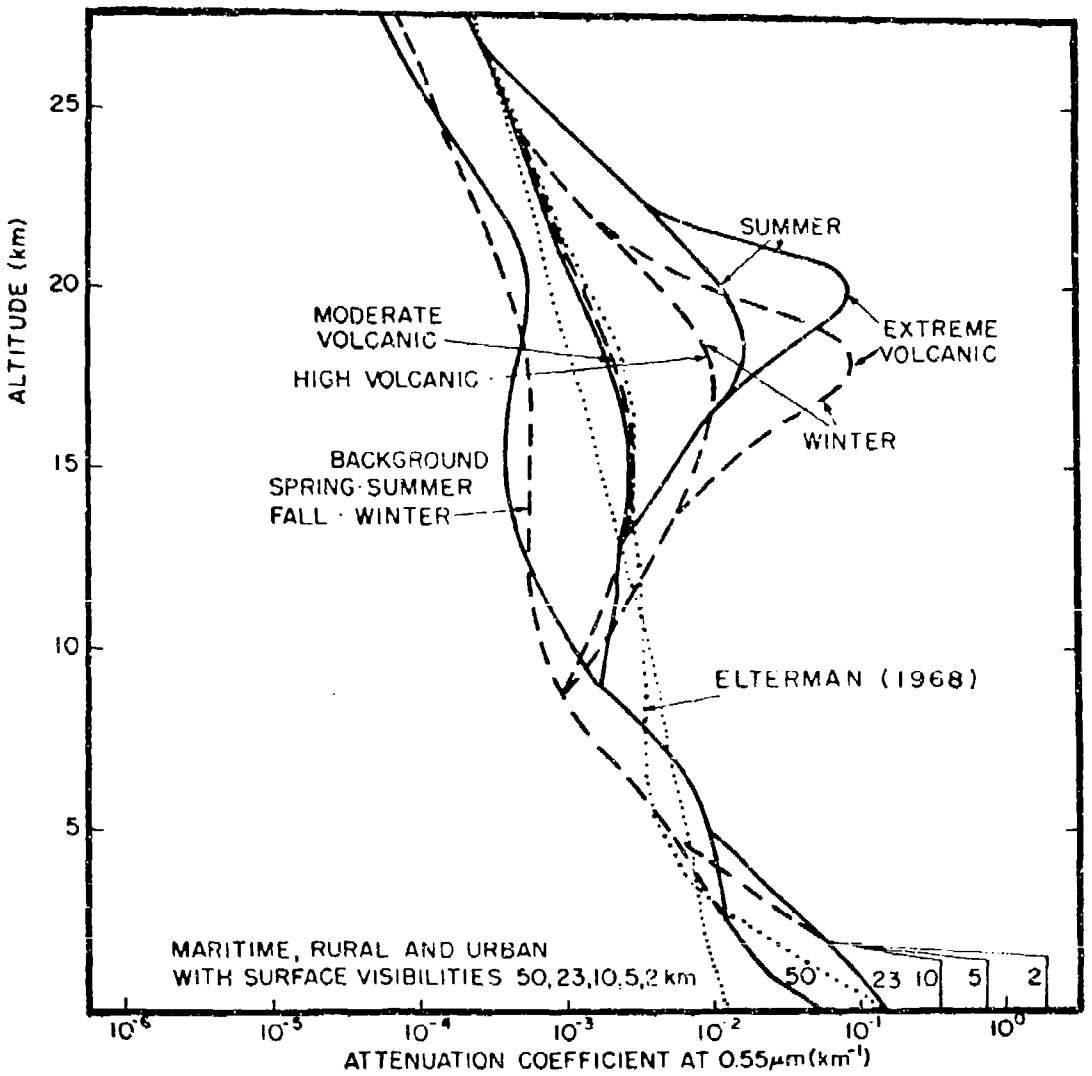

Figure 3.4. The vertical distribution of aerosol extinction (at 0.55 microns) for the different model atmospheres. Also shown for comparison are the Rayleigh profile (dotted line) and Elterman's (1968) Model. (From Reference 5).

data which show that the aerosol concentration very often has a rather different vertical profile. One finds that especially under low visibility conditions the aerosols are concentrated in a layer from the surface up to about 1 to 3 kilometers altitude and that this haze layer has a rather sharp top, (e.g. see DUNTLEY et al., 1972).

The vertical distribution for clear and moderately clear conditions, 50 and 23 kilometer meteorological ranges respectively, is taken to be exponential, similar to the profiles used by ELTERMAN (1964, 1968) following the work of PENNDORF (1954). For the hazy conditions (10, 5, and 2 km meteorological ranges) the aerosol extinction is taken to be independent of height up to 1 1/2 km with a pronounced decrease above that height.

When the atmosphere is clear the Elterman vertical distribution of aerosol extinction is appropriate. The Elterman distribution is given by

$$\sigma(z) = \sigma_o e^{-z/H} \tag{3.18}$$

where σ_o is the ground level extinction (scattering) coefficient and H is the scale height of the aerosol distribution.

When the atmosphere is hazy and there is a boundary layer at an altitude h_b below which the aerosol distribution is constant, the altitude variation of scattering coefficient may be expressed by the following relations

$$\begin{aligned} \sigma(z) &= \sigma_o && o < z \leq h_b \\ &= \sigma_o e^{-(z - h_b)H} && z > h_b \end{aligned} \tag{3.19}$$

We have examined three possible limiting cases of vertical distribution of aerosol scattering coefficients each having a slant visual range

of 10 km. The results are shown in Figure 3.5.

Case (1): Boundary Layer at 3 Kilometers

This is the situation where the boundary layer reaches to the maximum altitude of the RPV (10,000 ft.). The aerosol scattering coefficient is constant with altitude. Hence according to Equation 3.17 it must be equal to the mean value which is $\sigma = 0.3\ km^{-1}$.

Case (2): Boundary Layer at 1.5 Kilometers

Shettle and Fenn state this to be the most probable situation for hazy conditions. The aerosol scattering coefficient is a constant, $\sigma = 0.39\ km^{-1}$, from ground level to an altitude of 1.5 km. The distribution from 1.5 to 3.0 kilometers is found by substituting Equations (3.19) into Equation (3.17) with the mean scattering coefficient $\bar{\sigma} = 0.3\ km^{-1}$ and the scale height of the aerosol distribution $H = 1.2$ km (Elterman; Reference 3). The scattering coefficient at maximum altitude is found to be $\sigma = 0.106\ km^{-1}$.

Case (3): No Boundary Layer

An unlikely situation for hazy environments, but one which was investigated for the sake of completeness. Equation (3.18) must be substituted into Equation 3.17 with $\bar{\sigma} = 0.3$ and $H = 1.2$ kilometers as in Case 2. The ground level scattering coefficient $\sigma = 0.83\ km^{-1}$ and the scattering coefficient at maximum RPV altitude is $\sigma = 0.065\ km^{-1}$. Note that in this case the ground level horizontal visual range is only $V = 3.00/0.83 = 3.6$ km while the slant visual range from an aircraft at 10,000 ft is 10 km. (The horizontal visual range at 10,000 ft. is $V = 3.00/.065 = 46$ km).

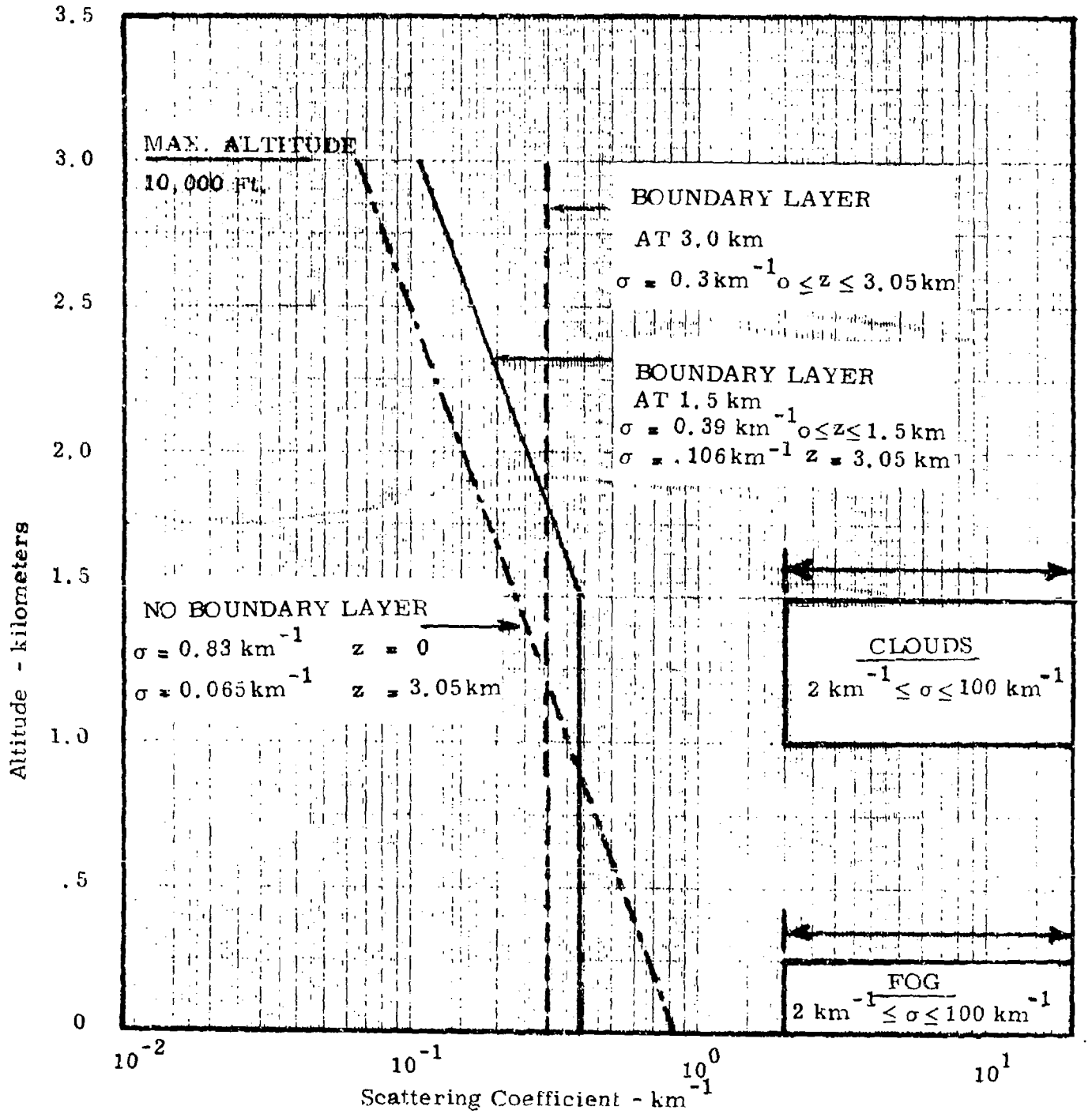

Figure 3.5. Vertical distribution of scattering coefficients corresponding to a Downward Slant Visual Range of 10 kilometers for three possible boundary layer situations.

On the basis of the investigations outlined above the limits on measurement of the aerosol scattering coefficient were established. These limits, i.e. the maximum and minimum values, are given in Table 3.3.

Table 3.3 Performance Requirements on Measurement of the Aerosol Scattering Coefficient by the Airborne Visibility Meter.

Limiting Value	Aerosol Scattering Coefficient
Maximum Value (Clouds/Fog)	100 km^{-1}
Minimum Value (Haze)	0.1 km^{-1}

The minimum value of aerosol scattering coefficient $\sigma = 0.1\ km^{-1}$ is based on the smallest value which is likely to be encountered at an altitude of 10,000 ft. when the downward slant visual range is SVR $\leq$ 10 km.

The maximum value $\sigma = 100\ km^{-1}$ is near the upper limit of scattering coefficients likely to be encountered in clouds or fog. It is not an AFGL requirement that the AVM be capable of measuring the scattering coefficients of clouds or fogs --- only that the instrument be capable of ascertaining whether the RPV is in or out of a cloud (or fog). However, to prevent the possibility of saturation of the amplifiers in the AVM we have required that the instrument electronics behave in a linear manner when the instrument is in a cloud or fog.

3.5 Aerosol Scattering Phase Function

It was previously indicated that the AVM is basically a fixed angle nephelometer, i.e. a radiometer which measures the amount of radiation scattered from a sample volume at a single angle (or more likely over a small range of angles centered on a nominal angle). Fixed angle nephelometers measure the angular scattering coefficient at their angle of operation.

The optical attenuation of the atmosphere is determined by the total scattering coefficient of atmosphere aerosols (in the absence of aerosol absorption or molecular absorption). In Koschmieder's law, for example, the total scattering coefficient is related to visibility by the relation $V = 3.912/\sigma$.

All forward-scatter nephelometers, including the AVM, are based on the principle that light scattered at certain angles in the forward direction may be linearly related to the total scattering coefficient. That is, the angular scattering coefficient $\beta(\theta)$ at a prescribed angle θ divided by the total scattering coefficient is a constant

$$\frac{\beta(\theta)}{\sigma} = \frac{\beta(\theta)}{2\pi \int_0^{\pi} \beta(\theta) \sin\theta \, d\theta} = \text{cons'} \qquad (3.20)$$

Sometimes it is convenient to relate the angular scattering coefficient $\beta(\theta)$ and the total scattering coefficient by means of a phase function $\Phi(\theta)$, thus we have

$$\Phi(\theta) = \beta(\theta)/\sigma \qquad (3.21)$$

Or, upon making the obvious comparison with Equation (3.20), we find that the requirement for converting fixed-angle nephelometer measurements to values of total scattering coefficient is that the phase function at a specific angle be constant over a significant range of atmospheric environments; i.e.

$$\Phi(\theta') = \text{const} = \Phi \qquad (3.22)$$

Perhaps the most thorough experimental investigations of the relationship between the angular scattering coefficient and the total scattering coefficient have been conducted by Barteneva (Reference 7) and Barteneva and Bashilov (Reference 8). The latter two authors conclude that for visual ranges between 0.5 and 220 kilometers the optimum angle of operation for fixed-angle nephelometers is 45 degrees. The authors further state, on the basis of their extensive measurements, that the phase function at an angle of 45 degrees is

$$\Phi(45^\circ) = 0.120 \pm 0.001 \qquad (3.23)$$

for the visibility range extending from 0.5 km to 220 km.

Barteneva and Bashilov estimate that the mean square error in the determination of horizontal visual range for any given situation on the basis of fixed angle nephelometer measurements made at 45 degrees will not be greater than $\pm$ 15 per cent if the value $\Phi = 0.120$ is employed for all environments extending over the entire visual range $0.5 \text{ km} \leq V \leq 220$ km. When the air is very clear, the optimum angle is greater (60 degrees for $V > 100$ km), they state. In fog situations the optimum angle is nearer 30 degrees.

Winstanley and Adams (Reference 9), on the basis of theoretical calculations, infer that the optimum forward-scatter angle to achieve a linear relationship lies between 30 to 40 degrees for fog environments ($2 \text{ km}^{-1} \leq \sigma \leq 60 \text{ km}^{-1}$) with the best correlation being achieved at 35 degrees.

The AVM must provide values of atmospheric scattering coefficients which will permit a determination of slant visual range to be made with an accuracy of $\pm$ 20 percent. We take this accuracy requirement to mean the standard deviation of the SVR. Barteneva and Bachilov on the other hand estimated a mean square error of $\pm$ 15 per cent if the value $\Phi(45^\circ) = 0.120$ is used over the entire visual range $0.5 \text{ km} \leq V \leq 220$ km.

The standard deviation is the square root of the mean square error (variance). Thus the standard deviation of the visual range determination if

one uses the value $\Phi(45°) = 0.12$ for the complete visual range $0.5\ km \leq V \leq 220\ km$ is likely to be $\pm \sqrt{.15} = \pm 39$ per cent.

The AVM must provide accurate measurements of the scattering coefficient over a very limited range of slant visibility conditions $.1\ km \leq V \leq 10\ km$. When the SVR > 10 km, there is no measurement accuracy required. Similarly, when the RPV is in clouds or fog, $V < 1$ km, there is no measurement accuracy required. We expect, therefore, that over the limited range $1\ km \leq SVR \leq 10\ km$, the measurement accuracy for a fixed angle nephelometer will be considerably better than that estimated by Barteneva and Bashilov.

Because of mechanical packaging constraints, we, of necessity, selected a central measurement angle of 55 degrees for the AVM. The use of this angle is justified on the basis that it is within the range of angles for which the scattering phase function is reasonably constant for all environments; also that the total angular coverage extends for $\pm$ 6 degrees on either side of the central angle; and finally that the calibration of the instrument will embrace the effects of different environments.

The phase function for aerosol scattering at an angle of 55 degrees is taken from the rural aerosol model of Shettle and Fenn (Reference 5). The value at 55 degrees is $\Phi(55°) = 0.08$. The complete angular distribution for the phase function is shown in Figure 3.6.

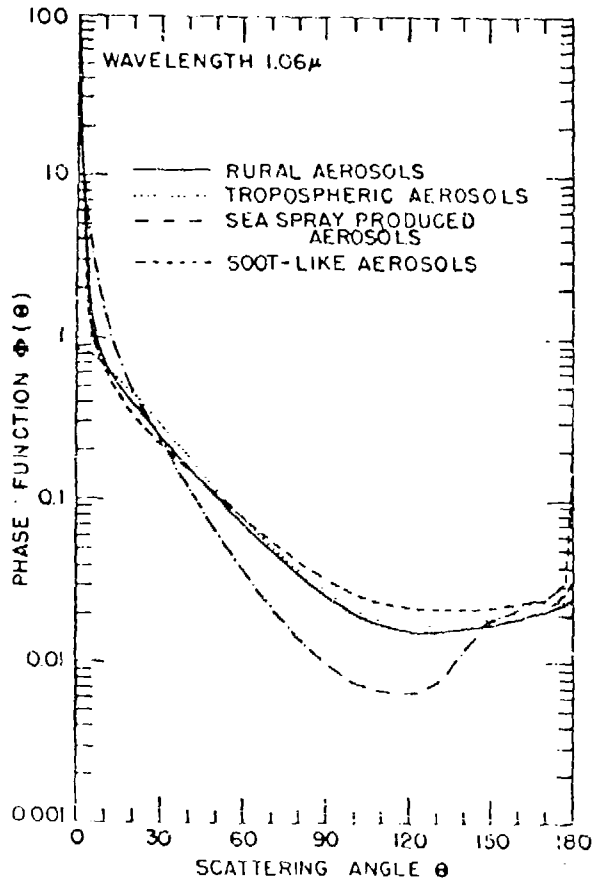

Figure 3.6. Angular distribution of scattered light for different lower atmospheric aerosol models, at wavelength of 1.06 microns. The phase function, $\Phi(\theta)$, is the differential probability of scattering by angle θ (From Reference 5).

4. AVM: LABORATORY MODEL DESIGN

4.1 Sampling Rate Considerations*

4.1.1 Cloud Sampling

When the operational constraints were imposed on the design of the Laboratory Model AVM (see Table 2.1), a 10 meter resolution was specified for the cloud presence capability. This constraint was imposed in a somewhat arbitrary manner and is certainly subject to change for any good reason which may arise at a later date.

The resolution requirement implies a sampling rate capability of one sample every 10 meters at the maximum RPV velocity, which was assumed to be 300 mph (134 m/sec). At the maximum RPV velocity, the sampling time interval to provide a reading every 10 meters is $10/134 = 0.075$ seconds.

When the RPV enters or exits a cloud, there will be an abrupt change in the scattering coefficient. We will require that the first reading taken beyond 10 meters from a cloud/clear-air boundary must be within 5 percent of the final value. Since three e-foldings with a time-constant of τ will result in a value which is 95 percent of an asymptotic value, we can require that the instrument have a time-constant given by

$$3\tau = 0.075 \text{ sec} \tag{4.1}$$

or

$$\tau = 0.025 \text{ sec}$$

The electrical frequency bandwidth of the system is taken to be

$$\Delta f = \frac{1}{4\tau} \tag{4.2}$$

thus, with a time-constant of $\tau = 0.025$ sec, the electrical bandwidth required of the system will be

$$\Delta f = 10 \text{ Hz} \tag{4.3}$$

*Note: These were the original design considerations and may not reflect the present operational deployment concepts.

4.1.2 Haze Aerosol Sampling

The sampling rate considerations which apply to clouds and fog do not apply to the measurement of haze aerosols. When the scattering coefficient of haze aerosols is to be measured, it is essential that a representative air sample be measured.

For a different instrument development program, where one of the operating wavelengths is .55μ HSS Inc has established that a volume of air equal to 250 cm^3 must be sampled to account for 95 percent of the cumulative attenuation, using Shettle and Fenn's Rural Aerosol Model with a visual range of 23 km. In this latter case aerosol particles less than 2 microns in diameter provide 95 % of the contribution and those larger than 2 microns in diameter add the remaining 5 percent attenuation.

There are only 0.1 particles per cm^3 in the size range 1.5 to 2.5 microns diameter. For good statistical sampling about 25 particles in this size range be sampled. Thus $25/0.1 = 250$ cm^3 must be sampled if the operating wavelength is 0.55 microns and the visual range is 23 kilometers. For a visual range of 10 km, we shall scale the volume requirement linearly. That is, a sample volume of $(10/23) \times 250 = 108$ cm^3 would be required.

To perform the above analysis required computer calculations by HSS Inc modeled after those of Shettle and Fenn in their determination of the "Cumulative Contribution (%) of aerosol extinction and scattering by various aerosol size ranges" (Reference 10) for the particular aerosol model and wavelength of interest.

The requirement that 25 particles of 2 microns size pass through the sample volume during one time constant of the instrument is extremely conservative. It states that the statistical fluctuation in the number of 2 micron particles; i.e. $\sqrt{25}$, will induce only a 20 per cent change $\left(1/\sqrt{25}\right)$ in the measured value of the scattering coefficient.

The instantaneous sample volume of the AVM has deliberately been kept small (approximately 1 cm^3) for reasons which will be discussed later. To assure that a truly representative aerosol sample has been measured requires that a sufficient amount of air be moved through the sample volume during a sample time period so that the time-integrated sample volume is equal to the representative sample volume. When the AVM is airborne, either on an RPV or as a drop-package, the motion of the parent vehicle will provide the necessary flow of air through the sample volume. When the AVM is operated statically winds must be depended upon to provide the proper sample volume.

A graph has been prepared (Figure 4.1) to assist in determining the sample time interval for various operational situations in which the AVM may be deployed. We have determined that the representative volume of air for a 10 km visual range situation which must be sampled is approximately 0.1 liter (100 cm^3). Given that volume we can find the proper sample time interval for each of three methods of deploying the AVM.

(1) RPV Deployment (100 to 300 mph)

From Figure 4.1 we see that a sample time interval of 0.03 seconds provides an integrated sample volume greater than 0.1 liters over the RPV speed range of 100 to 300 mph. This sampling rate is consistent with the sampling rate required for cloud diagnostics (0.075 seconds).

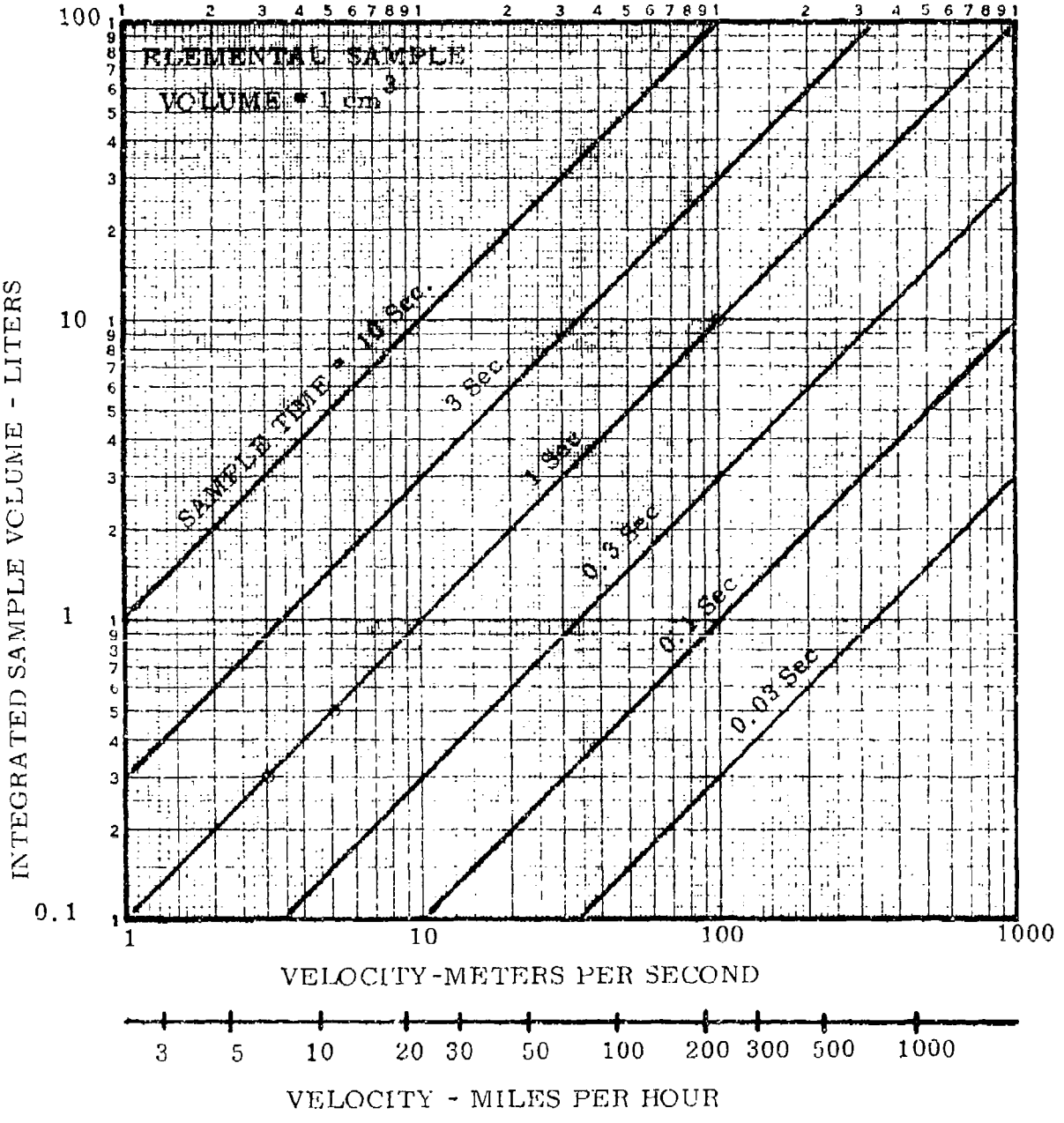

Figure 4.1. Integrated sample volume vs air speed for an elemental scattering volume of 1 cm^3 at six different sample times.

(2) Drop-Sonde Deployment

It is assumed that the drop-sonde package will have a retardation device to limit its fall velocity to 1000 ft/min (5.1 m/sec). A sample time interval of 1 second will provide an integrated sample volume of 0.5 liters --- more than is required to achieve a representative sample volume. If the sample rate is fixed at 1 per second an aerosol scattering coefficient measurement will be made at every 5 meter change in altitude. An aerosol vertical profile resolution of 5 meters more than satisfies our requirement for a 30 meter vertical resolution (see Table 2.1).

(3) Stationary Operation

When the AVM is operated in the stationary mode, a sample time of between 1 to 10 seconds will be required. If the sample time interval were 10 seconds, for example, the wind velocity need only be 0.2 mph to provide a truly representative sample volume.

There is no requirement that a single model of the AVM be capable of rapid conversion from one deployment method to another. In fact, for packaging reasons the RPV and drop-sonde deployment modes may require two different models of the AVM. In any case, the electronic circuit time constant τ can be adjusted to the particular deployment mode: approximately $3\tau = 0.1$ second for RPV deployment, and $3\tau = 1$ second for drop-sonde deployment. For stationary operation of the AVM, the circuit time constant can be temporarily adjusted to give a τ anywhere between 1 to 30 seconds.

4.2 Signal Analysis

We examined the signal flux equations for two types of light sources, a tungsten filament lamp and a light emitting diode, proceeded to select one source in preference to the other for the AVM, and then obtained signal flux predictions for that source.

The geometry of the AVM fixed-angle nephelometer is depicted in Figure 4.2. Light from a source, which in the case illustrated is a light emitting diode (LED), is projected by a lens through the region encompassing the sample volume. A receiver system, composed of a

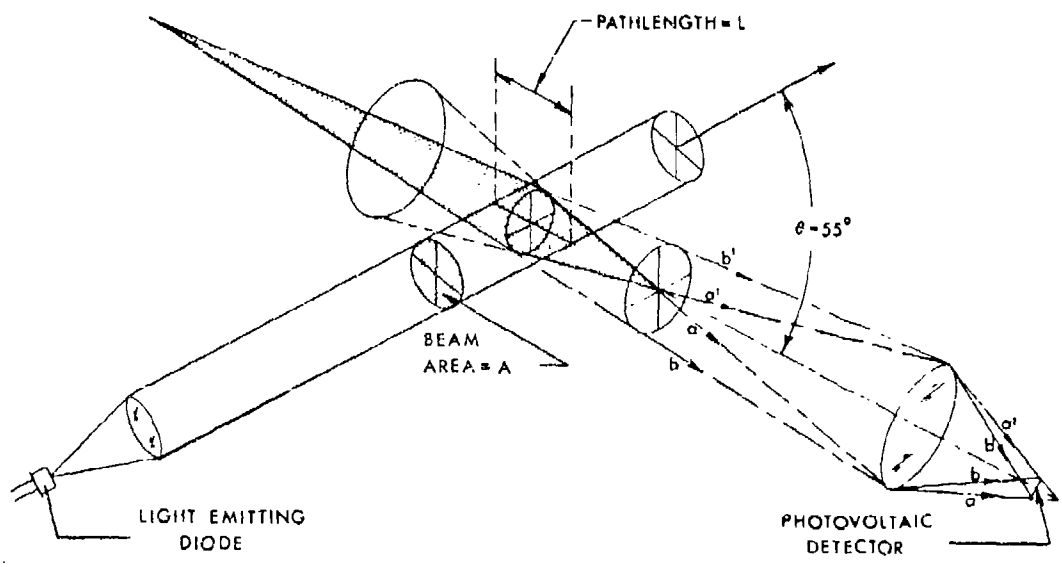

Figure 4.2. Schematic diagram of the optical system of the Airborne Visibility Meter.

photovoltaic detector and objective lens, collects light which is scattered by aerosols at a nominal scattering angle θ from the sample volume, which volume is defined by the intersection of the ray bundles of the transmitter and receiver optics.

Most, but not all, of the flux collected by the receiver will come from the region defined by the intersection of the collimated light bundle projected by the transmitter and the focal zone of the receiver system. The focal zone of the receiver is the shaded region shown in Figure 4.2 which has the appearance of two cones with a common base.

The maximum flux is collected by the receiver system when the sensing element of the detector is imaged into the center of the sample volume as shown in Figure 4.2; the base of the cones in the focal zone is actually the image of the detector projected into the sample volume. The focal zone is defined by four rays as shown in the figure. Rays a and a' terminate at the edges of the detector but cross the optical axis of the receiver lens beyond the detector, which implies that in object space they must cross the optical axis at a distance nearer to the lens than is the object. Similarly rays b and b' also terminate on the edges of the sensing element, but cross the optical axis in front of the sensor; hence, they must cross the optical axis beyond the object in object space. All other rays terminating at the sensor must be included within the locus of rays defined by the four rays a, b, a' and b' which in turn define the focal zone.

The focal zone thus defines a region in which the full lens acts to collect light from every scatterer in the illuminated part of the zone. There are regions around the focal zone where light can be scattered to the lens and reach the detector, but only a fraction of the lens can observe this light. Most of the light which can reach the detector will be that which originates within the focal zone. For signal analysis purposes, therefore, we need consider only the focal zone radiation. The small amount of light which will be contributed by the regions peripheral to the focal zone will be an added bonus.

When the light source is a tungsten lamp, the optimum flux transfer situation occurs if the lamp filament is imaged such that the maximum diameter of its focal zone (i.e. the image of the filament) intersects the maximum diameter of the receiver focal zone (i.e. the image of the sensor element). This is one of the two principles upon which the original AVM concept was based (this and a second principle described later dictate the optimal overall geometry for fixed angle nephelometers. The beneficial use of this combination of principles appears to have been first recognized by HSS Inc.).

For a tungsten lamp source, the flux, F_t, collected from the source by the transmitter lens is

$$F_t = \frac{\pi \epsilon_\lambda N_\lambda \Delta\lambda T_t(\lambda) A_s}{1 + 4 (f/n)_t^2} \quad \text{Watts} \qquad (4.4)$$

where:

A_s = Effective area of the source, cm^2

N_λ = Spectral radiance of the lamp filament, watts $cm^{-2}\ sr^{-1}\ \mathring{A}^{-1}$

$\Delta\lambda$ = Effective wavelength bandwidth of the instrument, $\mathring{A}$; (actually defined by a wavelength isolation filter in the receiver optics)

ϵ_λ = Average spectral emissivity of tungsten in the spectral region defined by $\Delta\lambda$

$T_t(\lambda)$ = Transmittance of the projection optics in the wavelength interval $\Delta\lambda$

$(f/n)_t$ = Relative aperture of the transmitter optics

The constant irradiance H throughout the focal zone of the transmitter lens is the ratio of the total flux collected by the transmitter lens to the effective area of the image of the filament, that is

$$H = F_t / A_1, \text{ watts cm}^{-2} \qquad (4.5)$$

The scattering cross section per unit volume of scatter (i.e. the scattering coefficient, σ) has the units cm^2/cm^3 or cm^{-1}. The product of σ and the irradiance H is the total flux σH scattered from the beam per unit pathlength in the beam. The flux F_1 scattered per unit volume per unit solid angle in the direction θ is determined by the phase function Φ

$$F_1 = \Phi \sigma H \text{ watts cm}^{-3} \text{ ster}^{-1} \qquad (4.6)$$

The radiance (brightness) ,B_1, of the sample volume as observed from the receiver lens is obtained by multiplying Equation 4.6 by that length L of the focal zone of the receiver system which is illuminated by the transmitter beam

$$B_1 = \Phi \sigma HL \text{ watts cm}^{-2} \text{ sr}^{-1} \qquad (4.7)$$

Finally, the scattered flux, F, collected from the sample volume by the receiver lens is given by the expression

$$F = \frac{\pi B_1 A_1 T_r(\lambda)}{1 + 4 (f/n)_r^2} \text{ watts} \qquad (4.8)$$

where: $(f/n)_r$ = relative aperture of the receiver lens (in object space)

A_1 = cross-sectional area of scattering volume as seen from the receiver lens, cm^2

$T_r(\lambda)$ = Transmittance of the receiver optics in the wavelength interval $\Delta\lambda$

Combining Equations 4.4 through 4.8 gives the complete expression for flux received at the detector

$$F = \frac{\pi^2 \Phi \sigma L \epsilon_\lambda N_\lambda \Delta\lambda T_t(\lambda) T_r(\lambda) A_s}{\left[1 + 4(f/n)_t^2\right]\left[1 + 4(f/n)_r^2\right]} \qquad (4.9)$$

HSS Inc appears to have been the first to recognize that Equation 4.9 can be written in the following form:

$$F = \Phi \sigma \epsilon_\lambda N_\lambda \Delta\lambda E_t \left(\frac{L}{A_1}\right) E_r \qquad (4.10)$$

where: $$E_t = \pi A_s T_t \left[1 + 4(f/n)_t^2\right]^{-1} \qquad (4.11)$$

is the throughput of the transmitter optical system and

$$E_r = \pi A_1 T_r \left[1 + 4(f/n)_r^2\right]^{-1} \qquad (4.12)$$

is the throughput of the receiver optical system.

Equation (4.10) is the basic design trade-off equation for fixed angle nephelometers where both the source and detector are imaged into the sample volume (which as we have seen is one of the optimal conditions for maximizing flux onto the detector).

The design trade-off equation permits an interpretation to be enunciated, which appears to have previously gone unnoticed. That interpretation is as follows: Once the source radiance $\epsilon_\lambda N_\lambda$ and detector bandwidth $\Delta\lambda$ have been chosen and the throughputs E_t and E_r of the transmitter and receiver have been maximized for the geometry permitted by the physical constraints on the instrument there remains a further means of maximizing flux on the detector namely the ratio (L/A_1).

To a first approximation $A_1 \simeq L^2$, thus we see that

$$F \sim \frac{1}{L} \qquad (4.13)$$

enabling the statement to be made that the flux on the detector is inversely related to the linear size of the sample volume. The smaller the sample volume the greater the amount of flux received by the detector.

The analysis outlined above is the basis for making the sample volume of the AVM as small as possible consistent with the requirement to measure scattering from representative samples of air. The AVM sample volume chosen for design purposes is 1 cm^3. The numerical value of the pathlength L is thus L = 1 cm and the cross-sectional area of the sample as viewed from the detector lens is A_1 = 1 cm^2.

For several reasons we elected to use a light emitting diode (actually an infrared emitting diode, IRED) as the light source for the AVM. The major argument against using an IRED (as opposed to a tungsten lamp) is that the measured scattering coefficients are not those of the visible spectral region; therefore, small errors may be introduced if the ratio σ (0.55 μ) / σ (0.88 μ) is not constant. On the other hand, the arguments in favor of the IRED are quite compelling:

(1) The IRED is much smaller than a tungsten lamp.

(2) Far less electrical power is required to produce the same irradiance at the sample volume.

(3) Negligible Heat is generated by the IRED.

(4) The IRED is modulated electronically; no chopper system is required.

(5) The state-of-the-art for LED's is constantly changing. Sources with greater power output at shorter wavelengths are continuously being developed.

It would appear to be only a matter of time before LED s with sufficient power output in the visible region will be available for use in an AVM. We feel that this step should be anticipated in advance and the inconvenience of the calibration factor required when an IRED source is used should

be tolerated for the time being.

When a IRED source is used, it becomes necessary to modify Equation 4.10 slightly. The emitting element of the IRED is so small that we can essentially treat the bundle of light from the transmitter optics as a collimated bundle. The flux on the detector is then expressed as

$$F = \Phi \sigma P_\lambda \Delta\lambda T_t(\lambda) \left(\frac{L}{A_1}\right) E_r \qquad (4.14)$$

where P_λ is the radiant power emitted by the IRED. (Note: it is assumed here that the relative aperture of the transmitter optics is fast enough to collect all the light emitted by the IRED).

The IRED will be square-wave modulated and the received signal will be synchronously detected in order to suppress noise due to background radiation. It is thus necessary to determine the rms signal flux on the detector. The rms signal flux is obtained by dividing Equation 4.14 by $\sqrt{2}$, giving

$$F_{rms} = \frac{1}{\sqrt{2}} \Phi \sigma P_\lambda \Delta\lambda T_t(\lambda) \left(\frac{L}{A_1}\right) E_r \qquad (4.15)$$

Table 4.1 lists the AVM instrument design parameters pertinent to the signal flux calculations. Table 4.2 gives the range of scattering coefficients, and their phase functions at $\theta = 55°$, which are also necessary for the signal predictions. The results of the signal flux calculations are given in Table 4.3.

Table 4.1. Design Parameters Used for the Laboratory Model AVM

INSTRUMENT PARAMETER	SYMBOL	VALUE
TRANSMITTER		
IRED Source Power	$P_\lambda \Delta\lambda$	12 mW
Center Wavelength	λ	8800 Å
Optical Bandwidth (HBW)	$\Delta\lambda$	800 Å
Lens/Window Efficiency	$T_t(\lambda)$	0.80
SAMPLE VOLUME		
X-Sectional Area	A_1	1 cm^2
Path Length	L	1 cm
Scattering Angle (Nominal)	θ	55°
RECEIVER		
Relative Aperture (Lens)	f/n	
(a) Object Space	--	5
(b) Image Space	--	1
Efficiency of Optics	$T_r(\lambda)$	0.40
(a) Lens/Window = 0.8	--	--
(b) 800 Å HBW Filters = 0.5	--	--
Optical Throughput	E_r	1.40×10^{-2} cm^2 sr
Photovoltaic Detector		
(a) Total Sensor Area	A_r	5.1 mm^2
(b) Useful Sensor Area	A_r	4.0 mm^2
Electrical Bandwidth	Δf	10 Hz
Time Constant	τ	0.025 sec
Sample Time Interval	T_s	0.1 sec
Detector NEP (88μ, 3000 Hz, 10 Hz)	NEP	2.75×10^{-13} watts
Detector Quantum Efficiency	$\eta(.88\mu)$	0.7

Table 4.2. Scattering Coefficients and Phase Functions Applicable to the AVM Design.

Environment	Maximum Scattering Coefficient	Minimum Scattering Coefficient	Phase Function $\Phi(\theta = 55°)$
Clouds or Fog (Heavy to Light)	100 km^{-1}	2 km^{-1}	0.033(1)
Rural Aerosol Haze (Heavy to Light)	2 km^{-1}	0.1 km^{-1}	0.080(2)

Note (1): D. Deirmendjian Cloud Model C1 (See Reference 11)

Note (2): Shettle & Fenn (See Figure 3.6)

Table 4.3. Predicted Signal Flux Values for Various Environmental Situations.

ENVIRONMENT	Scattering Coefficient km^{-1}	RMS Signal Flux watts
Heavy Clouds/Fog	100	2.79×10^{-9}
Light Clouds/Fog	2	5.57×10^{-11}
Heavy Rural Aerosol Haze	2	1.35×10^{-10}
Light Rural Aerosol Haze	0.1	6.75×10^{-12}
Mean Scattering Coefficient For Slant Visual Range = 10 km	0.3	2.03×10^{-11}

4.3 Noise Analysis

There are three potential sources of noise which are of concern in the design of the AVM: (1) Photon noise due to background radiation in the field-of-view of the instrument, (2) detector noise i.e. the NEP of the detector, and (3) amplifier noise. It will be assumed that by use of high quality electronic components combined with good design practice the third noise source, i.e. amplifier noise, can be neglected in comparison with the other two noise sources.

The NEP of the photovoltaic detector chosen for the Laboratory Model AVM is given in Table 4.1, i.e. NEP(0.88μ, 3000 Hz, 10 Hz) = 2.75×10^{-13} W. The NEP due to photon noise can be calculated from the relation (See Reference 12, p 11-40)

$$\text{NEP (Photons)} = \frac{4.46 \times 10^{-10}}{\eta} \left[\frac{F_b}{\lambda}\right]^{1/2} \sqrt{\Delta f} \qquad (4.16)$$

where: F_b = Flux at detector due to background radiation in the field-of-view of the receiver, watts.

η = Quantum efficiency of the detector.

λ = Wavelength of the photons, microns.

Δf = Electronic frequency bandwidth, Hz.

The flux at the detector F_b due to radiation from the terrain, or clouds, within the field-of-view of the receiver is given by

$$F_b = \frac{\pi A_d B_\lambda \Delta\lambda \; T_r(\lambda)}{1 + 4 (f/n)_r^2} \qquad (4.17)$$

where: B_λ = Average spectral radiance of background features, watt cm^{-2} sr^{-1} μ^{-1}.

$\Delta\lambda$ = Optical bandwidth of receiver, microns.

$T_r(\lambda)$ = Transmittance of receiver optics.

$(f/n)_r$ = Relative aperture of receiver optics in image space.

Substituting appropriate values of receiver parameters from Table 4.1 into Equations 4.16 and 4.17, and combining the two equations, we have

$$\text{NEP (photons)} = 6.88 \times 10^{-11} [B_\lambda]^{1/2} \text{ watts} \tag{4.18}$$

The signal-to-noise ratio (S/N) of the AVM may be derived from the expression

$$S/N = \frac{\text{RMS Signal Flux}}{\left\{[\text{NEP(Detector)}]^2 + [\text{NEP(Photons)}]^2\right\}^{1/2}} \tag{4.19}$$

or

$$S/N = \frac{F_{rms}}{\left\{7.56 \times 10^{-26} + 4.73 \times 10^{-21} B_\lambda\right\}^{1/2}} \tag{4.20}$$

Graphs of S/N ratio vs background spectral radiance have been made for three environmental situations using Equation (4.20); the results are shown in Figure 4.3. The three environments expressed in terms of their scattering coefficients σ are taken from previously described situations:

(a) $\sigma = 2 \text{ km}^{-1}$ Extremely heavy Rural Aerosol Haze, bordering on thin clouds or thin fog.

(b) $\sigma = 0.3 \text{ km}^{-1}$ The mean value of σ for a SVR of 10 km in a Rural Aerosol Haze.

(c) $\sigma = 0.1 \text{ km}^{-1}$ The least value of σ which the AVM need measure. It corresponds to the σ - value at 10,000 ft. when a boundary layer is present at 1.5 km and the SVR = 10 km.

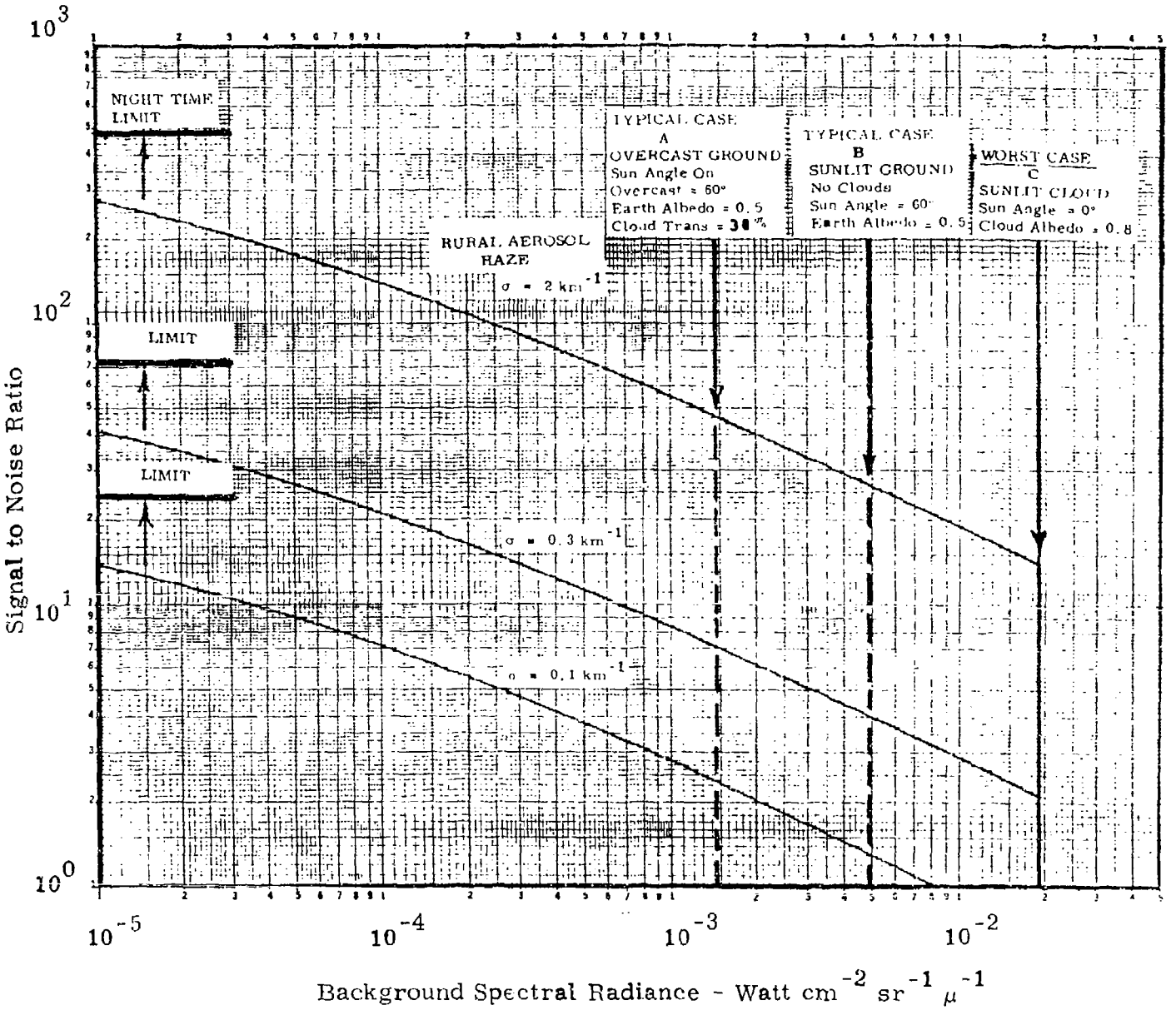

Figure 4.3. Predicted S/N ratio for the AVM vs background spectral radiance (at 0.88 micron) in the field-of-view for three environmental haze situations.

The worst background situation which the AVM could encounter (Case C) is indicated in Figure 4.3. The preferred orientation of the AVM aboard an RPV will be such that the receiver stares in the downward direction, invariably, therefore, at terrain. On rare occasions, however, the RPV may stare down at the top of sunlit clouds. This is the worst case situation, Case C, with the sun directly overhead.

More typical background situations are described by Cases A and B. Case A is an overcast situation with the RPV under the overcast, the ground albedo is 0.5, and the diffuse cloud transmittance is 30 percent. The spectral radiance B_λ of the background is calculated from the relation

$$B_\lambda = \frac{\omega H_\lambda T_c(\lambda) \cos Z}{\pi}, \text{ watts cm}^{-2} \text{ sr}^{-1} \mu^{-1} \qquad (4.21)$$

where: ω = Albedo of the background

H_λ = Incident solar irradiance on top of the cloud at normal incidence to direction to the sun, watts $\text{cm}^{-2} \mu^{-1}$

$T_c(\lambda)$ = Diffuse Transmittance of the Overcast

Z = Zenith angle of the sun

Case B is a typical situation when there is no cloud cover. The spectral radiance of the background can be found from the relation

$$B_\lambda = \frac{\omega H_\lambda \cos Z}{\pi} \qquad (4.22)$$

where the symbols are as previously described. The values of H_λ at $\lambda = 0.88 \mu$ were taken from Reference 12 in all cases treated here.

Figure 4.3 may be used to appraise the measurement accuracy of the AVM for the various situations treated in the figure. It is required that SVR determinations made from the AVM measurements for SVR ≤ 10 km have an accuracy of $\pm$ 20 percent (see Table 2.1). We can infer from this requirement that the signal-to-noise ratio must be at least S/N = 5 for a mean value of the scattering coefficient, $\sigma = 0.3\ \text{km}^{-1}$, when the slant visual range is 10 km. This condition is satisfied for the typical overcast situation, Case A, and very nearly satisfied for Case B. We do not believe that it is realistic to require that the condition be satisfied for Case C.

The reason for choosing to satisfy the condition S/N = 5 for the mean value of the scattering coefficient $\sigma = 0.3\ \text{km}^{-1}$ when the SVR = 10 km should be explained. At the top of the 10 km slant path the scattering coefficient could be as low as $\sigma = 0.1\ \text{km}^{-1}$, in which case the signal-to-noise ratio would be less than 5:1. On the other hand, at low altitudes the scattering coefficient will be much larger than the mean value in which case the accuracy of the measurement will be much better. We believe, therefore, that the net result of having a low accuracy at the top of the path and high accuracy at the bottom of the path can be properly appraised by evaluating the accuracy of the measurement for the mean value of σ over the total path.

4.4 Source Characteristics

Early in the design phase, our deliberations on a source for the AVM focused-in on a particular IRED (Model XC-88 FD) manufactured by the Xciton Corp. which had just appeared on the market. The Xciton Corp calls the series of IRED s of which this is a member, "Super High Output Infrared Emitters". These IRED s are gallium aluminum IR-emitting diodes in TD-46 style packages. Two features attracted us to the XC-88FD: (1) the peak wavelength of 8800 $\mathring{A}$ vs the peak wavelength of most IRED emitters which is 9400 $\mathring{A}$, and (2) the radiant power capability which is 12 mwatts.

At the time we selected the XC-88FD, its output power characteristics were superior to any other commercially available IRED at any wavelength. Since that time, however, other devices have become available with considerably more power output: (1) Plessey Model GAL-10, 45 mwatt at a peak wavelength of 9400 Å and a HBW of 500 Å; and (2) Zexco Model ZE 6000; 55 mwatt at a peak wavelength of 8800 Å, with HBW unspecified. Both the Plessey and Zexco IRED s are mounted on TO-66 headers.

A problem with the Plessey device is that to utilize the full 45 mwatts of radiation requires an optical component capable of intercepting radiation over a cone angle subtending 180 degrees (in other words a very strong parabolic or elliptical reflector). Such an optical component would have increased the physical size of the transmitter system beyond that which we deemed might be acceptable for use on an RPV or drop package.

There was no information available about the angular emission characteristics of the Zexco device. The similarity in characteristics between the Plessey and Zexco devices led us to conclude that the Zexco device probably suffers from the same angular emission problem as the Plessey device.

The laboratory model instrument was designed with the Xciton Model XC-88FD as the designated source of radiation. The same source was used in the prototype instrument because of the favorable experience in the laboratory model instrument. No new IRED s or LED s became commercially available in the time interval after test of the lab model and fabrication of the prototype instrument.

Laser diodes were given some consideration in reviewing the potential source of light for the AVM. However, they offered only one advantage over IRED s but had two distinct disadvantages. The cw power output of laser diodes is in the class of 10 mwatts at 9400 Å, so that there is no advantage gained from use of a laser diode over an IRED.

The advantage of laser diodes lies in their narrow wavelength bandwidths (HBW between 25 to 50 Å). By using equally narrow interference filters in the receiver system, a signal-to-noise advantage of at least $\sqrt{10}$ can be achieved.

The disadvantages of laser diodes are: (1) Cost; the cost of a laser diode is roughly 100 times that of an IRED (e.g. $300 vs $3), and (2) the eye-safety hazard created by the laser-diode.

The operating characteristics of the Xciton XC-88FD infrared emitting diode are listed in Table 4.4. An outline drawing of the device is shown in Figure 4.4 along with its angular radiation characteristics. Other pertinent characteristics of the XC-88FD are given in Figure 4.5. One curve of some significance shown in Figure 4.5 is the power output degradation vs time. The lifetime of IRED s is truly impressive, and the slight degradation in output after extended periods of use can be compensated for by periodic calibrations.

The output power of the XC-88FD is subject to variation with changes in the ambient temperature. This variation of output with temperature could lead to unacceptable errors in the measurement of aerosol scattering coefficients. The temperature coefficient of the power output is given in Table 4.4. The radiant power output vs temperature of the device is graphed in Figure 4.6.

To prevent temperature changes from being a problem, the XC-88FD will be housed in a miniature oven as shown in Figure 4.7. The oven (Ovenaire Model TO-5L) operates from 28 VDC power and has its solid state proportional control circuitry self-contained within the housing. The oven to be purchased for the AVM will have a pre-selected operating temperature of 35 °C. If the ambient temperature exceeds 35 °C, the oven ceases to control the temperature. In the temperature range between -35 °C and +35 °C, the oven will control the temperature of the IRED source to within

Table 4.4. Operating Characteristics of the Xciton XC-88-F Series and XC-88-P Series of IR Emitting Diode.

Opto-Electrical Characteristics at 25°C Ambient.						
			XC-88-FA XC-88-PA	XC-88-FB XC-88-PB	XC-88-FC XC-88-PC	XC-88-FD XC-88-PD
Package Style			O K	O K	O K	O K
Total Radiant Output Power, P_o	Min	mW @ 100 mA	7.0	9.0	10.5	12.0
Table of Characteristics for XC-88-F and XC-88-P Series						
Temp Coef of P_o, 25°C		%/°C		−.53		
Forward Voltage	Typ	V @ 100 mA		1.60		
	Max	V @ 100 mA		1.90		
Temp Coef of Fwd Voltage		mV/°C		−1.8		
Dynamic Resistance	Typ	Ohms		1.2		
Angle between Half Power Intensity Points	F P	Typ Degrees		65° 15°		
Peak Wavelength		nm		880		
Line Halfwidth		nm		80		
Reverse Current Max. at 25°C		μA @ −3.0 Volts		10		
Response Time (10% to 90%)	Typ	Rise Fall	μs	1.5		
Absolute Maximum Rating at 25°C						
Average Power Dissipation		mW		170		
Derate Linearly from 25°C		mW/°C		−1.4		
Average Fwd Current		mA		100		
Reverse Voltage		V		3.0		
Operating, Storage, or Process Temp Range		°C		−65 +125		
Solder Temp. 5 Sec 1/16 Inch from Case		°C		260		
Peak Pulse Current 10μ sec, 100Hz		Amp		3.0		

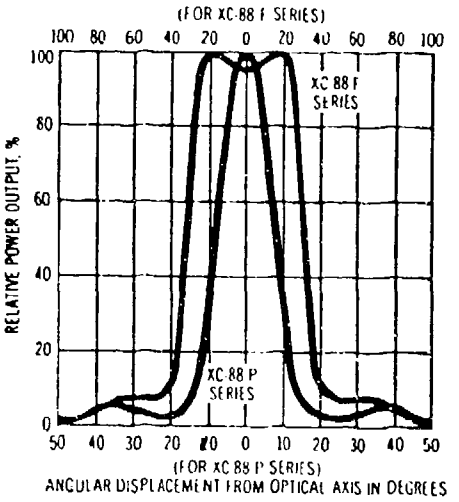

(a) Typical Radiation Pattern

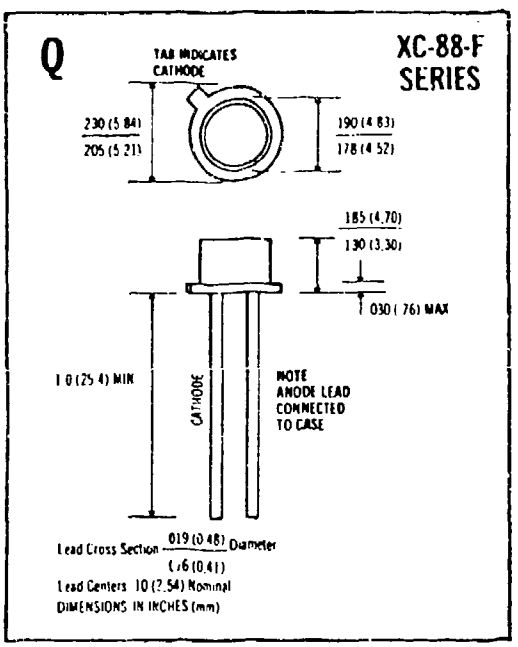

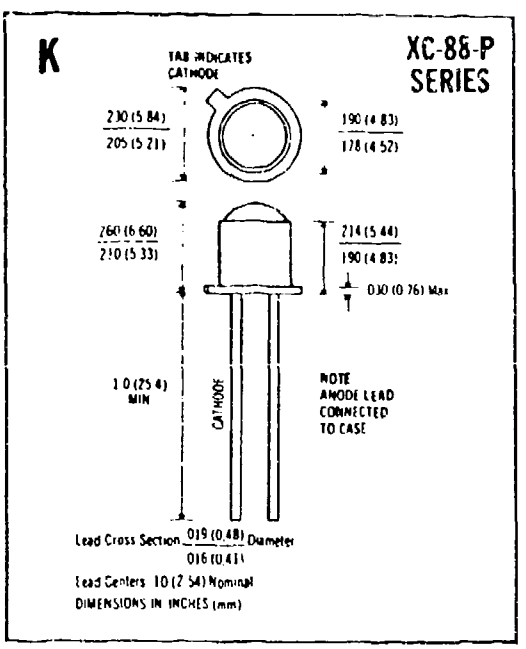

(b) Outline drawings of Package Styles Q & K

Figure 4.4. Radiation patterns and package styles of the Xciton XC-88-F Series and XC-88-P Series of IR Emitting Diodes.

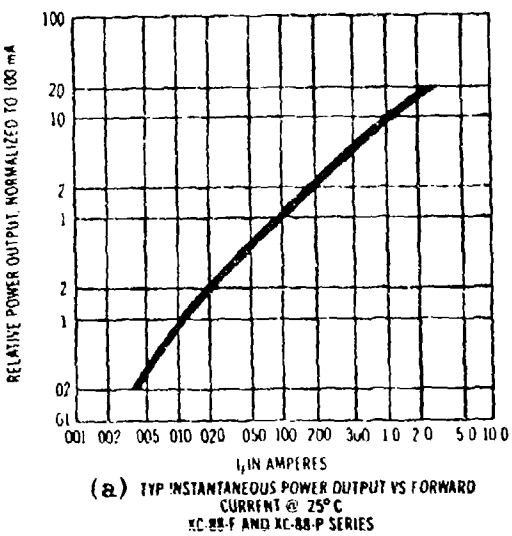

(a) TYP INSTANTANEOUS POWER OUTPUT VS FORWARD CURRENT @ 25°C
XC-88-F AND XC-88-P SERIES

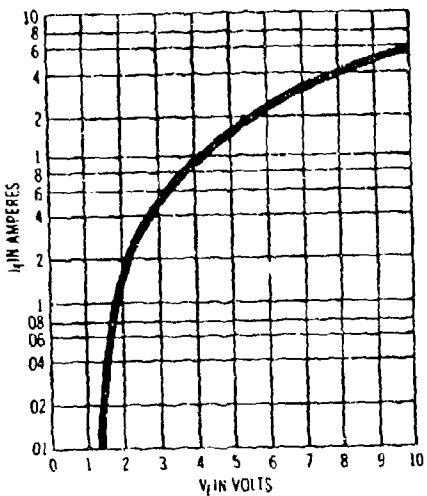

(b) TYP FORWARD VOLTAGE VS FORWARD CURRENT @ 25°C
XC-88-F AND XC-88-P SERIES

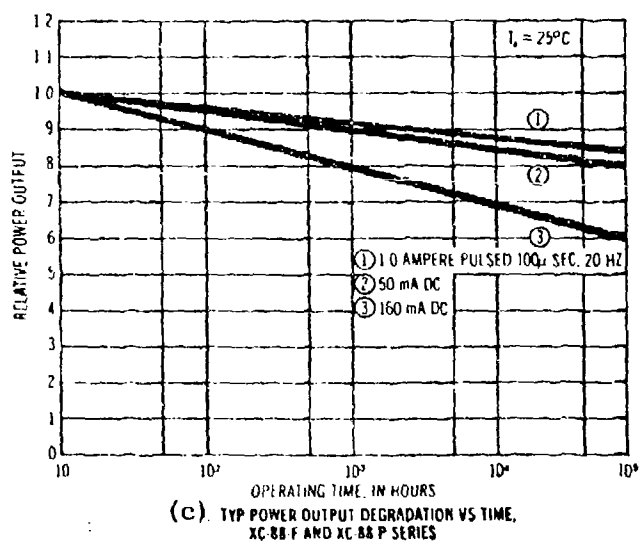

(c) TYP POWER OUTPUT DEGRADATION VS TIME,
XC-88-F AND XC-88-P SERIES

Figure 4.5. Operating characteristics of the Xciton XC-88-F Series and XC-88-P Series of IR Emitting Diodes.

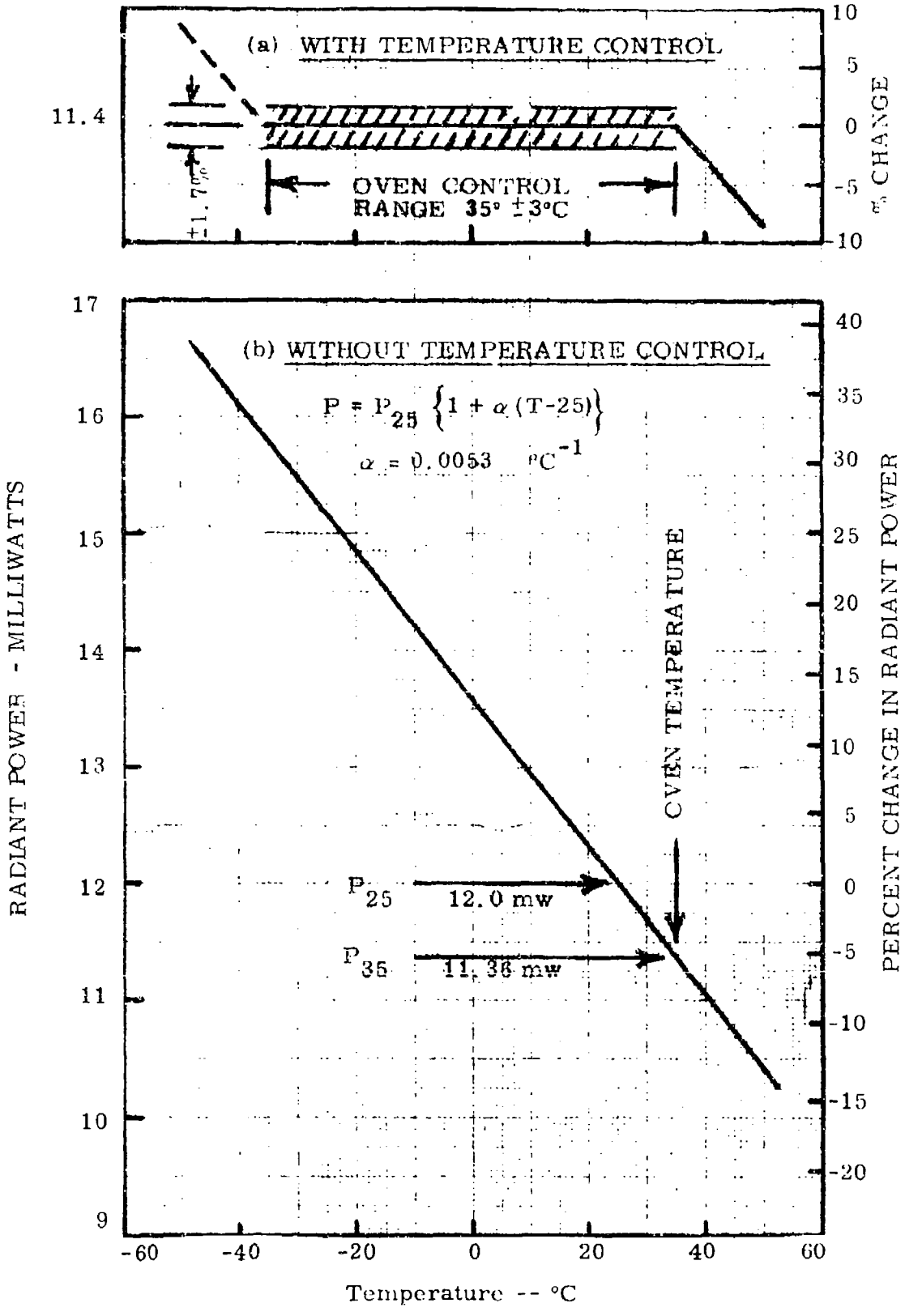

Figure 4.6. Radiant Power Output of Xciton LED Type XC-88-FD with and without Temperature Control.

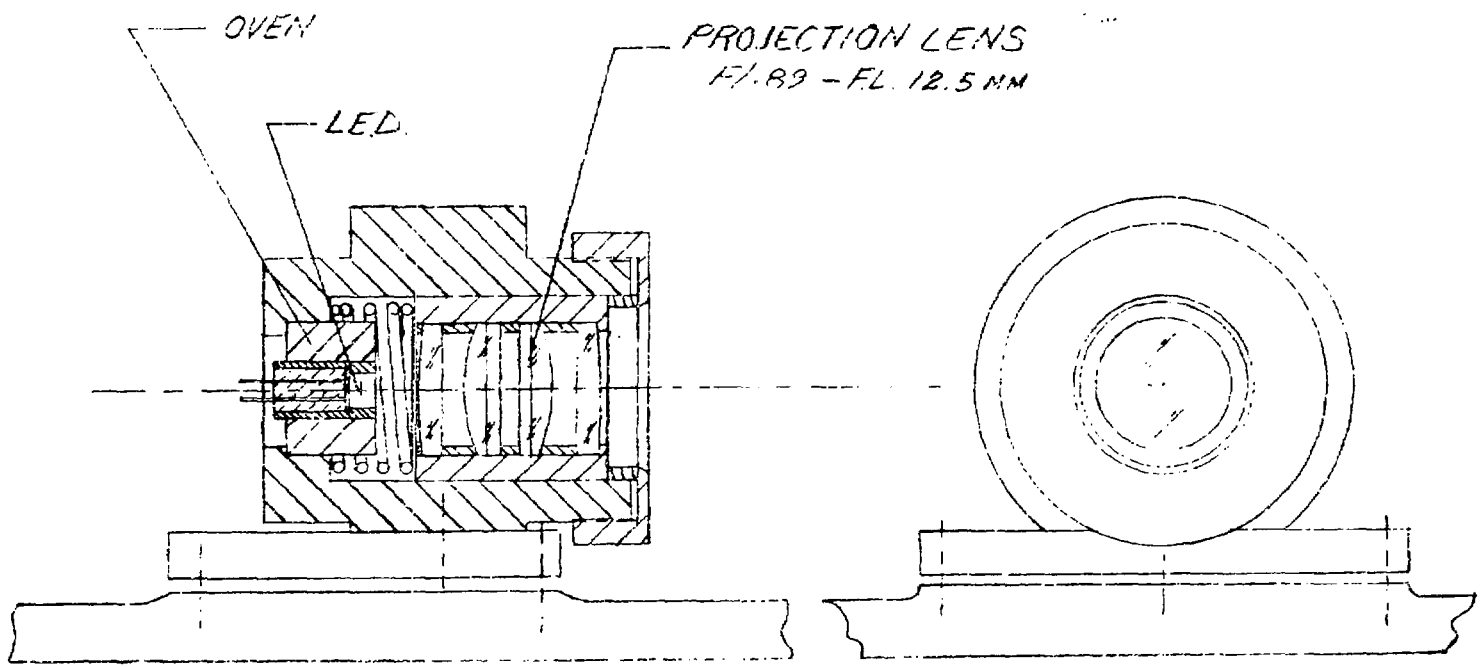

Figure 4.7. Layout drawing of the transmitter optical system and IRED source housed in a temperature regulating oven.

± 3 °C. For a temperature change of ± 3 °C, the corresponding change in radiant power output of the XC-88FD will be ± 1.7 per cent. The resulting behavior of the XC-88FD enclosed in the temperature regulated oven is shown in the upper portion of Figure 4.6.

4.5 Detector Characteristics

The detector chosen for use in the AVM is the EG&G Model HUV-1000B photovoltaic detector. This detector is a hybrid silicon-sensor/operational-amplifier combination which offers great stability, very low noise and linearity over a wide dynamic range.

The typical operating characteristics of the HUV-1000B detector may be found in Figure 4.8. The spectral response of the detector is shown in Figure 4.9. Note that the response at 0.88 microns is very near the maximum response.

The deviation of detector response with temperature is also shown in Figure 4.9. The temperature coefficient of responsivity is $\leq$ 0.05 percent at 0.90μ. The internal operating temperature range of the AVM is acknowledged to be -35 °C to 50 °C. Over this range, the deviation in responsivity is -3 percent to +1 percent from the responsivity at 25 °C. This responsivity change will induce corresponding changes, of like magnitude, in the scattering coefficient measurements. We considered these these potential errors to be readily acceptable and did not provide any temperature control of the detector.

If the wavelength of operation for the AVM had been chosen to be 9400 Å instead of 8800 Å, it is most likely that temperature control of the detector would have been required. Referring to Figure 4.9 (b) we see that above wavelengths of 9000 Å the variation of responsivity with temperature begins to change dramatically. The deviation at -35°C is not indicated in the figure so that it is not possible to determine the full range of deviations which would occur at an operating wavelength of 9400 Å.

OPERATIONAL AMPLIFIER/PHOTODIODE COMBINATIONS

CHARACTERISTIC	HAV-1000 MIN	HAV-1000 TYP	HAV-1000 MAX	HUV-1000B MIN	HUV-1000B TYP	HUV-1000B MAX	UNITS AND CONDITIONS
ACTIVE AREA		5.1			5.1		mm^2
SPECTRAL RANGE	350		1150	200		1150	nm
RESPONSIVITY AT 900 nm	9.0	9.4		11	12		10^7 volts/watt, R_f = 200 MΩ
RESPONSIVITY AT 230 nm	-	-	-	3.0	3.5	-	10^7 volts/watt; R_f = 200 MΩ
FREQUENCY RANGE	DC	-	1	DC	-	1	MHz, R_f = 10 kΩ
NOISE VOLTAGE AT 20 Hz	-	1	-	-	10	-	10^{-6} volts/$Hz^{\frac{1}{2}}$; R_f = 200 MΩ
NEP (900, 20, 1)	-	1.11	-	-	0.87	-	10^{-13} watts/$Hz^{\frac{1}{2}}$
NEP (230, 20, 1)	-	-	-	-	3.0	-	10^{-13} watts/$Hz^{\frac{1}{2}}$
OPEN LOOP GAIN	2×10^4	2×10^5		2×10^4	2×10^5		
BIAS CURRENT	-	3	50	-	3	50	pA (1),(2) at 25°C
OFFSET CURRENT	-	0.5	-	-	0.5	-	pA
OFFSET VOLTAGE (3)	-	10	20	-	10	20	mV
OFFSET VOLTAGE DRIFT	-	-	75	-	-	75	μV/°C
OUTPUT RESISTANCE	-	80	-	-	80	-	Ω
SLEW RATE	-	6	-	-	6	-	V/μ sec
SUPPLY VOLTAGE	±6	-	±18	±6	-	±18	volts
SUPPLY CURRENT	-	3.4	6.0	-	3.4	6.0	mA
POWER CONSUMPTION	-	102	180	-	102	180	mW
OPERATING TEMPERATURE	0	-	70	0	-	70	°C
STORAGE TEMPERATURE	-65	-	150	-65	-	150	°C

(1) Without external trim
(2) Doubles every +10°C
(3) Adjustable to 0 volts with external trim potentiometer.

MECHANICAL – HAV-1000 & HUV-1000B

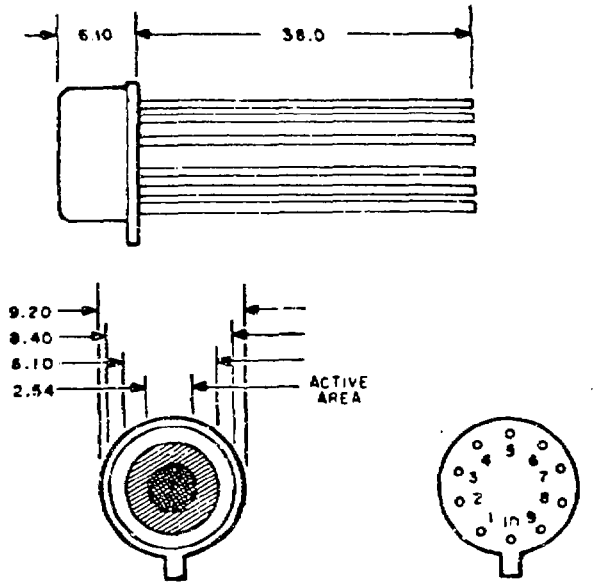

ALL DIMENSIONS IN MILLIMETERS

PACKAGE – TO-5-GOLD PLATED KOVAR LEADS, BASE, AND CAP
LEAD RADIUS – 2.54mm.
WINDOW – 6.15mm DIAMETER, 0.75mm THICK. DISTANCE OF OUTER WINDOW TO ACTIVE SURFACE IS 2.92mm NOMINAL.

CORNING 7052 GLASS FOR HAV-1000
QUARTZ FOR HUV-1000B

Figure 4.8. Operating Data and Specifications for EG&G Model HAV-1000 and HUV-1000B Photovoltaic Detectors.

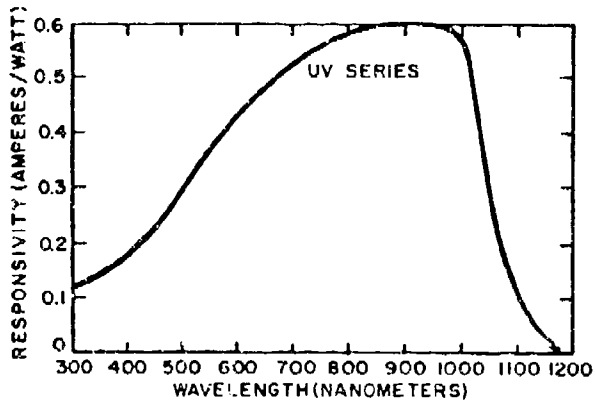

(a) Typical responsivity vs. wavelength

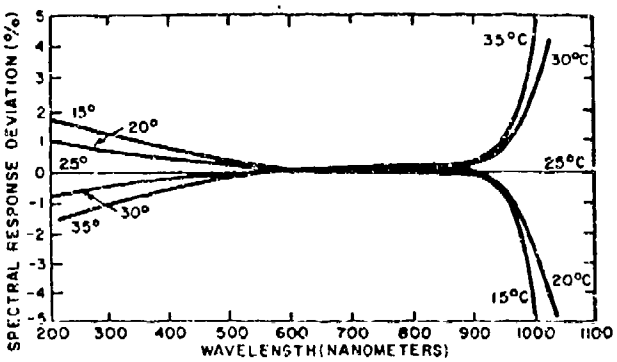

(b) Typical deviation of responsivity with temperature

Figure 4.9. Spectral response characteristics of EG&G silicon photovoltaic detector Model HUV-1000B.

The manufacturer's stated value for the noise equivalent power (NEP) of the HUV-1000B detector is, as taken from Figure 4.8,

$$\text{NEP}\ (0.9\mu,\ 20\ \text{Hz}, 1\ \text{Hz}) = 8.7 \times 10^{-14}\ \text{Watts}/\sqrt{\text{Hz}} \qquad (4.23)$$

where the 20 Hz refers to the chopping frequency and 1 Hz refers to the bandwidth of the measuring system. The AVM will operate at an effective chopping frequency of 3000 Hz with a frequency bandwidth of 10 Hz. The NEP shown in Table 4.1, which was used for the S/N calculations was derived from the manufacturer's rated value by multiplying by the square root of the 10 Hz bandwidth,

$$\text{NEP}\ (0.88,\ 3000,\ 10) = \text{NEP}\ (0.9,\ 20,\ 1)\sqrt{\Delta f = 10} \qquad (4.24)$$

4.6 Transmitter Electronic System

The transmitter electronics generates a 12 milliwatt square wave optical signal. The repetition frequency is 3 kHz with a 50 percent duty cycle. It also provides a synchronizing signal to the synchronous rectifier. The transmitter electronic system includes an oscillator, the source driver, the IRED, and a phase shifter. A block diagram of the transmitter system is shown in Figure 4.10. The oscillator is an astable multivibrator composed of a timer and associated circuitry. The frequency is determined by 2n RC-network. With the assigned component values, the circuit oscillates at 3 kHz providing a 50 percent duty cycle with a 15 volt peak square wave signal.

The IRED driver circuit provides a square wave voltage of constant amplitude to the IRED. It is composed of two circuits, an adjustable but stable pulse voltage generator, and a pulse amplifier. The pulse generator is driven by the oscillator. A potentiometer is adjusted to set the IRED power output level.

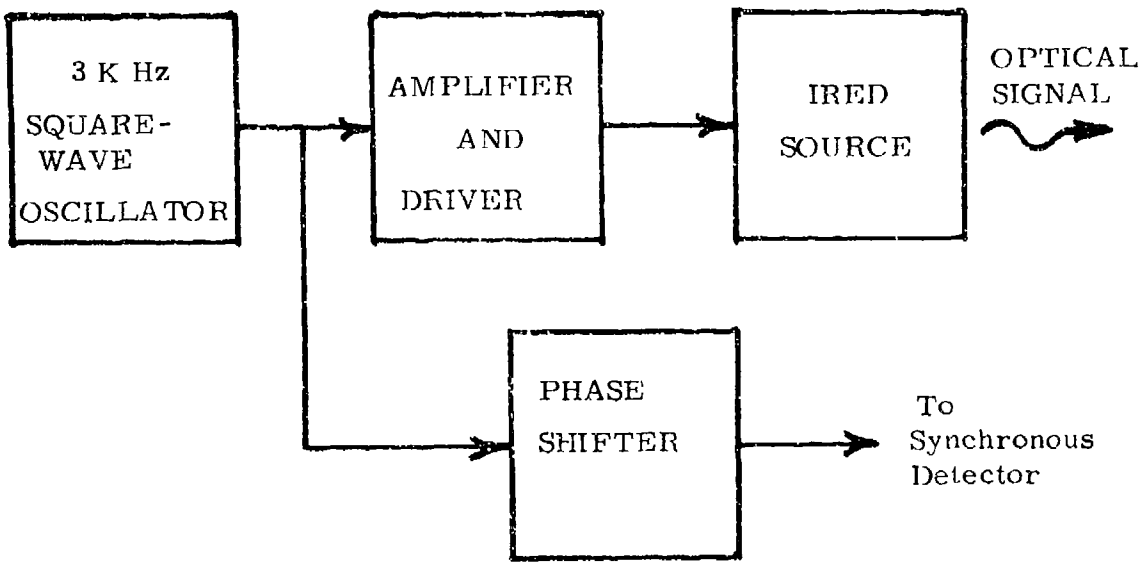

Figure 4.10. Transmitter Block Diagram.

The pulse amplifier of the driver circuit provides a voltage gain of two, can supply pulse currents up to 200 milliamperes, and has an output impedance of 2.5 ohms. This impedance provides temperature compensation for the IRED optical signal. The IRED output for a fixed drive current has a negative temperature coefficient. Since the LED junction voltage also has a negative temperature coefficient, the low driver output impedance provides increased current drive as temperature increases, providing a relatively stable optical output signal.

The phase shifter output signal is used to control the receiver synchronous rectifier. It generates a phase delayed signal synchronous with the IRED optical signal. The delay is adjusted to match the delay that occurs in the receiver filter and amplifiers. This delayed signal is

generated by using a second timer in a Schmitt Trigger configuration. Its input is the oscillator output signal delayed through an RC-filter network. A pot-adjust is required to provide the correct phase shift for the synchronous rectifier.

4.7 Receiver Electronics System

The receiver consists of the optical detector with integrated preamplifier, a 3 kHz center frequency bandpass filter, the synchronous rectifier including a phase splitter, and a low pass filter as shown in the block diagram (Figure 4.11). Each amplifier stage provides signal gain. The output voltage range is 0 to 10 volts DC for input-chopped optical signals of 0 to 6 nanowatts.

The detector-preamplifier is an EG&G HUV-1000B which uses a silicon photovoltaic diode. In its basic configuration, the overall responsivity of the detector circuit is 500,000 volts per watt. The load resistor is selected to provide the maximum output signal for the internal amplifier without saturation of the amplifier due to the optical background (up to 20 microwatts). Maximizing the output signal also maximizes the signal to noise for the detector.

The band pass filter is a four pole Butterworth design with 3 dB frequencies of 1.5 kHz and 6 kHz, geometrically centered at 3 kHz. Its low frequency attenuation is designed to severely attenuate variations in the background signal which otherwise could swamp out the desired signal in this high gain receiver. The filter's high frequency attenuation eliminates noise at odd harmonics of the synchronous rectifier. This filter provides a signal voltage gain of 100.

The phase separator consists of a non-inverting amplifier and an inverting amplifier driven from the same signal. Each

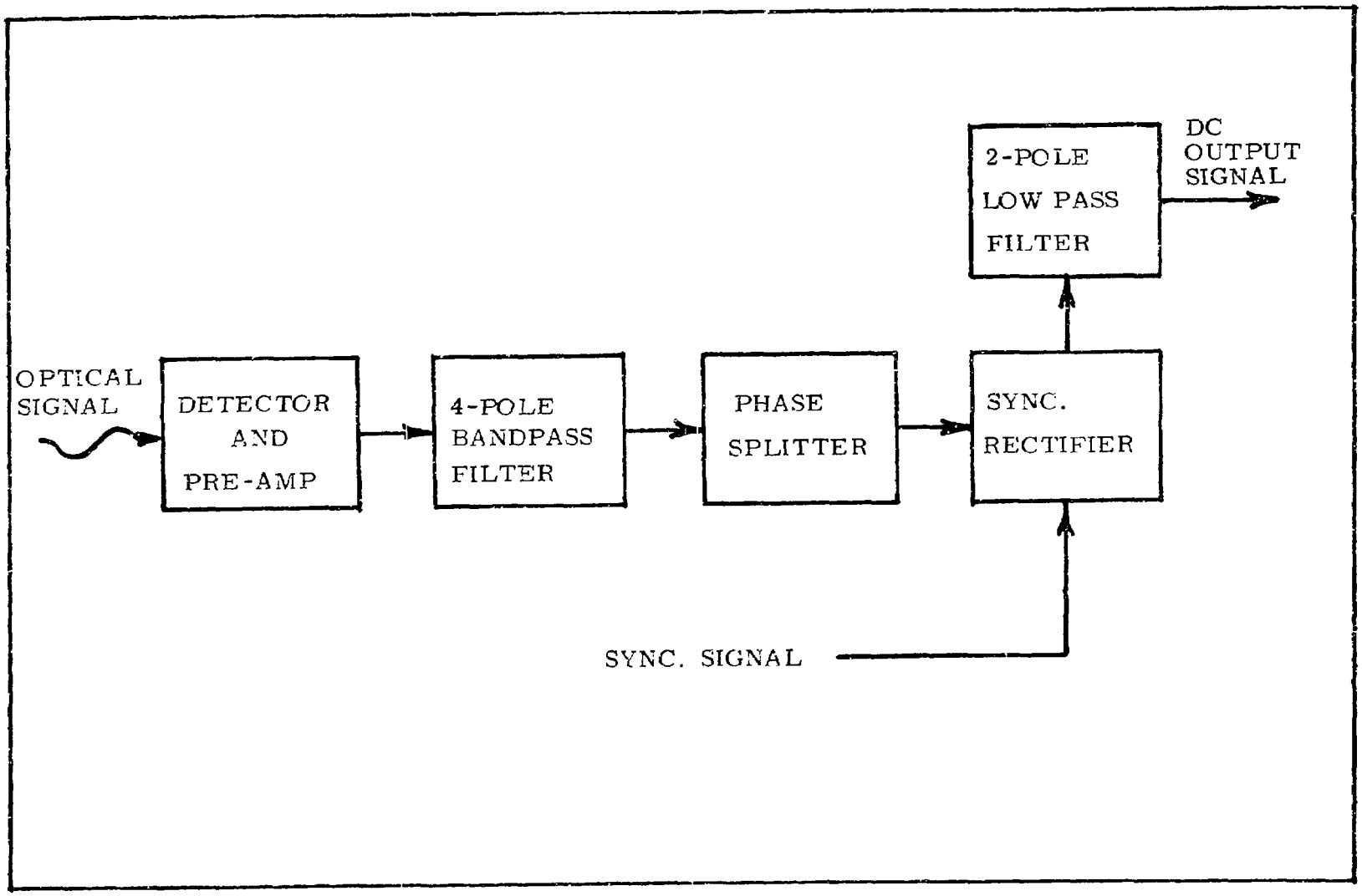

Figure 4.11. Receiver block diagram.

amplifier has a design voltage gain of 10. A potentiometer is used to adjust the gain of one amplifier to match that of the other amplifier.

The synchronous rectifier consists of an analog-switch, integrated circuit controlled by the delayed oscillator signal from the transmitter circuit. It alternately selects the outputs of the phase separator amplifiers for the input to the low pass filter. Since the two input signals are complementary, the net unidirectional (i.e. DC) signal at the synchronous rectifier output is due to the signal in phase with the switch control signal. This is the detected optical signal.

The low pass filter provides the "narrow band" filtering required by the receiver to increase the overall signal to noise to acceptable levels. This filter also provides the last stage of amplification of the signal with a low output impedance (less that one ohm). It consists of an op-amp and its associated components. It is a two pole Butterworth filter with a bandwidth of 6 Hz and has a voltage gain of 6.

4.8 Instrument Layout -- Laboratory Model

A layout of the Laboratory Model of the Airborne Visibility Meter is presented in Figure 4.12. The housing of the instrument serves also to provide the structural rigidity required to support all internal optical and electronic components and to preserve the alignment of the optical system. To minimize design and construction costs the Laboratory Model Instrument was fabricated from aluminum plate (typically 1/4" thick). One side of the housing was removable for ease in servicing of the instrument.

The transmitter optical unit is an integral assembly containing the transmitter lens, the IRED source and the oven which maintains the IRED at a constant temperature. The transmitter was fixed-mounted

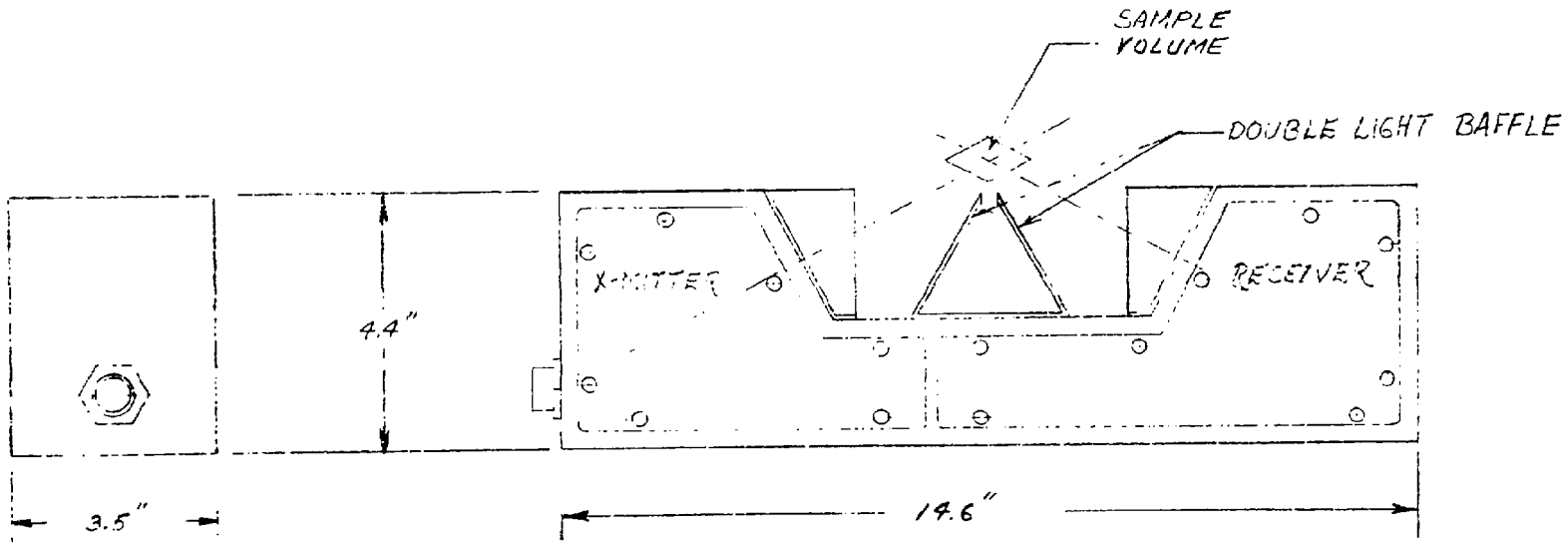

Figure 4.12. Layout drawing of the laboratory model Airborne Visibility Meter.

to the base of the instrument with no adjustments for steering of the light beam.

The instrument is divided into two compartments, one which houses the transmitter system, the other which houses the receiver system. This feature is intended to provide RFI shielding of the receiver electronics from external influences, and to prevent the 3 k Hz square-wave modulation of the IRED source from becoming a problem.

The receiver optical unit consists of the detector, receiver lens, and interference filter for restricting the radiation reaching the detector to an optical pas band equal to that of the IRED source. The receiver optical unit is provided with alignment and focus adjustments to center the image of the detector in the transmitted beam of radiation.

The Laboratory Model Instrument was intended only to prove that the instrument concept is a sound one and that the instrument can properly perform the scattering coefficient measurements specified under the performance requirements section of Table 2.1.

No dew-heaters were provided for each of the two windows of the Laboratory Model instrument to prevent condensation of moisture from occurring.

A photograph of the completed laboratory model instrument is shown in Figure 4.13. An On/Off switch and pilot light were provided for convenience. These devices are probably superfluous in an operational instrument.

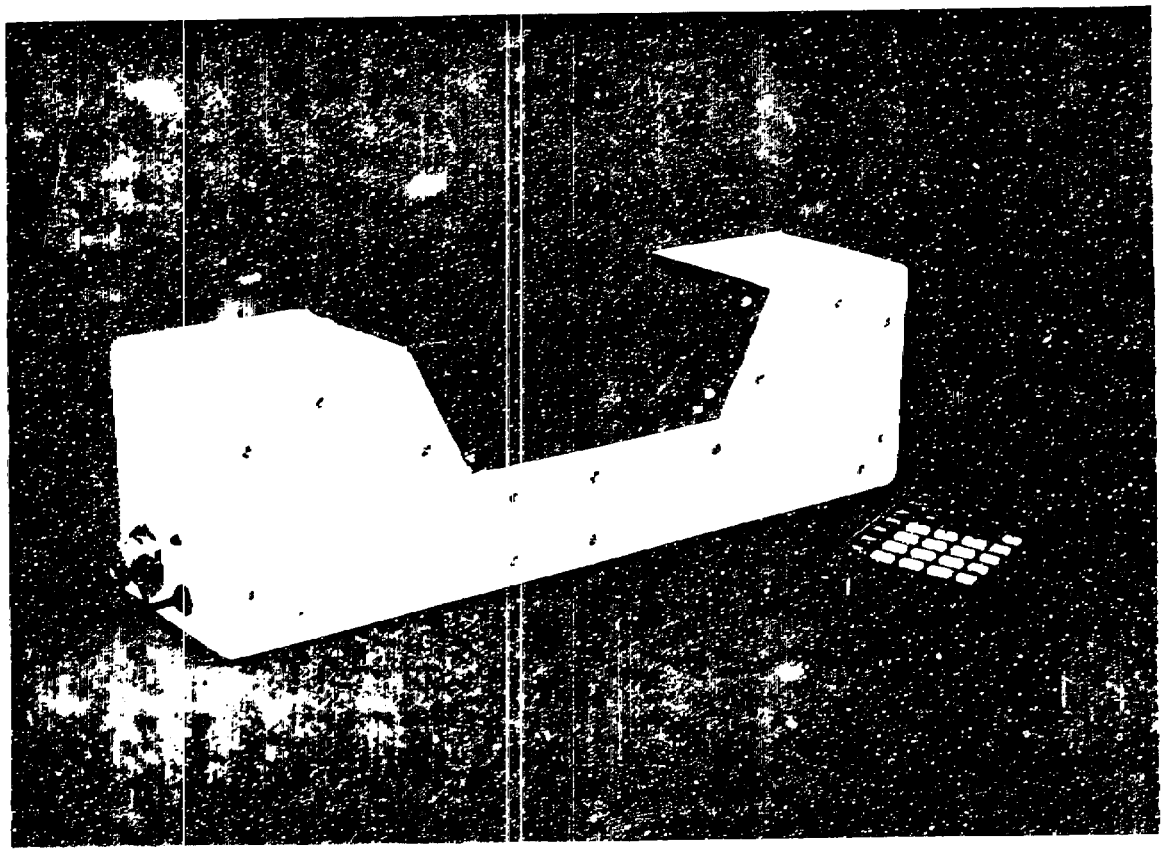

Figure 1-1. Photograph of the laboratory model AVM with a hand calculator shown for scale.

5. TEST AND ACCEPTANCE PLAN NO. 1

5.1 Test Location

An important step in the development of the airborne visibility meter under the contract terms was the testing of a laboratory model version of the instrument in an environmental test chamber where fog and haze situations of known optical attenuation characteristics could be generated. The following test plan is presented in the form originally submitted to AFGL.

The test program for the laboratory model instrument was scheduled for the four day period 14 to 18 September 1981 at the CALSPAN Environmental Test Chamber in Ashford, N.Y. The CALSPAN test chamber is a facility devoted to atmospheric simulation, air pollution, cloud physics, and aerosol research studies. The test chamber is 9 meters high and 9 meters in diameter making it one of the largest test chambers in the United States and valuable for minimizing wall effects and for closely simulating actual atmospheric conditions.

5.2 Test Objectives

The general objective of the test program to be conducted at the CALSPAN Environmental Test Facility is to evaluate the measurement performance of the laboratory model instrument over the entire range of operational environments it is required to perform measurements on.

The goal of the Air Force is to develop a small, lightweight nephelometer capable of performing measurements of the vertical profile of the atmospheric aerosol scattering coefficient for use in pre-strike surveillance missions. The instrument would also be used to determine percent cloud cover over a target area. When collecting cloud data, it would be deployed on an RPV (Remote Piloted Vehicle). When making aerosol measurements, it could be deployed either as an airborne package on an RPV or as part of an expendable drop-sonde package. In either method of deployment, there

are two specific performance requirements the instrument must meet; these are:

(1) Cloud Presence: At any instant of time, the instrument must signify whether it is in or out of clouds at altitudes ranging from sea level to 20,000 feet. It is not required that the instrument measure the scattering coefficient of clouds, only that it is in or out of a cloud. A typical visible-light scattering coefficient for moderately dense clouds is 20 km^{-1}; for heavy clouds it may range from 40 km^{-1} to a maximum of 100 km^{-1}.

One option in the design of the instrument was to let the receiver-amplifier saturate whenever the instrument entered a cloud, since a measurement is not required and saturation of the amplifier would readily indicate the presence of a cloud. This approach would simplify the electronics somewhat since it would require considerably less linear dynamic range. However, when operating in this manner the recovery time of the amplifier would inhibit the ability to discriminate the time of exiting from a cloud. It was felt, therefore, that the instrument should have linear response for all but the heaviest of clouds or fogs.

For compatability with most signal processing and telemetry systems with which it must interface, the range of signal output (analog) of the instrument is required to be 0 to 5 volts. The instrument actually has an output range of 0 to 13 volts with the first 10 volts believed to be linear to within 0.1 per cent. Electronic gains in the receiver have been adjusted, by

a design analysis, such that in the presence of a cloud with a scattering coefficient of 20 km^{-1} the output signal voltage should be approximately 5 volts. The exact correspondence will, of course, be established by the test program in the environmental chamber.

(2) Visual Range. It is required that the instrument be capable of performing measurements of the atmospheric aerosol scattering coefficient over a range of values which will permit the determination of slant visual ranges up to 10 kilometers with an accuracy of 20 percent. For slant ranges greater than 10 kilometers, the instrument measurements need only indicate whether the slant visual range is greater or less than 10 kilometers.

Slant visual range determinations are to be made from vertical profile measurements of the atmospheric scattering coefficient for all altitudes up to 10,000 feet. It was established in the design evaluation report for the instrument that the instrument must, therefore, be capable of measuring aerosol scattering coefficients as small as 0.1 km^{-1} in order to satisfy this requirement.

Having stated the general performance objectives of the instrument, we may now proceed to discuss the more subtle aspects of these same requirements.

The indication of entering or exiting a cloud is greatly influenced by the time-constant of the receiver. The design evaluation established that a desirable time-constant for the instrument would be .025 seconds if it were on an RPV traveling at a maximum speed of 300 mph (134 m/sec). The time-constant of the receiver in the laboratory model instrument, however, has been set at 0.5 seconds for purposes of static testing in the environmental test chamber and possible outdoors tests at the AFGL

Weather Test Facility at Otis AFB.

It is important that the instrument "observe" a representative sample of the atmospheric aerosol size distribution within the time-constant of the receiver. At that time, we were uncertain whether a representative sample volume of air was 1 liter or 0.1 liter for visible or near visible optical radiations in typical environments. (Calculations to be performed by AFGL established this value as $\sim$ 100 cm^3.

Since the instantaneous sample volume of the instrument is small (of the order of 1 to 2 cm^3), it is essential in static measurement situations that the time-constant of the receiver be long so air motion will allow a measurement to be performed on a representative sample of the aerosol size distribution. If one assumes the worst case; i.e. a 1 liter volume must be sampled, then a time constant of 15 seconds is highly desirable for static situations (See Figure 4.1). If the instrument were flown on an RPV, or installed in a drop-sonde package, the rapid motion of air through the sample volume will permit a short time constant to be used in the receiver.

It was not possible to install the necessary components within the housing of the instrument which would increase the time constant from 0.025 to 15 seconds. The increase in time constant was achieved by a two-step process. Internal to the instrument, the time constant was increased to 0.5 seconds and external to the instrument, an auxiliary "signal conditioner" package was added. The signal from the instrument can be fed to the signal conditioner where it is passed through an active filter having a time constant of 15 seconds. The output of the filter is then further processed so that there are two signal outputs from the signal conditioner, one with a X 1 gain and the other with a X 25 gain with respect to the input signal.

One result of the increase in receiver time constant is a bonus increase in signal-to-noise ratio (the increase is equal to the square root

of the ratio of time constants). The X25 Gain output signal from the signal conditioner was added to take advantage of the improved signal to noise ratio created by the signal conditioner.

For many reasons the light source in the Airborne Visibility Meter (AVM) is an electronically modulated IRED whose radiant power output is contained in an 800 Å bandwidth centered at 8900 Å. The silicon photovoltaic detector in the receiver has a bandwidth limiting optical filter tailored to the spectral characteristics of the source. This filter greatly limits the amount of background radiation incident on the detector.

The AVM, like all visibility meters, is intended to measure daylight visual range. Quite properly, therefore, an ideal light source would have daylight spectral characteristics and the ideal detector for such instruments would have the spectral response of the standard (CIE) photopic eye. In essentially all cases, practical reasons dictate otherwise.

When scattering coefficient measurements are not made using the spectral characteristics of sunlight and the photopic eye, errors can be introduced into visual range determinations if the scattering coefficients happen to be wavelength dependent.

Figure 3.2 illustrates the wavelength dependence of several environments. Fogs (and clouds) have essentially no wavelength dependence throughout the visible and near-visible spectral regions. Rural aerosols have a small wavelength dependence and as visibility approaches the Rayleigh limit (i.e. scattering by air molecules alone), there is a strong wavelength dependence.

Visual ranges are quoted as if the measuring wavelength were 0.55 μm. The AVM measures at a wavelength centered at 0.89μm. There will be no error in fog or cloud scattering coefficient measurements introduced by this wavelength difference. There will be a small error introduced for haze measurements. The CALSPAN tests may indicate that this error can be calibrated out if it is a constant (or nearly a constant) over the slant visual ranges of interest to the Air Force (i.e. VR $\lesssim$ 10 km).

A slight problem may arise with the CALSPAN calibrations because of the instrumentation and techniques used by CALSPAN to determine the visual range in the test chamber. Visual range in simulated clouds or fogs is monitored by transmissometers for the visual range from 30 meters to 4000 meters (i.e. $\beta = 130\ km^{-1}$ to $\beta = 1.0\ km^{-1}$, where β is the extinction coefficient). The transmissometers utilize tungsten lamps and blue-sensitive photomultiplier tubes. Clouds and fogs show little wavelength dependence when the extinction coefficient is large. When the extinction coefficients are low $\beta \sim 1\ km^{-1}$, there may be some spectral dependence in which case the CALSPAN calibration itself will introduce a small error.

Visual ranges in haze conditions are monitored by an MRI integrating nephelometer which can cover the visual range from 3 to 80 kilometers ($\beta = 1.3\ km^{-1}$ to $\beta = .05\ km^{-1}$). At this time, there is no information available to us on this instrument. Whether it has wavelength dependencies which might introduce errors will be a subject of discussion at CALSPAN.

The AVM is a fixed angle nephelometer (i.e. it measures scattering coefficients in a small range of scattering angles centered on 55°. This angle was dictated by size constraints imposed on the instrument by the RPV capabilities. The rationale for selecting the fixed-angle nephelometer configuration for the AVM centers around considerations of sensitivity, size, weight and ease of adaption of this configuration to airborne packages.

The angular scattering coefficients of clouds and fogs differ from those of hazes because of the differences in particle size distributions. Also, the angular scattering coefficients of advection fogs differ from those of radiation fogs, the latter class of fogs having smaller size particles than the former.

Typical droplets of advection fogs range from 7 to 12 μm in radius making them similar to some stratus clouds. Radiation fogs have particles ranging from 3 to 8 μm in radius and in that respect are much like cumulus clouds.

Because clouds and fogs are composed of droplets much larger in size than the aerosols which make up hazes, the angular scattering coefficient for clouds and fogs differs from that of hazes. The angular scattering coefficient $\beta(\theta)$ can be considered as having two components, a phase function $\Phi(\theta)$ and the total scattering coefficient, σ; that is,

$$\beta(\theta) = \Phi(\theta) \times \sigma \qquad (1)$$

where θ is the angle of scatter of the radiation incident on a sample volume.

Light scattered from cloud and fog particles tends to be scattered into smaller forward angles than light scattered from haze particles. At an angle of $\theta = 55°$ the phase function for clouds and fogs is smaller than that of hazes by more than a factor of two. At angles much smaller than 55° the situation would be reversed; that is, the phase function for clouds and fogs is greater than for hazes.

The ideal nephelometer response is given by the relation,

$$V = K\sigma \qquad (2)$$

where V is the output (signal) voltage of the instrument, σ is the scattering coefficient of the ambient aerosols, and K (the calibration constant) is a true constant over the full range of σ that is of interest. We indicated earlier that the scattering coefficients of hazes are slightly wavelength dependent and that the phase function of hazes differs from that of clouds and fogs. For these two reasons, we cannot expect that K will be a singular constant over the full response of the AVM.

The predicted response of the AVM is shown in Figure 5.1. The predicted response function is discontinuous in the region from $\sigma = 1\ km^{-1}$ to $\sigma = 3\ km^{-1}$ because of the difference in phase functions between hazes and fogs both of which can exhibit scattering coefficients of these magnitudes

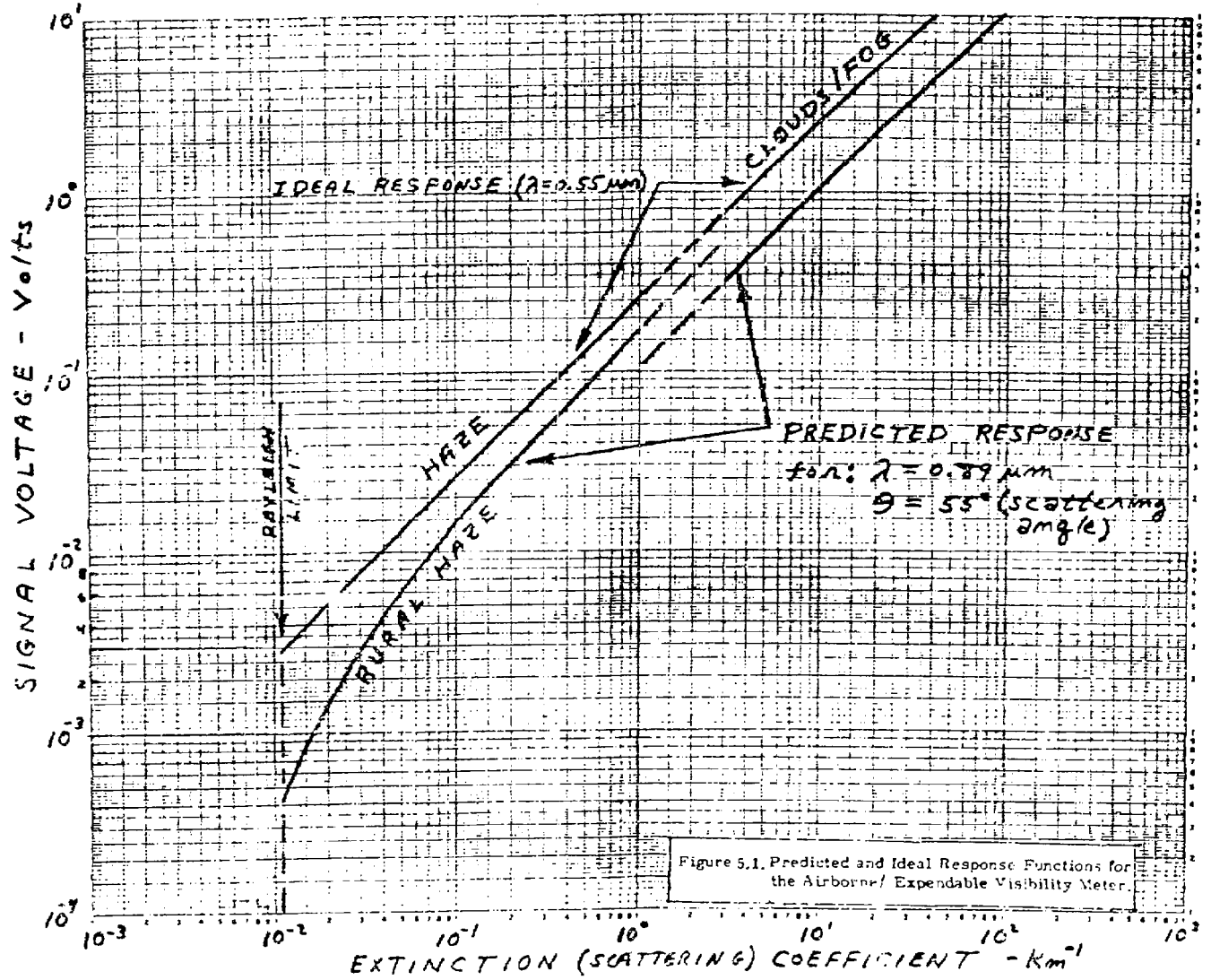

Figure 5.1. Predicted and Ideal Response Functions for the Airborne/Expendable Visibility Meter.

Figure 5.1. Predicted and Ideal Response Functions for the Airborne/Expendable Visibility Meter.

(the maximum values of σ for hazes and the minimum values of σ for clouds and fogs overlap in the region between σ = 1 km^{-1} to 3 km^{-1}).

Scattering coefficients of hazes and fogs are, essentially, equal to their extinction coefficients in the visible and near visible spectral regions, there being little or no absorption by the aerosols. There is, however, a wavelength dependence to the scattering coefficient which differs from one class of haze aerosols to another (e.g. maritime, rural, urban, etc). The predicted response of the AVM for only the case of rural aerosol hazes is shown in Figure 5.1.

For scattering angles between 30° and 60°, the phase function does not vary significantly from one haze class to another. Nor does it vary significantly within a given haze class when the scattering coefficient varys between strong and weak values. In the predicted response to rural haze shown in Figure 5.1, we have assumed that the phase function is a constant.

The ideal response of the AVM nephelometer is also shown in Figure 5.1. This response behavior assumes that the instrument measures the total (i.e. integrated over angles) scattering coefficient and, thus, is not subject to any variations in phase function of the scattering medium. The ideal response is also measured at the wavelength of maximum response of the eye (0.55 μm). Thus ideal response values of the scattering coefficient can be immediately converted into horizontal visual range VR using Koschmieder's relation

$$VR = \frac{3.912}{\sigma\ (0.55\mu)}$$

AVM applications of most interest to the Air Force will result in measurements of haze scattering coefficients ranging between σ = 0.1 km^{-1} and σ = 2 km^{-1}. Over that range of σ values, there is only a slight variation in the wavelength dependence. In Table 3.2 we show that the ratio $\sigma\ (0.55\mu)/\ \sigma\ (0.88\mu)$ varies from 1.78 in the case of rural aerosols with 0 per cent relative humidity to 1.53 at 99 per cent relative humidity, with a mean value of 1.66.

If CALSPAN is able to provide us with σ (0.55μ) values for each test run, then in all likelihood we should find that the response function for hazes is linear over the range of σ-values of interest to the Air Force. Also we should find that the response function for clouds and fogs is linear but that the constant of proportionality is different for the hazes and fogs.

5.3 Test Procedures and Equipment

The following brief description of the procedures followed in the production of laboratory fogs and hazes was extracted from a recent CALSPAN Report (Reference 13).

> The first step in preparing the chamber for fog formation is the establishment of near saturated conditions within the chamber. This is accomplished by wetting the entire inner surface of the chamber with distilled water from any of several remotely-controlled spray-nozzle systems. With the relative humidity in the chamber typically in excess of 95 % following the washdown, specific nuclei can be added to the chamber to serve as condensation sites for fog formation. These nuclei can be added by a number of methods: e.g., pyrotechnically, by dissemination of dry powders or by the nebulization of an aqueous solution of which the solute is the desired parent material of the nuclei. The number of nuclei in the chamber (and, hence, the number concentration of resultant fog droplets) may be controlled simply by filtering down to the desired number.
>
> Subsequently, the chamber is pressurized to about 30 mb above ambient atmospheric pressure.

During this statue of pressurization, usually maintained for about 10 minutes, a mixing fan within the chamber aids in restoring equilibrium and in increasing the RH of air within the chamber. Following this period to equilibrate, pressure is rapidly decreased within the chamber by withdrawing air at a metered rate of 3-5 mb min^{-1}. Initially, the pressure is dropped abruptly, producing a state of supersaturation within the chamber. This initial supersaturation activates fog nuclei and secures the desired growth of fog droplets. Later, a continuous pressure reduction of $\sim$ 1 mb min^{-1} is required to maintain the fog by negating the effects of heating from warmer chamber walls. While fogs have been sustained for periods longer than one hour in the chamber, their microphysical characteristics (i.e., LWC, drop sizes, and visibility) change appreciably over such long intervals; hence, fog tests are usually terminated after $\sim$ 30 minutes.

Visibility measurements in the chamber fogs are obtained at two heights (1.2 and 4.5m) above the floor with two in-house built transmissometers. Visibility (V) determinations are obtained from measurements of the extinction (β) of a once-folded, collimated beam of white light, having a path length (X) of $\sim$ 18m.

In this manner, visibility is monitored continuously throughout an experiment in a useful visibility range of from 30 to 4000m. Visibility in haze conditions (i.e., 3-80 km) is monitored with an MRI Nephelometer.

The CALSPAN Droplet Sampler is used to obtain measurements of fog droplet size spectra. In operation, foggy air is drawn through a sampling tube by a high capacity blower,

and droplets are collected by impaction on gelatin-coated slides. The sampling airspeed is measured by a pitot tube and static source mounted in the unit, and a standard aircraft air-speed indicator is used to read the airspeed through the sampler. Airspeed is adjustable from 20 to 80 m sec^{-1}, but typically an impaction velocity of $\sim$ 50 m sec^{-1} is used.

Droplet samples are taken by injecting a narrow, gelatin-coated, glass slide into the high speed flow through an opening in the sampling tube. Slide injection is accomplished through the use of a modified 35 mm photographic slide changer. When the coated slide is exposed to the air flow in the tube, droplets in the air volume swept out by the 4 mm wide glass slide impinge on the gelatin coating and form crater-like depressions. Development work on this technique (Jiusto, 1965 and Mack, 1966) has shown that there is approximately a 2:1 ratio between the crater diameter and the diameter of the impinging droplet. Exposure times are typically approximately 0.2 sec, but can be extended to minutes as might be required for light hazes.

For 4 mm wide slides and the sampling velocities of 40-60 m/sec typically employed in the drop sampler, it is seen that collection efficiencies are better than 70 % for droplets larger than 3 μm radius and $>$ 90% for droplets larger than 5 μm radius. It should also be noted that collection falls off rapidly for droplets below 2 microns radius. This feature places a lower limit on the drop sizes that can be sampled with any degree of confidence. The limit is about 2 μm radius but is of little consequence since fog droplets are typically larger than 2 μm radius.

Reduction of the droplet data is performed manually from photomicrographs (of the sample slides) obtained with a

phase contrast microscope. Where possible, a minimum of 200 droplets is measured, with an accuracy of $\pm$ 10 % of drop radius, for each drop size distribution.

HSS Inc installed the AVM nephelometer in the chamber such that the mple volume will be located approximately 42 inches above the chamber floor, roughly at the same height as the lower CALSPAN transmissometer. Two large light traps were also installed in the vicinity of the AVM, one to intercept the IRED radiation from the transmitter section of the AVM, the other will act as the background for the receiver optics of the AVM. Each light trap was located several feet away from the AVM along the optical axes of the transmitter and the receiver.

The output voltage of the AVM was monitored in a laboratory room adjacent to the test chamber. Chart recorders and digital volt meters were used to monitor the output of the AVM directly or via the signal conditioner. Power to the AVM were supplied from a 28 VDC power supply also located external to the test chamber.

Prior to the start of each test run, a standard scatter plate (hereafter referred to as the reference standard) were inserted into the sample volume and output voltage readings were recorded. These readings served to establish reference points in the calibration.

5.4 Test Responsibilities.

CALSPAN Responsibilities: HSS Inc/AFGL contracted with CALSPAN to provide at least 10 chamber tests of approximately 30 minutes duration during the course of the four day test program. The breakdown of these ten tests into fogs or hazes, and the range of σ-values to be covered were left to on-site discussions between representatives of CALSPAN, HSS Inc, and AFGL.

CALSPAN provided transmissometer and/or MRI nephelometer measurements of extinction coefficients and visual range at frequent intervals during the course of each test run. CALSPAN also provided droplet size spectra from five slides exposed during fog tests; HSS Inc/AFGL decided which slides were to be evaluated.

HSS Inc/AFGL Responsibilities: HSS Inc personnel installed and operated the AVM, the light traps and all associated measuring equipment. HSS Inc and the AFGL Representative collaborated on all decisions affecting the test plan and test schedule so that a maximum amount of data could be collected in the time available.

5.5 Test Schedule

The AVM test program was scheduled for the four day period 15-18 September. Set-up and check out of equipment took approximately one-half days as did roll-up upon completion of the tests. Approximately three days were devoted to the actual test program.

CALSPAN personnel recommended a sequence of fog/haze simulations that made for optimum utilization of the test chamber and the time available for tests. That sequence is as follows: The first simulations of each day should start with large droplet fogs (advection fog or stratus cloud simulations). Those tests should then be followed by simulations of small droplet fogs (radiation fog or cumulus clouds). The final test runs of any given day should be devoted to simulation of hazes (beginning with high population density hazes).

CALSPAN personnel also recommended that the test program should commence with a "shot gun" series of approximately four simulation tests which will range from heavy fog to light haze. Based on the results from this quick-look survey we (CALSPAN, HSS Inc and the AFGL Representative) formulated the details of the full test program.

Specific objectives of the full test program are outlined below:

Fog and Cloud Simulations

(1) Saturation Value of σ, Advection Fog

(2) Saturation Value of σ, Radiation Fog

(3) Response Function, $1\ km^{-1} \leq \sigma \leq 100\ km^{-1}$, for Advection Fog and Radiation Fog.

(4) Saturation Values and Response Functions for basic instrument plus signal conditioner (both channels), Advection Fog and Radiation Fog.

Haze Simulations

(1) Response Function, $0.05 \leq \sigma \leq 2\ km^{-1}$, for high aerosol population density haze.

(2) Response Function, $0.05 \leq \sigma \leq 2\ km^{-1}$ for low aerosol population density haze.

(3) Nighttime Noise Limit of the AVM Measurements.

(4) Daytime Noise limit of the AVM Measurements (This test may not be possible within the confines of the test chamber.

6. CALIBRATION AND TEST--EXPERIMENTAL MODEL AVM

6.1 Calibration Curve

A total of fourteen fog and haze tests were conducted with the AVM in the CALSPAN Environmental Test Chamber. A brief summary of the test environments is given in Table 6.1. Data from nine of the fourteen tests were used to derive the calibration curve for the laboratory model instrument. The nine data sets used in the derivation of the curve are listed in Table 6.2. Also given in that table are the reasons why the five remaining data sets were not included.

The calibration curve for the laboratory model instrument is shown in Figure 6.1. An accompanying set of notes (see Table 6.3) provides pertinent details about the test procedures at CALSPAN. A preliminary analytic expression has been derived for the best fit curve to the test data. This analytic expression is valid for values of atmospheric attenuation coefficient $\beta \geq 0.1\ \text{km}^{-1}$. For atmospheric attenuation coefficients less than $0.1\ \text{km}^{-1}$ the analytic expression departs from the test data.

The best fit to the test data is a straight line on a log-log plot for $\beta \geq 0.1\ \text{km}^{-1}$, indicating a gentle power-law behavior. The curvature on a log-log plot for $\beta < 0.1\ \text{km}^{-1}$ is believed due to a wavelength effect. CALSPAN measurements of the atmospheric attenuation coefficient in hazes were made with an MRI Integrating Nephelometer. This nephelometer performed its measurements with blue-white light from a Xenon flash tube and a blue-sensitive photomultiplier tube. The laboratory model AVM utilizes near-infrared radiation (an 800 Å band centered at 8900 Å). For attenuation coefficients $\beta \geq 0.1\ \text{km}^{-1}$ the scattering coefficient for blue light and near-infrared radiation are essentially equal. For values of $\beta < 0.1\ \text{km}^{-1}$ a wavelength variation of β appears to set in, being greater for blue light than for the near-infrared. This curvature could also be explained by a zero offset in the MRI integrating nephelometer.

Table 8.1. Summary of Fog and Haze Tests Conducted at the CALSPAN Environmental Test Facility

Test Run	Date	Objective	Aerosol/Nuclei
1	15 Sept	Large Droplet Fog	Ambient Nuclei
2	15 Sept	Small Droplet Fog	Cigar Smoke
3	15 Sept	High Humidity Haze	Salty Dog (1 gm)
4	16 Sept	Large Droplet Fog	Ambient Nuclei
5	16 Sept	High Humidity Haze	Salty Dog (.1 gm)
6	16 Sept	Low Humidity Haze	Salty Dog (1 gm)
7	16 Sept	Low Humidity Haze	Cigar Smoke (White Owls)
8	17 Sept	Large Droplet Fog	Ambient Nuclei
9	17 Sept	Large Droplet Fog	Ambient Nuclei
10	17 Sept	Small Droplet Fog	Cigar Smoke
11	17 Sept	High Humidity Haze	Cigar Smoke
12	18 Sept	Low Humidity Haze	Salty Dog (6 gm)
13	18 Sept	Low Humidity Haze	Cigar Smoke (White Owls)
14	18 Sept	Low Humidity Haze	Burning Diesel Oil

Table 6.2. Test Data Employed in

Calibration Curve for the Model VR101 Visibility Meter

Fourteen Test Runs were made in the CALSPAN Environmental Test Chamber. This note lists the nine runs which were included in the compilation of a calibration curve for the instrument and provides an explanation for the exclusion of the test data from five of the runs.

Test Runs Included

Tests: 1, 3, 5, 6, 10, 11, 12, 13, 14

Test Runs Not Included

Test Data Set	Reason Not Included
2	Points Overlap Data Set from Run 10.
4	This Data set (on large droplet fogs) has initial agreement with other data sets then begins to drift as if the transmissometer zero were drifting.
7	This data (taken in a cigar smoke haze) behaves as if there were an offset in the integrating nephelometer measurements. Test 13 was conducted to check this hypothesis. Data from Test 13 fell on the calibration curve.
8	CALSPAN Transmissometer Failure; No Extinction Data.
9	Behavior similar to Test Run 4 but drift is in opposite direction.

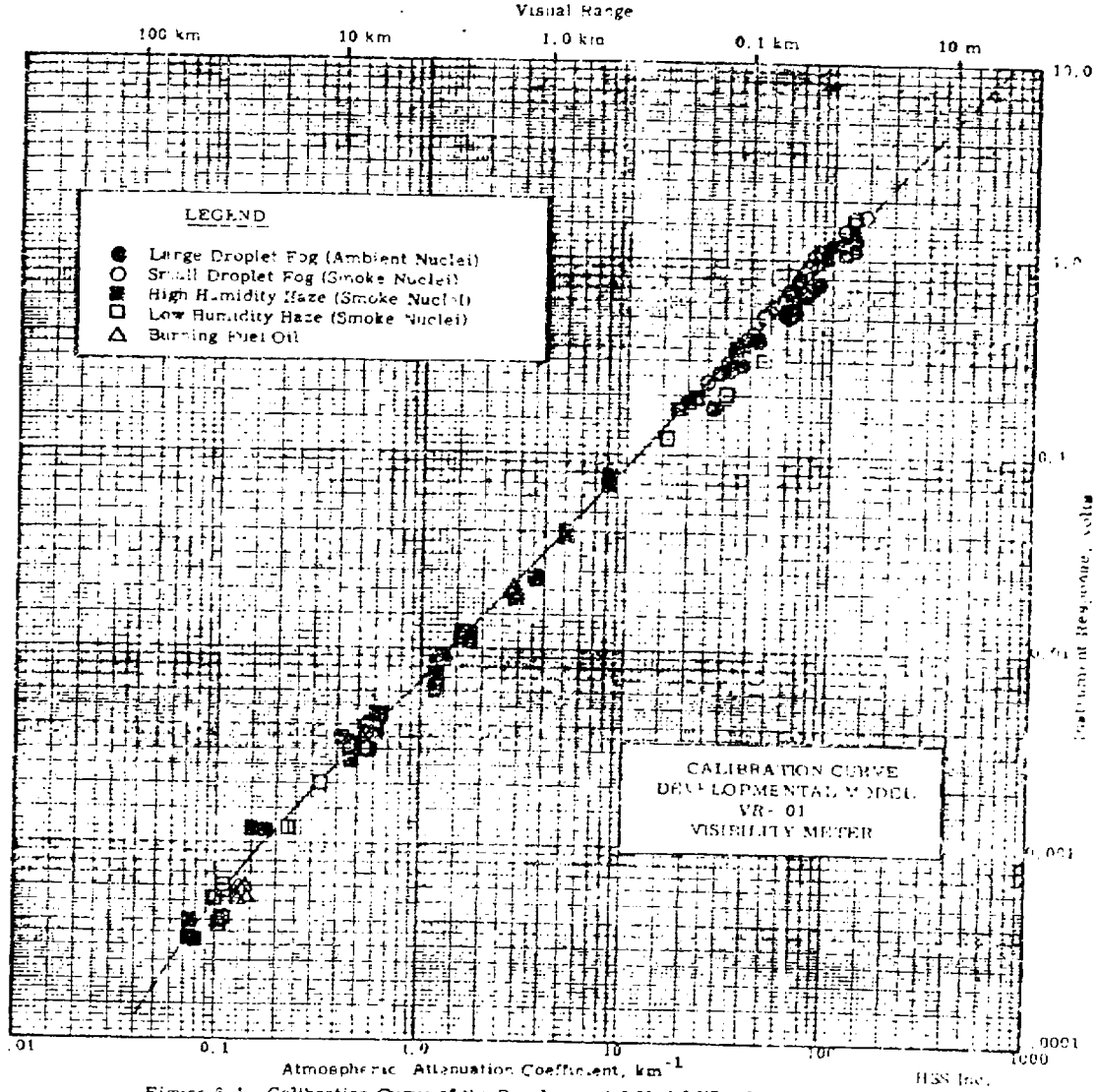

Figure 6.1. Calibration Curve of the Developmental Model VR-101 Visibility Meter.

2 Alfred Circle
Bedford, Ma. 01730
(617) 275-2020

HSS INC
TECHNICAL DATA SHEET

Table 6.3.
Model VR101
Sheet 1
Date 1 Dec 1981

Table 6.3.

NOTES ON VR101 CALIBRATION CURVE

1. Data for calibration curve were obtained from tests conducted at the CALSPAN Environmental Test Chamber in Ashford, N.Y. during the period 14 to 18 September 1981.

2. The atmospheric attenuation coefficients β provided by CALSPAN were obtained from two instruments whose ranges of reliable measurements were approximately as follows:

   (a) CALSPAN Transmissiometer $\beta \geq 8\ km^{-1}$

   (b) MRI Integrating Nephelometer $.08\ km^{-1} \leq \beta \leq 8\ km^{-1}$

3. The linear dynamic range of the VR101 extends to a maximum of 10 volts and a minimum 0.1 m volt. The rms noise limit is approximately 0.3 m volts when a time constant of 15 seconds is employed.

4. A small signal amplifier was employed external to the instrument to provide a X25 external gain for use at low signal levels. The X25 gain output was used to overcome any potential noise pickup in the long cable length between the instrument and the chart recorders. The X1 output was used for all intermediate and high level output signals. For ease of presentation all data points in the calibration curve are presented on an X1 external gain basis.

5. The upper limit of the VR101 calibration was determined by the maximum fog attenuation (approximately $\beta = 200\ km^{-1}$) which can be produced in the CALSPAN Chamber. The lower limit of the VR101 calibration was set by the minimum sensitivity level of the integrating nephelometer.

6. Smoke nuclei were introduced into the chamber by the burning of a cigar or a small measured quantity of "Salty Dog" - a pyrotechnic smoke-generating-material consisting principly of NaCl and KCl.

7. A preliminary best-fit equation to the test data is

$$V = 6.83 \times 10^{-3}\ \beta^{\,1.108} \qquad (1)$$

where V is the output voltage of the VR101 in volts and β is the attenuation coefficient in km^{-1}. This expression leads to the following calibration

Table 6.3 (Cont)

equation for the development model instrument

$$\beta = 90.1\ V^{.903} \qquad (2)$$

One can only speculate as to why the exponent in either Equation (1) or (2) differs from unity. A possible explanation lies in the variation of aerosol sizes between low humidity hazes, high humidity hazes and advection (large particle) and radiation (small particle) fogs. The angular scattering coefficient varies with aerosol particle size, the scattering being more forward-scattering for larger particles than for smaller particles.

6.2 Calibration Reference Standard

Three reference standards for the AVM were calibrated during the CALSPAN tests. These reference standards are disks of neutral optical attenuating material which have small, micron-size scatterers dispersed through the material. During a calibration (or calibration check), the reference standard is mounted in the opening of a large opaque disk. The opaque disk is then mounted on the AVM such that the reference standard is situated in the sample volume of the instrument. The calibrations obtained for these three reference standards were as follows:

REFERENCE STANDARD	AVM OUTPUT VOLTAGE	
	X 1 GAIN	X 25 GAIN
A	.173 volts	4.33 volts
B	.342	8.55
C	1.916	OFF SCALE

The approach we have taken for obtaining reference standards to perform periodic calibration checks on the AVM has been demonstrated to be successful. The CALSPAN experience has demonstrated that some improvements in the technique are required, however. The most significant deficiency noted during the CALSPAN tests was that the homemade reference standard disks were not completely uniform in their attenuating and scattering properties; this in turn made the output response of the AVM sensitive to their polar orientation in the sample volume. There was very little sensitivity of the AVM output response to small transverse excursions of the reference standards in the sample volume.

6.3 Response to Precipitation

The operational objectives of the AVM are such that it was optimally designed for the measurement of atmospheric scattering coefficients in haze and cloud/fog environments. The particular approach taken to satisfy the operational objectives has been demonstrated to be highly successful. A question was raised by the AFGL contract technical monitor concerning the behavior and response of the AVM when subjected to precipitation.

The design approach taken with the AVM involved the use of a small sample volume. The use of a small sample volume permitted the design of a small, compact, lightweight instrument with high sensitivity. These features are of importance for an instrument which is to be carried on an RPV. But it can be demonstrated that all these features are directly related to the choice of a small sample volume.

At issue, in the case of precipitation, is the question of whether a small sample volume can provide an output signal response which correlates with visual range in a precipitation environment. This question has two aspects: (1) does a small sample volume permit adequate precipitation statistics to be obtained, and (2) what is the instrument response to a single particle of precipitation passing through the sample volume.

An investigation of the AVM response to precipitation was outside the scope-of-work of the contract. Nevertheless, it was decided to conduct a brief investigation into that question because it has impact on future RPV operational objectives under consideration by AFGL.

Subquestion (1) which was stated above has, in turn, two facets depending upon the mode of deployment of the instrument: (a) when the instrument is employed on an RPV the small sample volume will sweep out a large integrated sample volume during any reasonable measurement time-interval

(e.g. a liter volume will be swept out in 0.2 seconds for an RPV velocity of 100 mph). Thus reasonable good statistics can be anticipated; (b) when the instrument is mounted on a stationary platform, the statistics for a one-second measurement time period are poor. However, the statistics for a 15 second measurement time period offer reasonable hope of obtaining a meaningful correlation with visual range in precipitation (an instrument time-constant of 15 seconds would in all likelyhood be employed when the instrument is operated on a stationary platform).

Subquestion (2), stated above, concerns the response of the laboratory model AVM to an individual particle of precipitation traversing the sample volume. This was the specific question addressed by a small laboratory investigation which is described in the next section.

6.4 Laboratory Investigation

Set Up: A hypodermic needle attached to a funnel was installed well above the AVM which was mounted on a tripod in the laboratory. Light traps were placed in both the transmitter and receiver optical beams to eliminate scattered light effects from the walls of the room. Water drops from the funnel/hypodermic needle arrangement fell through the sample volume at the rate of about one per second. The drops were approximately 3 mm in diameter.

Measurements: Signal amplitudes were measured at the output of the portion of the amplifier chain prior to the synchronous detector. The signal amplitudes, which were measured with an oscilloscope, were approximately four volts peak-to-peak for the 3 mm diameter water drops.

Conclusions: The signal amplitude produced by the 3 mm drop would have saturated the final output amplifier stages. Because the

signal pulses from large drops exceed the maximum permissible voltage which can enter the amplifier chain without producing saturation, clipping of the signal pulses will occur. The response of the electronic circuitry under these circumstances could exhibit a non-linear behavior. Thus, even though good statistical sampling may be achieved, an incorrect attenuation coefficient might be measured.

Recommendations: Based on the laboratory investigation, we believe that additional electronic circuitry could ultimately be added to an AVM which would permit the instrument to perform two additional functions (i.e. beyond the capability to measure the atmospheric scattering coefficient in fogs and hazes). Those functions would be : (1) to identify the presence of precipitation and (2) to present an additional (or alternative) signal output which would have a linear response to precipitation and presumably, therefore, have some degree of correlation with transmission through precipitation. The degree of correlation would, naturally, have to be a subject of investigation at a test facility such as the Weather Test Facility at Otis AFB. But, it is much more probable that a correlation can be found if the response to individual particles of precipitation is linear rather than non-linear.

An added bonus resulted from the precipitation investigation. Our thinking, at one point, was directed toward a method for increasing the sample volume while maintaining some of the attributes of the instrument; namely, its small size, compactness, light weight, and low power consumption. The trade-off parameter for increased sample volume was taken to be sensitivity---since the signals from precipitation were far too large anyway. An instrument concept was ultimately arrived at which had a large sample volume (0.5 to 1.0 liter). This concept could lead to a low-cost, ground-based instrument for handling precipitation (which would handle fogs and haze equally as well as does the AVM).

7. RESULTS OF EVALUATION OF LABORATORY MODEL AVM

7.1 Basis of Evaluation

A description of the evaluation of the experimental model instrument is presented in terms of five categories of attributes: (1) measurement performance, (2) stability of calibration, (3) physical characteristics, (4) electronic/electrical characteristics and (5) serviceability. The criteria used in making the evaluation are the design goals as outlined in the design evaluation (See Sections 1 to 4).

7.2 Measurement Performance

It was concluded in the design evaluation that the AVM must be capable of measuring an atmospheric aerosol scattering coefficient of 0.3 km^{-1} with a S/N ratio of 5:1 (this is equivalent to measuring a visual range of 10 km to an accuracy of $\pm$ 20%). The measurement must be made with a time constant no greater than 0.5 seconds when the instrument is deployed on a drop-sonde package and no greater than 0.1 to 0.25 seconds for RPV deployment.

An evaluation of the measurement performance of the instrument is based on the tests conducted at the CALSPAN Environmental Test Chamber. A time constant of 0.5 seconds was built into the instrument. However, on the basis of reasoning outlined below it was concluded that static tests of the instrument should be conducted with a time constant of at least ten seconds. An external signal conditioner was, therefore, fabricated having a time constant of 15 seconds, and used for all tests conducted at CALSPAN.

The necessity for a long time constant when deploying the instrument statically is based on the following reasoning: The AVM employs a small sample volume ($\sim$1 cm^3). Such a small sample volume may not contain a statistically significant number of aerosol particles of all sizes which are important to the measurement of visual range. When preparations for the CALSPAN tests were being made there was great uncertainty as to what the

proper, time-integrated, sample volume should be for the AVM. The only information available were AFGL/OPA calculations for 10 μm wavelength (Reference 10). Based on these calculations it was concluded that a sampling of, approximately, 10 seconds would be required for stationary operation of the instrument to guarantee that a truly representative aerosol size distribution had been properly sampled. (The assumption being that wind velocities would be about 0.7 mph or greater).

When the instrument is operated on an RPV the motion of the vehicle permits the small instantaneous sample volume (~1 cm^3) to sweep out a large measurement volume - in any measurement time of importance (e.g. at a speed of 150 mph a volume of 6.7 liters is swept out in 0.1 seconds). Note that a similar volume is swept out in 15 seconds for a wind velocity of 1 mph when the instrument is stationary.

Subsequent analysis, performed jointly by HSS Inc and AFGL/OPA, indicate that a much smaller integrated sample volume is required when the operating wavelength is in the visible spectral region. A sample volume of a few tens of cm^3 is quite adequate to properly sample the aerosol size distribution. The necessary sample volume can thus be swept out in one second for a wind velocity of 0.7 mph.

The tests at CALSPAN indicate that the experimental model AVM was capable of measuring a scattering coefficient $\sigma = 0.02\ km^{-1}$ with a S/N = 1. (This is an extrapolated value since the CALSPAN monitoring equipment could not measure σ-values below $\sigma = 0.08\ km^{-1}$). Based on these observations we conclude that the experimental model AVM can measure a scattering coefficient of $\sigma = 0.1\ km^{-1}$ with a S/N = 5. However, all these values are appropriate to a measuring time constant of 15 seconds. To obtain the S/N ratio appropriate to another time constant τ we must employ the relation

$$(S/N)_\tau = \sqrt{\frac{\tau}{15}} \times (S/N)_{\tau = 15}$$

From this relation we may calculate the S/N ratio for various time constants and for the case of $\sigma = 0.3\ km^{-1}$.

Time Constant (sec)	S/N Ratio (σ 0.3 km^{-1})
15	15
1.7	5
0.5	2.7
0.25	1.9

The S/N values listed above apply to the case where there is no background radiation incident on the detector. When background radiation is present the photon noise will degrade the S/N ratio from the values quoted. Degradation by as much as a factor of three can occur under daytime conditions where a bright sky appears in the receiver field of view.

On the basis of the above results it must be concluded that the design goal on measurement performance has not quite been achieved. In spite of that, it has been demonstrated that the performance of the experimental model AVM equals the capability of any commercially available visibility meter; and it does so with much less power and considerably less size and weight.

There are several ways of improving the S/N of the AVM. Some of them are not very desirable. An increase in size and weight would occur if a larger source, greater optical throughput, or a larger detector were used. A smaller instantaneous sample volume would also lead to improved S/N ratio, but aerosol sampling statistics might again become a concern. Increasing the load resistor of the hybrid silicon photovoltaic detector-amplifier could improve S/N ratio, but the maximum value of this load resistor is set by the brightest background expected to occur in the field of view of the detector. This latter possibility was

explored with negative results as will be described later.

The primary reason for a very short time constant in the AVM results from its dual-role requirement: the AVM is required to recognize whether it is in or out of a cloud as well as measure the aerosol scattering coefficient. A very short time constant (0.2 sec to 0.5 sec) is necessary if the instrument is to respond rapidly upon entering or exiting a cloud.

The desired S/N performance requirement can be achieved in an operational AVM if a few seconds of data is averaged by the data processing system. Since atmospheric aerosols invariably are horizontally stratified no error will be incurred by taking an average of a few seconds of data whenever the RPV is flying horizontally. When the RPV is in a spiral ascent or descent the averaging technique may or may not be useful depending upon the rate of climb or descent.

Two approaches for increasing the S/N ratio, without increasing the time constant, should be pursued: (1) search for an IRED with greater output power and (2) decreasing the forward scatter angle.

7.3 Stability of Calibration

The calibration of the experimental model AVM has been checked periodically over the four month time-interval since the calibration was performed at CALSPAN. A calibration check is performed with the reference standard plaque which was calibrated during the CALSPAN tests. No detectable change has been noticed in the calibration of the instrument.

Based on these observations we recommend no basic changes in the electronic circuitry of the transmitter system, receiver system or of the calibration technique.

7.4 Physical Characteristics

The primary characteristics of concern in the AVM development

program are the size, weight and configuration of the instrument.

The experimental model AVM was designed to minimize the number and size of weather-tight seals. No consideration was given to achieving any form of aerodynamic shape. Major emphasis was placed on minimizing the size of the instrument, but no great emphasis was placed on weight, the thought being that if we make it small it will automatically be light. Very little consideration was given to ease of assembly or ease of serviceability.

The prototype instrument represents a complete mechanical redesign of the laboratory model AVM package. In the redesign of the instrument considerable emphasis was placed on those features which had been de-emphasized in the first design: accessibility, lightness and aerodynamic form.

The design of the prototype AVM has a central strut which also serves as the optical bench and which supports all mechanical, electrical and optical components. The housing of the instrument consists of three removable sections, as shown in the drawings. Once the housings are removed there is complete access to all electronic and optical components.

The prototype instrument is designed to be lighter in weight than the experimental model. The housing is to be fabricated of lighter gauge aluminum and the transmitter and receiver optical assemblies, which were excessively heavy in the experimental model, were redesigned to lessen the fabrication costs and lighten their weight. Focusing of the transmitter and receiver optical assemblies will, in all probability, be required only once during the lifetime of an instrument (i.e. at assembly). Hence, it was decided to do all focusing by shimming rather than by providing more costly mechanical focusing adjustments. (There is also less probability of the focus shifting over a period of time when shims are used.)

7.5 Electronic & Electrical Characteristics

Of primary consideration in the transmitter and receiver electronics is stability, both short term and long term, and over an extreme temperature range. All testing, to date, has shown that this goal has been achieved. In the case of the receiver electronics there is an additional goal of minimizing the noise contribution from the early stages of signal amplification. Measurement and calculations show that the noise characteristics of the instrument are near the theoretical limit.

We recommended no basic changes in the electronic circuits of the instrument. There were, however, a few minor changes which would improve the usefulness of the instrument. These changes were as follows:

Gain Change: The gain of the receiver eledtronics should be increased by a factor of five.

The amplifier gain in the experimental model AVM was chosen somewhat arbitrarily. With considerable operational experience now behind us, we believed the added gain factor would be beneficial. As it now stands a signal voltage of 0.0001 rms volts represents the threshold of detection of the instrument. The MAWS system operated at Otis AFB by AFGL has a minimum of 0.0025 volts, some 25X larger than the threshold detectability level of the experimental model AVM. The upper level of the dynamic range of the present instrument is 10 volts which is set by the operational amplifier characteristics. Thus, the present dynamic range of the instrument is about five decades (from 0.1 mv to 10 volts). Increasing the gain by a factor of five would cut the dynamic range to 20,000:1 because the 10 volt limit would remain fixed. The primary reason for increas-

ing the gain is that signal levels of the order of one millivolt or less cannot be transmitted over cable lengths longer than 10 to 20 feet in many environments without being contaminated by electrical noise pickup. If the electronic gain is increased by a factor of five as we recommend the lowest measurable visual range will be increased from 5 meters to 25 meters. The corresponding maximum measurable fog scattering coefficient will be reduced from 800 km^{-1} to 160 km^{-1}. Since the scattering coefficients of heavy fogs rarely exceed 200 km^{-1} there will be little likelihood that loss of data will result from the gain change.

Time Constant: The time constant of the basic receiver electronics is 0.5 seconds in the experimental model AVM. The signal conditioner, when used, increases that time constant to 15 seconds. The prototype instrument was to be tested over a several month period at the AFGL Weather Test Facility at Otis AFB. Its measurements were to be compared with those of other visibility meters and transmissometers having time constants of the order of 15 seconds. The comparison should be made, we felt, with similar instrument time constants so that any localized scattering phenomena (such as occur in fogs) are measured in an identical manner. For this reason, the prototype AVM was to be fabricated with a time constant of 15 seconds. The time constant can easily be changed to a different value at a later date.

Gain Adjustment: The receiver electronics of the model AVM were not provided with a potentiometer for adjusting the gain over a limited range. This was done deliberately so that any long term drifts could be detected. We recommended, however, that the receiver electronics of the prototype AVM be provided with a potentiometer for introducing a small range of gain change. Over the course of a year's continuous operation one expected some decrease in the light output of the IRED source. The ability to introduce a small gain change was a convenience if such a drift were to occur. Changing the gain slightly would obviate the necessity for changing the calibration constant in the calibration equation.

An experiment was performed to determine if the detector load resistor could be increased and thus provide some improvement in S/N ratio. A white panel was set normal to the direction to the sun at noon-time on a clear day in early December. The experimental model AVM was situated in a manner that allowed the FOV of the receiver optics to be filled by the sun-illuminated plaque. Under these viewing conditions the voltage across the load resistor was found to be slightly over 13 volts (which is on the threshold of saturation of the amplifier stage internal to the detector).

The experiment was intended to simulate the maximum possible background radiation which an operational AVM would be subject to, i.e. a sunlit cloud. The conclusion reached was that the load resistor could not be increased; if anything it should probably be slightly decreased.

7.6 Serviceability

The prototype visibility meter was fabricated with MIL-SPEC, or equivalent quality, electronic components. The life-time of the IRED source is estimated to be greater than 10 years. The expectancy, therefore, is that there will be very little need for servicing the instrument. If, however, servicing of the electronics ever is required the new design will permit easy access to all electronic components. The design of the experimental model AVM did not permit ease of servicing. In fact assembly of the instrument proved to be an extremely tedious affair, consuming much more time and, therefore, money than should be expected. Again, on the basis of serviceability we must recommend the new design over the previous design.

8.0 PROTOTYPE AVM DEVELOPMENT

The experimental model of the Airborne Visibility Meter (AVM) was completed by mid-August 1981 and underwent testing and calibration in mid-September 1981 at the CALSPAN Environmental Test Chamber at Ashford, N. Y. The test program and the results are summarized in Section 6 of this report.

In the time period from September 1981 to mid-January 1982 the Experimental Model AVM was operated at HSS Inc to gain additional operational experience prior to submitting the design evaluation report for the Prototype AVM. An evaluation of the Experimental Model AVM was then performed based on both the CALSPAN tests and post-CALSPAN testing at HSS Inc. The results of this evaluation were presented in a design evaluation report (Section 7 of this report).

Based on the results of the evaluation of the experimental model AVM a complete mechanical redesign of the instrument was performed. No basic changes were made in the electronic circuits of the instrument; however, a few minor changes were made to improve the versatility of the AVM. The mechanical redesign was begun in early February and completed by late February. Fabrication of the Prototype AVM began in early March and was completed by late April.

The AVM Instrument Development Program outlined in the contract statement of work did not specify any use for the Experimental Model AVM after its calibration and test at CALSPAN. It occurred to the contract technical monitor and to HSS Inc that the Experimental Model AVM could be installed at Otis AFB to begin an evaluation of the long-term performance of the AVM under adverse environmental conditions. This use of the Experimental Model AVM could act as a partial substitution for the evaluation of the Prototype AVM at Otis AFB -- which is a contract Line Item. Operation of the Experimental Model at Otis AFB could not fully substitute for operation of the Prototype instrument at Otis AFB since the prototype

instrument incorporates some design changes which could have a slight influence on the performance of the instrument.

The Experimental Model AVM was installed at Otis AFB on 28 January 1982 and has been in operation continuously since then, except for a three-week period in early May when it was returned to HSS Inc for a zero-drift check. What was thought to be an instrument problem turned out to be a problem in the MAWS data collection and recording system.

Fabrication of the Prototype AVM was completed just prior to the CALSPAN tests of the SWIR Nephelometer. With the concurrence of the contract technical monitor, the installation of the Prototype AVM at Otis AFB was deferred in favor of performing a no-cost calibration and test of the Prototype AVM by piggy-backing on the SWIRN CALSPAN tests.

The CALSPAN tests of the Prototype AVM and SWIR Nephelometer were conducted during the time period from 3 to 7 May 1982. The CALSPAN tests indicated that some minor modifications to the electronic circuitry of the Prototype AVM were in order. These modifications have since been effected.

The CALSPAN tests and subsequent circuit modifications caused a delay in the installation of the Prototype AVM at Otis AFB. Further delay was encountered because of the necessity to purchase lightning surge arrestors for the instrument signal leads, prior to the installation at Otis AFB. Personnel at Otis AFB warned that the thunderstorm season was approaching and that the Prototype AVM and Experimental Model AVM should not go unprotected.

The basic problem is that the many meteorological sensors and visibility meters at the Otis Weather Test Facility are connected to the MAWS system by fairly long signal leads. These leads can pick up con-

siderable voltage surges during lightning storms. Such voltage surges invariably cause considerable damage to the instruments if they are not protected by surge arrestors. HSS Inc ordered voltage surge arrestors for the two instruments in early June. The surge arrestors were delivered on 1 July. On 2 July the Prototype AVM was installed at Otis AFB. Lightning surge arrestors are now installed on the signal leads of both instruments. The 115 V AC/28 V DC converter which powers the two instruments was left unprotected. The AFGL power supply is relatively inexpensive and it will absorb any voltage surges on the 115 V AC line thus protecting the two visibility meters from a voltage surge on their power inputs.

An optical schematic drawing of the prototype AVM is shown in Figure 8.1. The complete AVM Visibility Meter System is illustrated in Figure 8.2. The system consists of the basic instrument plus four fub-assemblies: (1) an aerodynamic fairing for airborne use of the instrument, (2) a calibrator holder, (3) a baffle assembly for static operation of the instrument and (4) a calibrator reference standard.

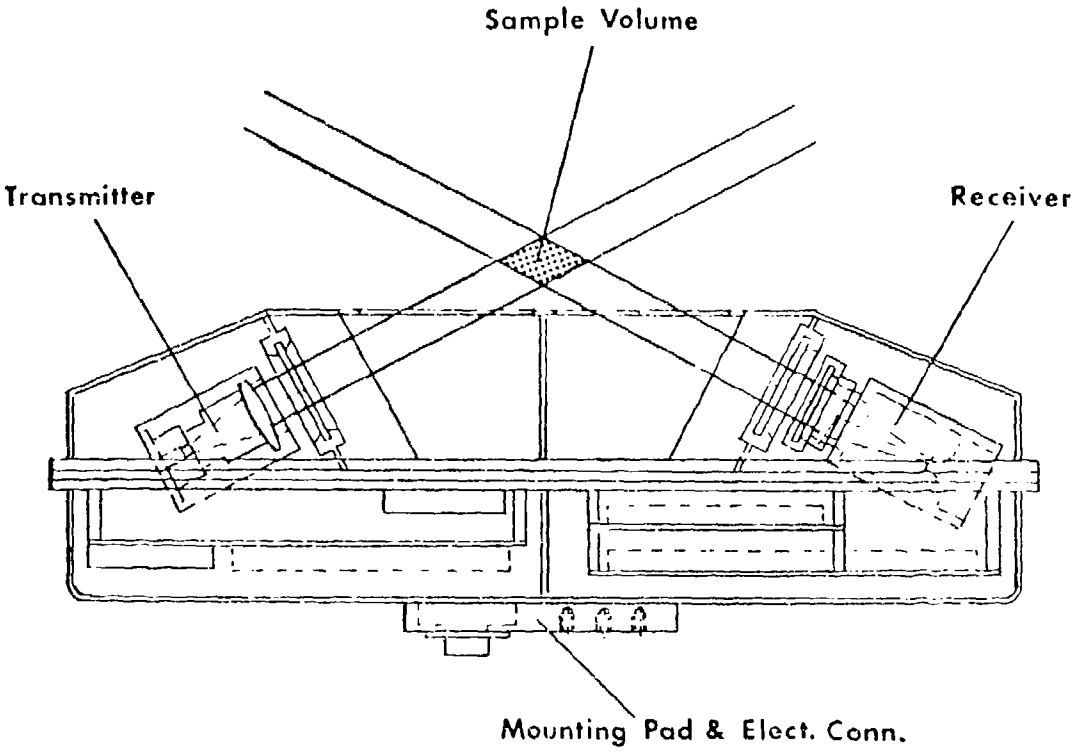

Figure 8.1. Optical Schematic of the Airborne Visibility Meter.

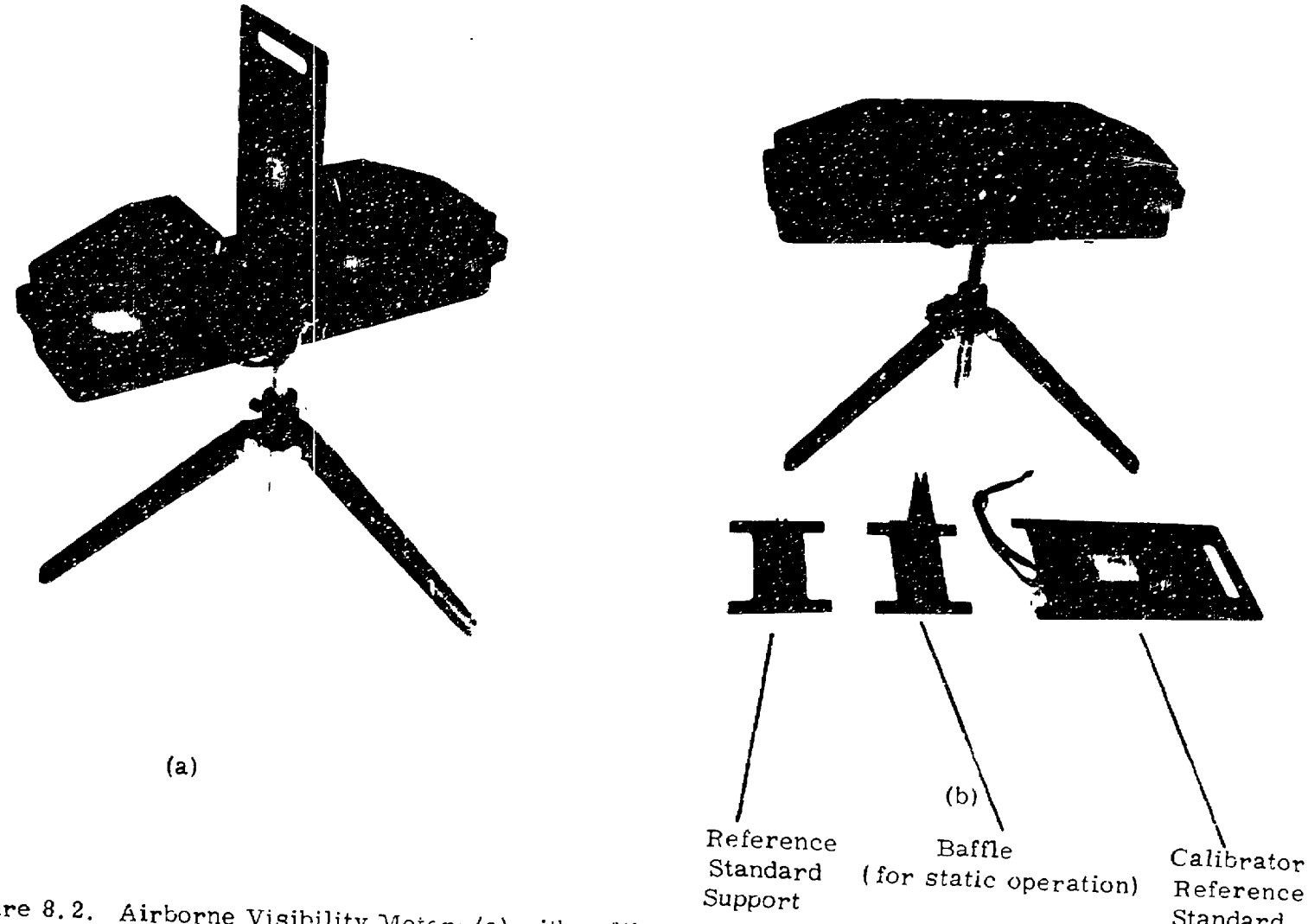

Figure 8.2. Airborne Visibility Meter: (a) with calibration reference standard installed (b) with aerodynamic fairing in place and also showing major instrument accessories.

9. PROTOTYPE AVM CALIBRATION

9.1 Calibration Curve

A total of fourteen fog and haze tests were conducted in the CALSPAN Environmental Test Chamber during the five day period 3-7 May 1982. A summary of the test environments is given in Table 9.1.

Seven of the test runs were used to devise a calibration curve for the Prototype AVM. The calibration curve is shown in Figure 9.1. The test data from the other seven runs were not suitable for incorporation into the calibration curve, for one reason or another (e.g. there were several fog runs which were aborted because of difficulties encountered by CALSPAN in generating fogs due to high chamber temperature).

The calibration equation for forward scatter visibility meters has the general expression

$$\beta = K\,(V - b)^n$$

where β is the atmospheric attenuation coefficient in km^{-1}, V is the output voltage of the instrument, b is the zero offset voltage, K is the calibration constant and n is an exponent derived from plotting the experimental data on a log-log plot.

An insufficient number of zero readings and reference calibrator readings were taken during the course of the tests. This has caused minor problems in establishing the best possible calibration equation for the Prototype AVM.

The zero reading prior to Test Run No. 1 was 6 millivolts. The zero reading was not checked again. The instrument output voltage when the reference calibrator was inserted after Test Run No. 14 was 1.122 volts. Based on these checks and the equivalent extinction of the calibrator (10.6 km^{-1}), which was established from the calibration curve, the calibration equation for the prototype AVM is

$$\beta = 9.532\,(V - 0.006)^{0.97}$$

Table 9.1. Summary of Fog and Haze Tests Conducted at the CALSPAN Environmental Test Facility.

Test Run	Date	Objective	Aerosol/Nuclei
1	3 May	Low Humidity Haze	Salty Dog (200 gm)
2	4 May	Large Droplet Fog	Ambient Nuclei
3	4 May	Large Droplet Fog	Ambient Nuclei
4	4 May	Medium Droplet Fog	Ambient Nuclei
5	4 May	Small Droplet Fog	Cigar Smoke
6	4 May	High Humidity Haze	Salty Dog (20 gm)
7	5 May	Large Droplet Fog	Ambient Nuclei
8	5 May	Large Droplet Fog	Ambient Nuclei
9	5 May	Small Droplet Fog	Cigar Smoke
10	5 May	High Humidity Haze	Salty Dog
11	6 May	Small-Med. Droplet Fog	Ambient Nuclei
12	6 May	Small Droplet Fog	Ambient Nuclei
13	6 May	High Humidity Haze	Salty Dog (50 gm)
14	7 May	Low Humidity Haze	Phosphorus

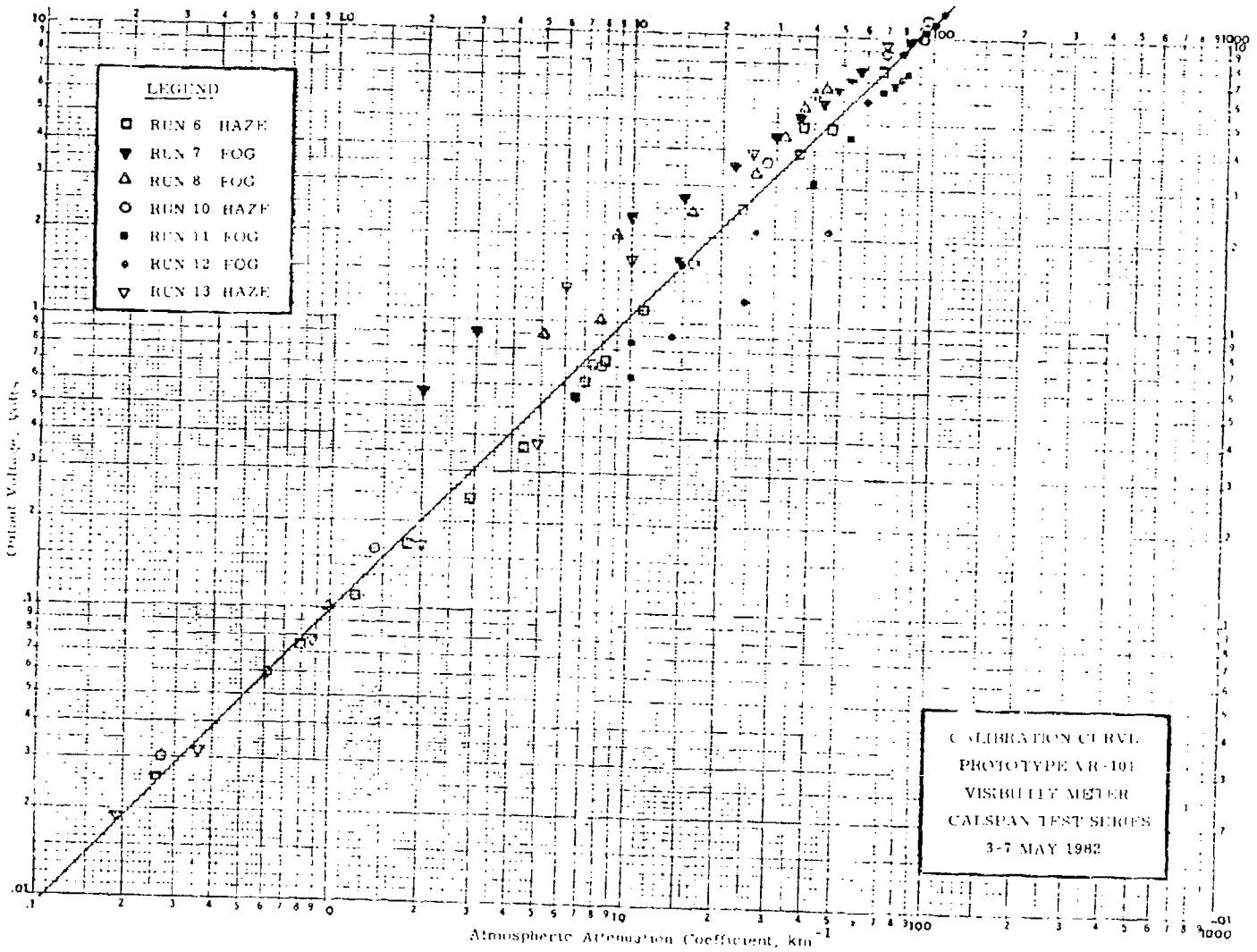

Figure 9.1 Calibration Curve Prototype VR-101 Visibility Meter.

The value of n = 0.97 was also established from the calibration curve.

The above calibration equation was appropriate to the Prototype AVM configuration at the time of the CALSPAN tests. Subsequent to those tests some circuit modifications were made in order to eliminate a high frequency oscillation in the output amplifier which was present whenever a long signal cable was attached to the instrument. The oscillation, which caused a zero offset voltage to occur, was undoubtedly present during the CALSPAN tests, but not during bench tests at HSS Inc before shipping to CALSPAN. Because of the circuit modifications revision to the calibration equation should be made prior to the instrument being sent to Otis AFB.

The exponent n = 0.97 in the calibration equation for the Prototype AVM differs significantly from that of the experimental model AVM which was n = 0.90. We have no good explanation for this difference in exponent values.

There is a more general question related to the exponent in the calibration equation. Most manufacturers and users of forward scatter visibility meters assume that n = 1.00. The reason for having to make that assumption is the degree of difficulty involved in generating a calibration curve over a large range of attenuation coefficients. A large range of attenuation coefficients is required to determine an accurate slope of the curve on a log-log plot.

Calibration of forward scatter visibility meters invariably takes place by comparison with transmissometer measurements of atmospheric attenuation. But transmissometer measurements are subject to large errors for visual ranges which exceed 10 to 20 times the baseline of the transmissometer, thus the calibration of forward scatter meters is invariably restricted to fog situations.

The calibration of the AVM instruments was carried out at CALSPAN by comparison with transmissometer measurements in simulated fog situations and by comparison with an MRI integrating nephelometer in simulated haze

situations. The calibration was carried out over a range of 1000:1 in attenuation coefficients.

The CALSPAN calibrations cannot be considered definitive in the matter of determining the exponent in the calibration equation for forward scatter meters. There are limitations to the CALSPAN calibrations: (1) the CALSPAN transmissometers tend to drift, leading to a bias in the fog data, (2) the fogs do not have a high degree of uniformity which leads to scatter in the fog data as measured by point visibility meters, and (3) the simulated hazes are biased toward small particles and are not typical of real atmospheric hazes.

The entire case for the exponent $n = 1.00$ rests on the measurements of the MRI integrating nephelometer used by CALSPAN to measure the attenuation coefficient in haze situations. An instrumental error in that instrument could bias the calibration of other instruments in such a way that an exponent different from unity is found for their calibration equations.

The Air Force and AFGL in particular has several programs, including the development of an AVM, where visual range in haze situations is of importance. The potential for calibrating visibility meters in all forms of real weather situations exists at the AFGL Weather Test Facility (WTF) at Otis AFB. At present that capability is limited to fog situations. We strongly urge that the WTF capability be expanded to provide for calibrations in haze situations. Only then can the issue of the correct exponent value be settled.

10. AVM PERFORMANCE EVALUATION

10.1 Otis AFB Test & Evaluation

The experimental model AVM was installed at Otis AFB in late January 1982 and has been operated there essentially continuously to this date (early October 1982).

It was returned to HSS Inc once during the month of May for a three week period for a check on a possible zero drift in the instrument. The problem turned out not to be in the instrument but in the MAWS data collection system.

The prototype AVM was installed at Otis AFB in early July. It has been returned to Bedford twice for brief periods of time; once to replace an electrolytic capacitor which failed (because its polarity was inadvertently reversed during fabrication), and again for demonstration purposes by AFGL at a PRESSURS meeting. Otherwise, the prototype AVM has also seen continuous service.

At Otis AFB the two instruments are connected to the MAWS (Modular Automatic Weather System) meteorological sensor network. The MAWS network at Otis AFB is composed of a large variety of meteorological sensors including visibility meters of several types. Each sensor in the network is interrogated every 12 seconds by the MAWS system and its output reading is recorded on magnetic tape. During data processing, once a week at AFGL, the calibration formulae of each instrument is applied to the readings and five readings are averaged to give one-minute mean values.

Starting in early February AFGL has furnished HSS Inc with weekly computer print-outs of the one-minute averages of the readings from the two AVM s along with the readings from several other instruments. Measurements of other instruments, both standard meteorological sensors and other types of visibility sensors are needed to properly evaluate the measurement performance of the two AVM sensors and to characterize the environment.

A typical computer print-out covering a one-hour time period is shown in Table 10.1. A legend is provided in Table 10.2 so that readings of the particular sensors can be identified. It should be noted that, in addition to the two AVM sensors, which are located near C-tower in the MAWS network, there are five other visibility meters whose readings are used for comparison with those of the AVM sensors: (1) a 500 foot base line transmissometer, (2) a 300 foot EG&G Model 207 forward scatter meter (C-10), located near C-tower, (4) an EG&G Model 207 forward scatter meter (X) located near the crossover between the beams of the two transmissometers whose baselines form a cross, and (5) an HSS Inc Model 301 visibility meter which is also located in the vicinity of C-tower.

Caution must be exercised in the comparison of the atmospheric extinction coefficients measured by the various visibility meters. Measurements of extinction coefficient made by the two AVM sensors and the VR-301 are tabulated in units of km^{-1}, whereas the measurements of the two transmissometers and the EG&G forward scatter meters are in units of $km^{-1} \times 10$.

A significant amount of data similar to that shown in Table 10.1 has accumulated since early February. This data has been studied at length, in order to evaluate the performance of the two AVM sensors during all kinds of weather environments and to determine the measurement accuracy of the instrument.

10.2 Reliability and Maintainability

In the design and fabrication of the AVM sensors HSS Inc chose to specify and use only electronic and optical components of very high quality to assure stability and long life. The source of light (the IRED) is, for example, rated to have a lifetime of over ten years. Wherever possible components were selected whose operating temperature range was -55° C to +55°C.

Table 10.1. Computer Printout of Data Collected by the AFGL Modular Automated Weather System (MAWS) for a One-Hour Period.

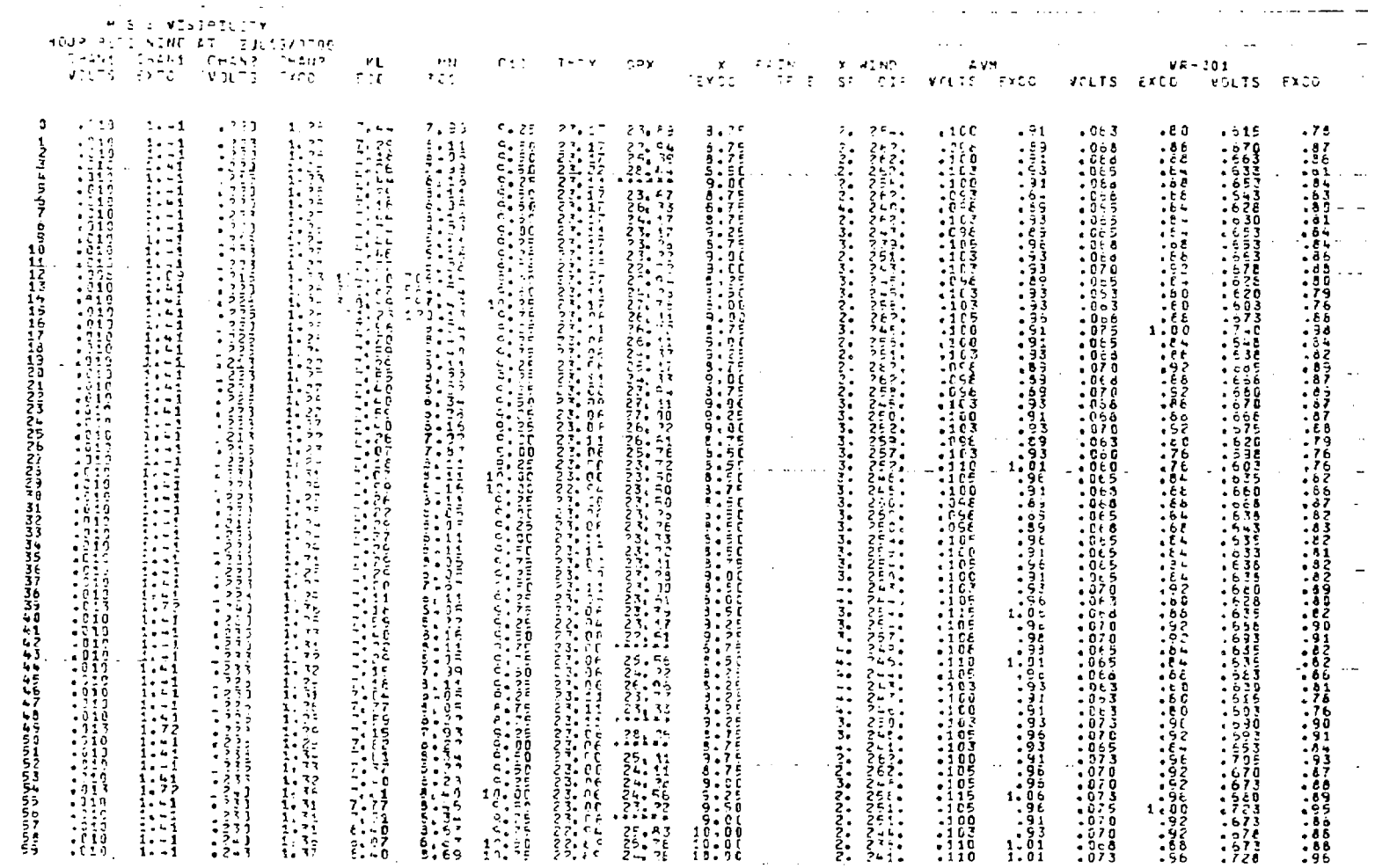

Table 10.2 Identification of Legend Symbols Used in Computer Print-Out of MAWS Data.

Column No.	Identification/Description	Measurement Units
1	Minute of time over which readings are averaged	
2	AVM-XM; Voltage Output X1; Channel 1	Volts
3	AVM-XM; Extinction Coefficient; Channel 1	km^{-1}
4	AVM-XM; Voltage Output X10; Channel 2	Volts
5	AVM-XM; Extinction Coefficient; Channel 2	km^{-1}
6	500 Ft. Baseline Transmissometer; Extinction Coeff.	km^{-1} x 10
7	300 Ft. Baseline Transmissometer; Extinction Coeff.	km^{-1} x 10
8	EG&G 207 Vis. Meter near C-tower; Extinction Coeff.	km^{-1} x 10
9	Temperature	°C
10	Dew Point Depression	°C
11	EG&G 207 Vis. Meter at Cross-Over; Extinction Coeff.	km^{-1} x 10
12	Accumulated Monthly Rainfall	0.01 inch
13	Wind Speed	Knots
14	Wind Direction	Compass Degrees
15	AVM-P; Voltage Output	Volts
16	AVM-P; Extinction Coefficient	km^{-1}
17	VR-301; Voltage Output X1; Channel 1	Volts
18	VR-301; Extinction Coefficient Channel 1	km^{-1}
19	VR-301; Voltage Output X10; Channel 2	Volts
20	VR-301; Extinction Coefficient; Channel 2	km^{-1}

The radiant power output of IRED s according to the manufacturer's specifications, declines by approximately 10 percent over the first 1000 hours of operation and declines by only another 10 percent over the next 10 years of operation. This 10 percent reduction of light output during the first thousand hours of operation was noticeable in both instruments. The AVM-XM has no provision for gain adjustment in the electronic circuitry; hence, its readings were not changed to compensate for the drop in output power. The gain adjustment feature in the AVM-P was used, after two months of operation, to re-establish the correct output voltage using the calculator reference standard.

The AVM-XM sensor has operated for eight months with no component failures and no repairs of any parts. Except for the failure of the incorrectly installed electrolytic capacitor, the AVM-P has operated for over three months with no component failures. It would appear that the operational reliability of the AVM is well established by this performance history.

Ease of maintenance of the AVM sensors was also clearly established. Periodic trips to Otis AFB indicate that the only maintenance required of the instrument is a cleaning of the windows, approximately, once every three months. A check of the instrument calibration at that same interval of time would be a worthwhile part of the routine maintenance procedure.

The AVM is not intended for, nor was it so designed, for operation as a static ground-based visibility meter. Some modifications were made to enable the instrument to function as a ground based visibility meter. These modifications were:

(1) The aerodynamic fairing was replaced by a two-component baffle system to increase the accessibility of wind-induced air flow to the sample volume (see Figure 8.2).

(2) The time constant was increased to 15 seconds. The volume of air contributing to the measurement was, thus, increased by allowing wind to move air through the sample volume for a longer time period.

Despite these modifications to the instruments, operation of the AVM s as ground based visibility meters led to problems in some environmental situations: (1) under freezing rain conditions droplets of rain froze to the edge of the baffles. Droplets frozen on the edge of the first baffle picked up stray transmitter radiation, relayed it to droplets frozen on the edge of the second baffle, which then projected the stray radiation into the receiver optics giving erroneous readings, and (2) both AVM s responded properly to all haze and fog environments plus mist and drizzle environments. For other precipitation environments the small sample volume led to poor statistical sampling despite the 15 second time constant.

During the fabrication phase of the prototype AVM, a second identical instrument was made under a subcontract to the University of Texas. The U of T, under contract to the Army, engaged in a series of atmospheric profile monitoring experiments at WSMR using an RPV. This second AVM prototype visibility meter has already been flown by the U of T in one series of flights at WSMR. Details of the measurements are not yet available. However we have been told by the U of T program manager, Mr. Carlos MacDonald, that the instrument performed well during the entire mission. During flights to determine the vertical profile of the atmospheric attenuation coefficient, the readings from the AVM permitted U of T personnel to discern the presence of boundary layers in the atmosphere.

The RPV, upon which the U of T AVM was flown, suffered several minor crashes while landing. We were told that the AVM, although subject to rather violent impacts, continued to perform flight-after-flight with no apparent problems due to the crashes.

10.3 Measurement Performance

The measurement performance of the AVMs can best be evaluated by a comparison of their readings with those of other visibility sensors which

are subject to the same environmental conditions. Operation of the AVM s in the MAWS meteorological network at Otis AFB provided an excellent opportunity to conduct just such comparisons.

When comparing visibility sensors under poor visibility conditions transmissometers are invariably accepted as the standard against which all other visibility meters should be compared. For this reason we include the measurements of the 500 ft. baseline transmissometer in all comparisons which are made. Two facts should be borne in mind when comparing the readings of the AVM with those of a transmissometer and other forward scatter visibility meters: (1) the sensors in the MAWS network are not collocated but are, in some instances, as much as several hundred feet apart; hence, inhomogeneities in fogs tend to produce some differences in readings which are due purely to the separation of the instruments, and (2) the AVM visibility meters have small sample volumes which when the instrument is operated on an RPV will sweep out a large integrated sample volume during the time constant of the instrument, thus, reducing somewhat the effects of small local inhomogeneities in the atmospheric environment.

At Otis AFB the experimental model AVM and the prototype AVM are the only visibility sensors which are collocated. They are mounted on arms extending from the same vertical pole, and are about 10 feet above the ground level (as are all other visibility meters). The experimental model AVM is mounted such that the sample volume is in a horizontal plane parallel to the ground, thus, permitting precipitation to fall through the sample volume. The prototype AVM is mounted so that the sample volume is below the instrument and is shielded by the body of the instrument from direct incidence of any precipitation. This choice of different mounting configurations for the two AVM's was based on addressing a question currently being raised in meteorological circles; i.e. how much of the extinction coefficient measured during precipitation episodes is due to fog and how much is due to precipitation.

The cross-over point of the two transmissometers is located several hundred feet south of the AVM s. The EG&G-207(X) forward scatter meter is located near the cross-over point. The VR-301 is about fifty to sixty feet southeast of the AVM s, and the EG&G-207(C-10) forward scatter meter is probably 100 feet south of the AVM s. All sensors are oriented such that their receivers generally face a northern direction, away from the sun.

Thin Fog/Haze Eposide: During the hours of 0100 to 0400 GMT on 18 July an episode occurred in which the environment varied between thin fog (defined as β = 1.5 to 3.0 km^{-1} by the international visibility code) and haze (β= 0.75 to 1.5 km^{-1}), and finally meandered into light haze (β= 0.30 to 0.75 km^{-1}). Figures 10.1 through 10.4 present the one-minute averaged reading for four forward scatter meters, which are compared in each case with the readings of the 500 foot baseline transmissometer. The measurements of all forward scatter meters are highly correlated with those of the transmissometer. The correlation appears to be slightly better with the prototype AVM than with any of the other forward scatter meters. The small differences in readings between the five instruments are most likely due more to the spatial variability of the fog than to any real instrumental difference. (Note: once each hour the light source of the transmitter is turned off for five minutes so that a background check can be made on the receiver readings. This check produces the gaps one observes in the plots of transmissometer readings).

Light Fog Episode: On 20 July a light fog (β= 3.0 to 6.0 km^{-1}) to moderate fog (β= 6.0 to 15 km^{-1}) episode occurred. Figures 10.5, 10.6 and 10.7 compare the measurements of six visibility sensors; i.e. five forward scatter meters and the 500 foot baseline transmissometer over a three hour period. In this instance, it is difficult to judge which forward scatter meter correlates best with the transmissometer; all correlate very well. Again, the differences in readings are attributed to spatial variations in the fog rather than to instrumental differences.

Thick Fog Episode: A highly variable thick fog episode (defined as β = 15 to 60 km^{-1}) occurred during a three hour period on 19 August. A comparison of the measurements of six visibility sensors is given in Figures 10.8, 10.9 and 10.10. The readings of the forward scatter meters depart slightly more from those of the trans-

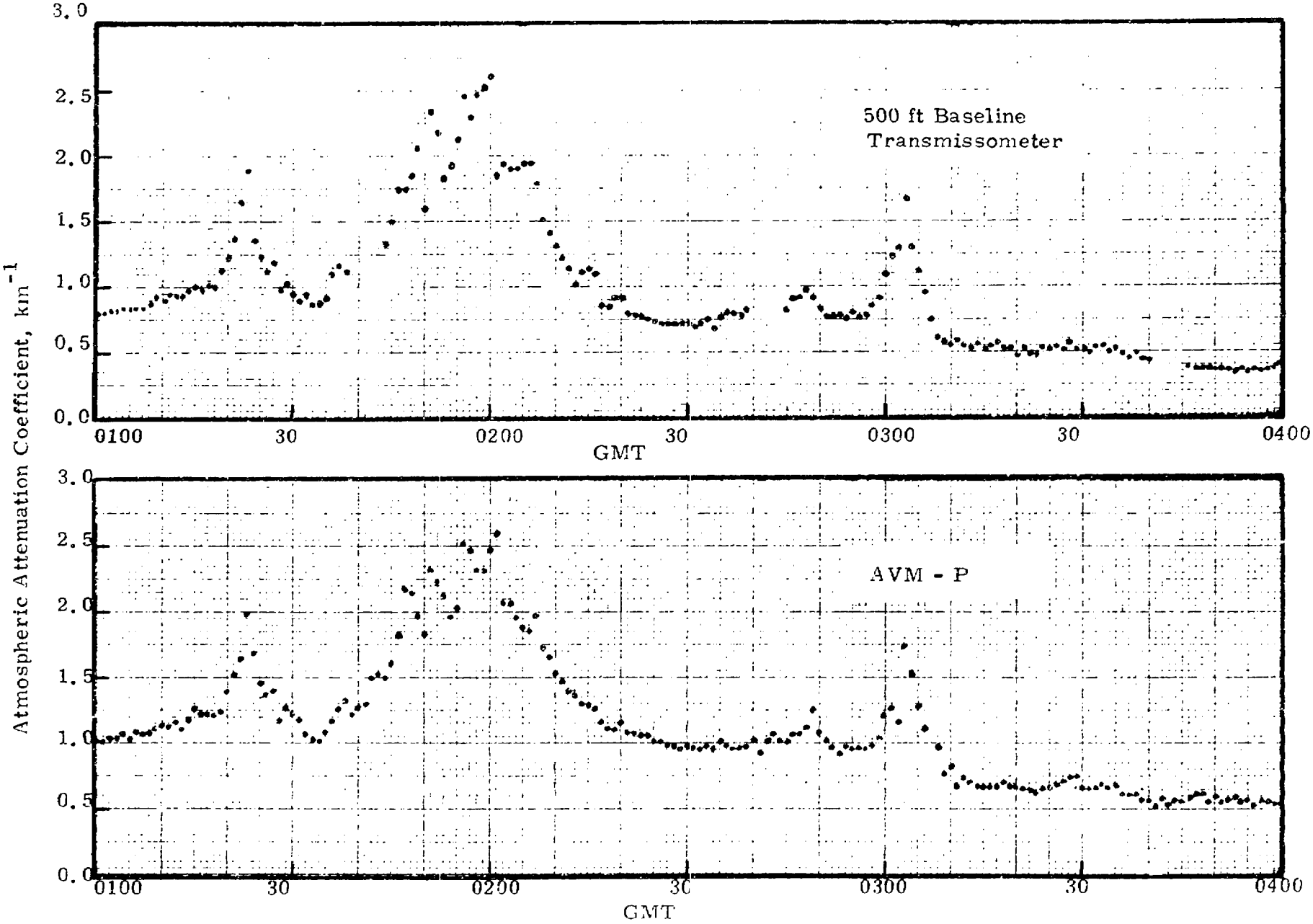

Figure 10.1. Thin Fog/Haze Episode, 18 July 1982, Otis AFB.

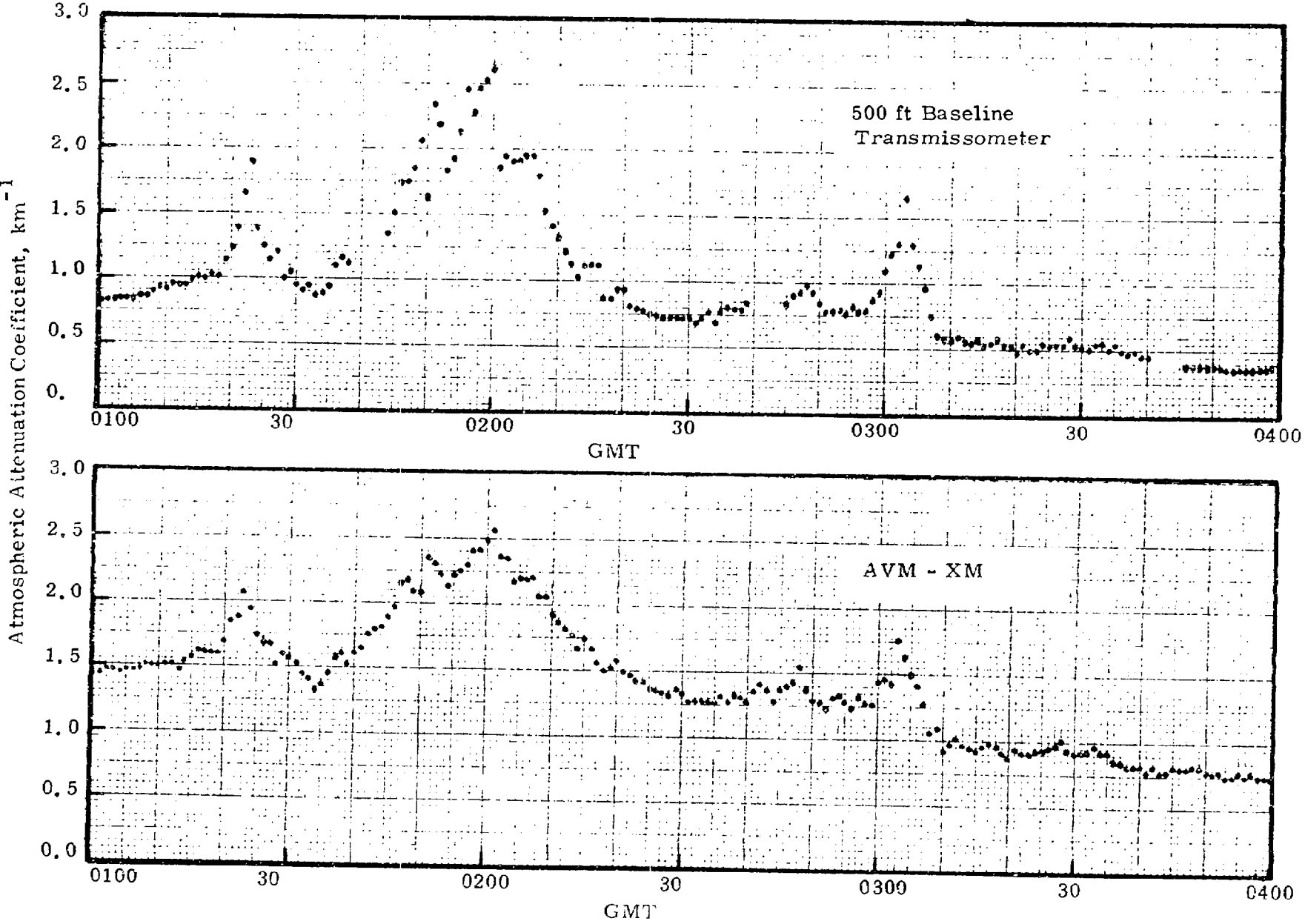

Figure 10.2. Thin Fog/Haze Episode, 18 July 1982, Otis AFB.

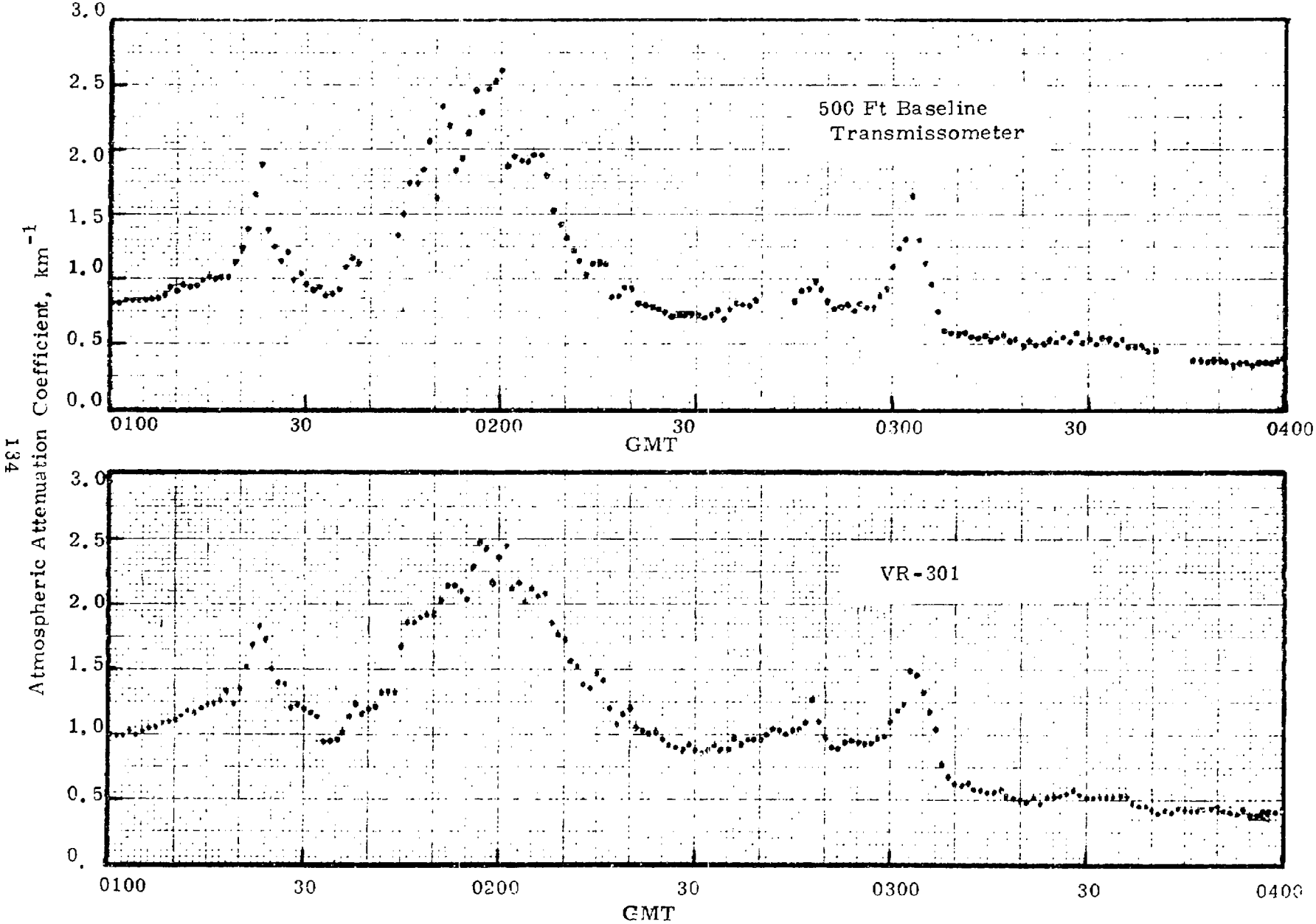

Figure 10.3. Thin Fog/Haze Episode, 18 July 1982, Otis AFB.

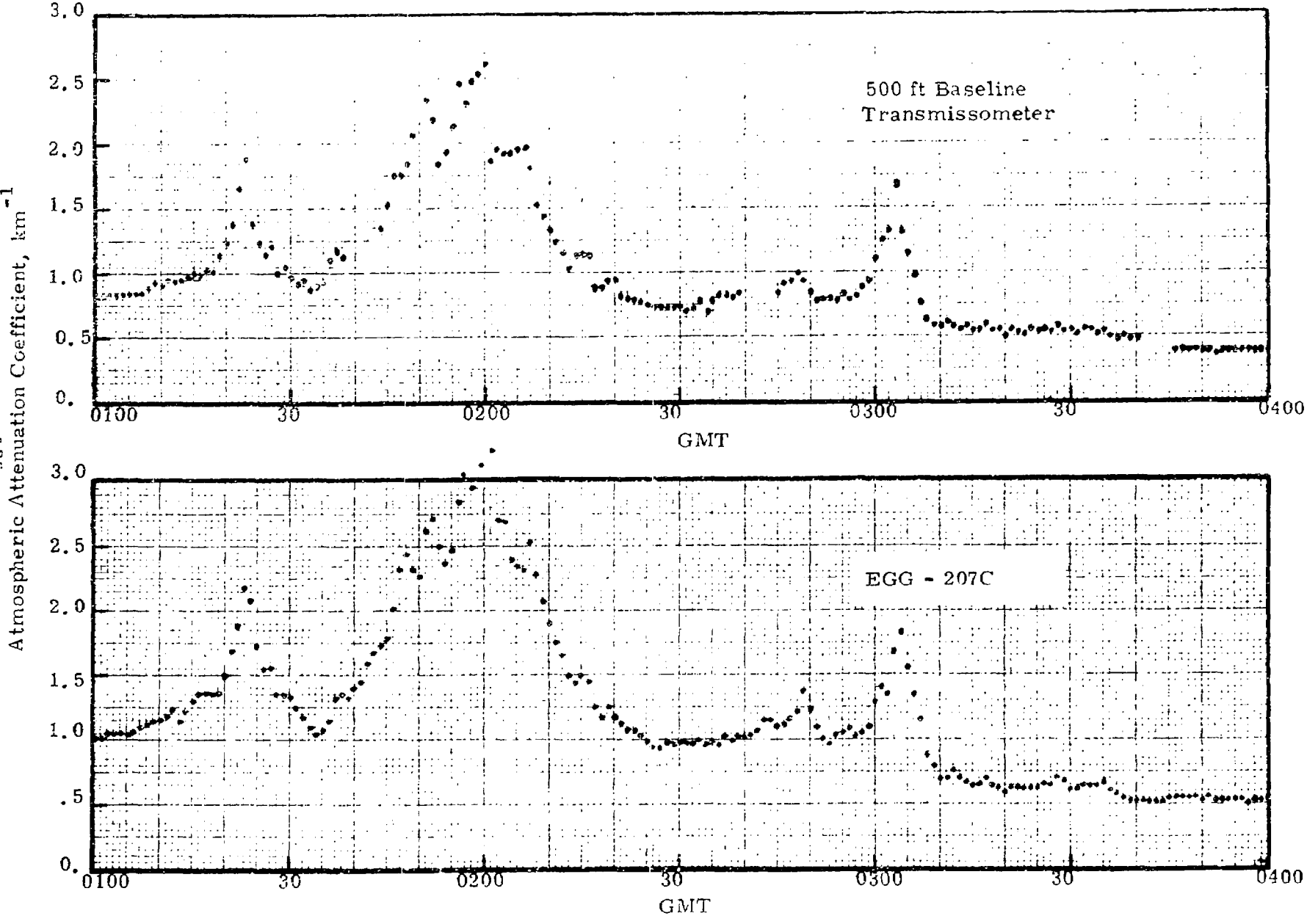

Figure 10.4. Thin Fog/Haze Episode, 18 July 1982, Otis AFB.

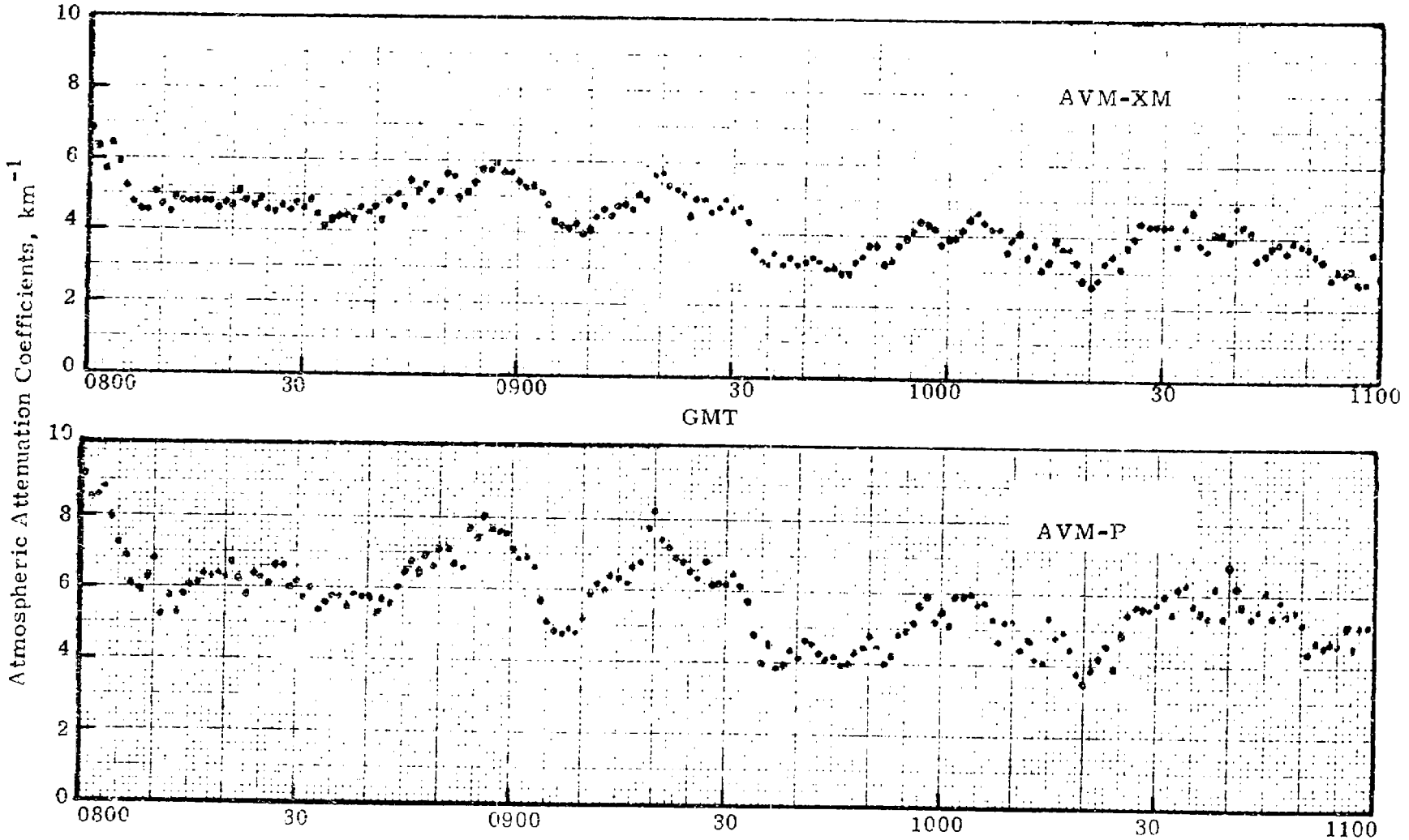

Figure 10.5 . Light Fog Episode, 20 July 1982, Otis AFB.

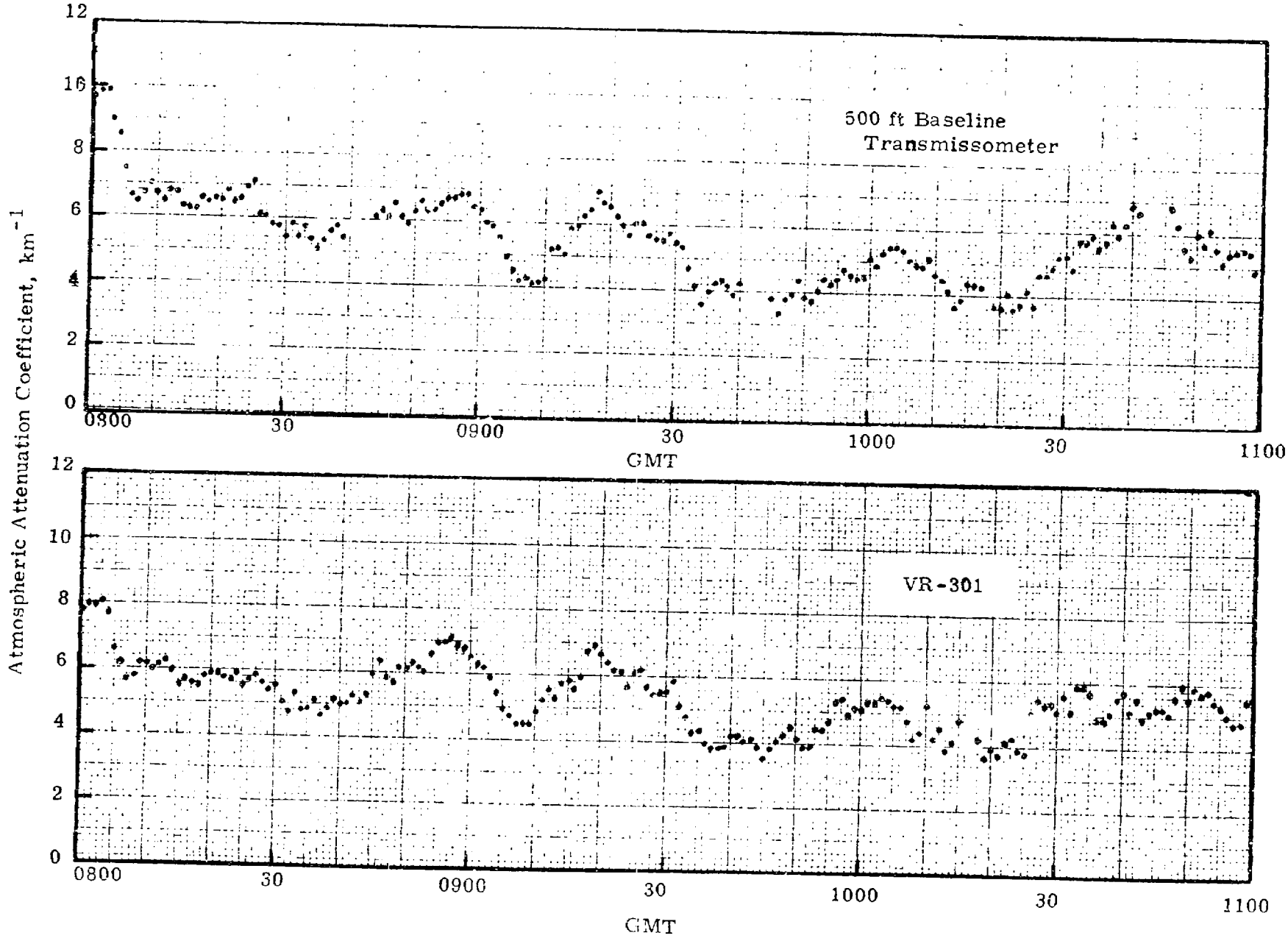

Figure 10.6. Light Fog Episode, 20 July 1982, Otis AFB.

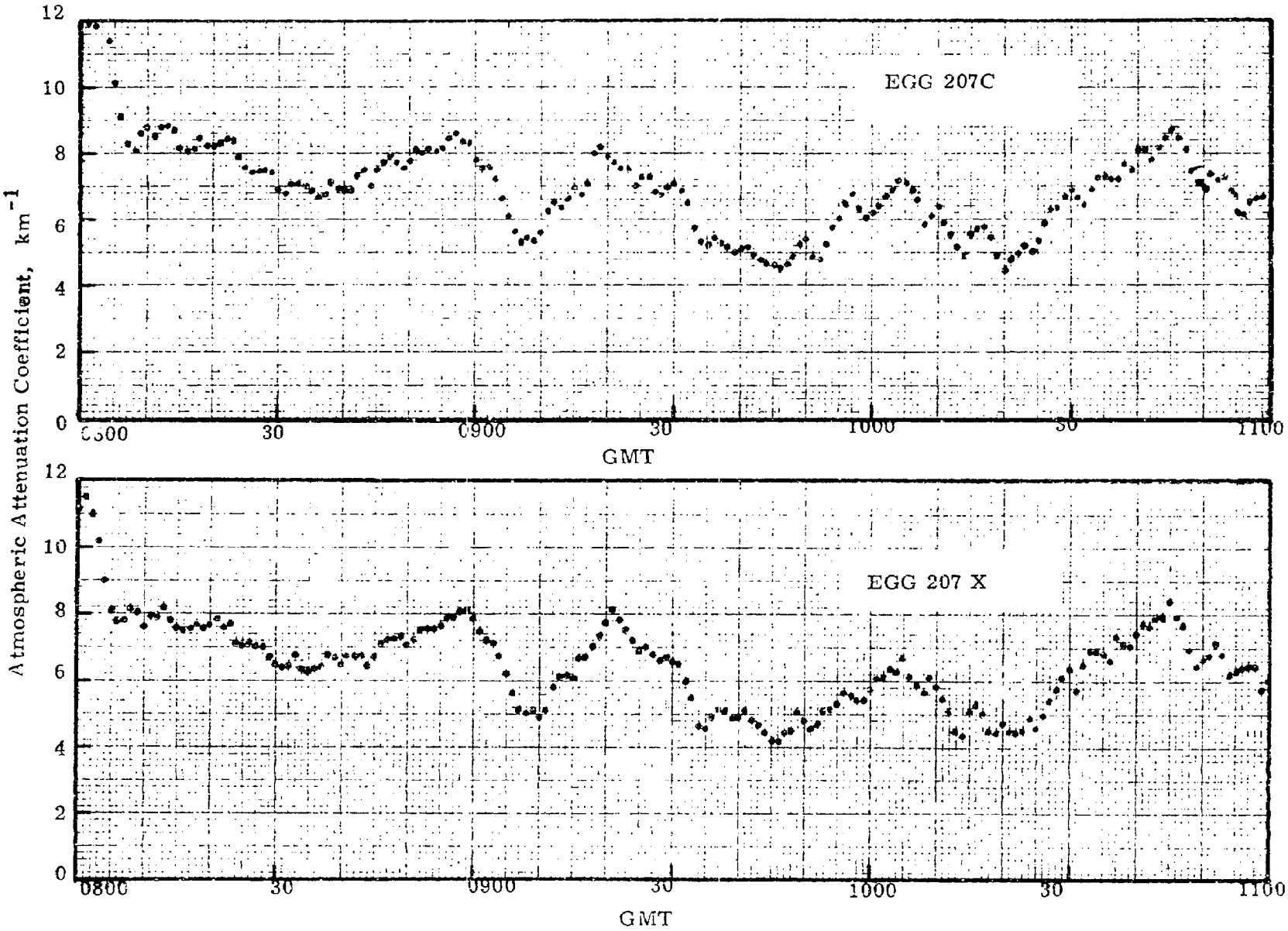

Figure 10.7. Light Fog Episode, 20 July 1982, Otis AFB.

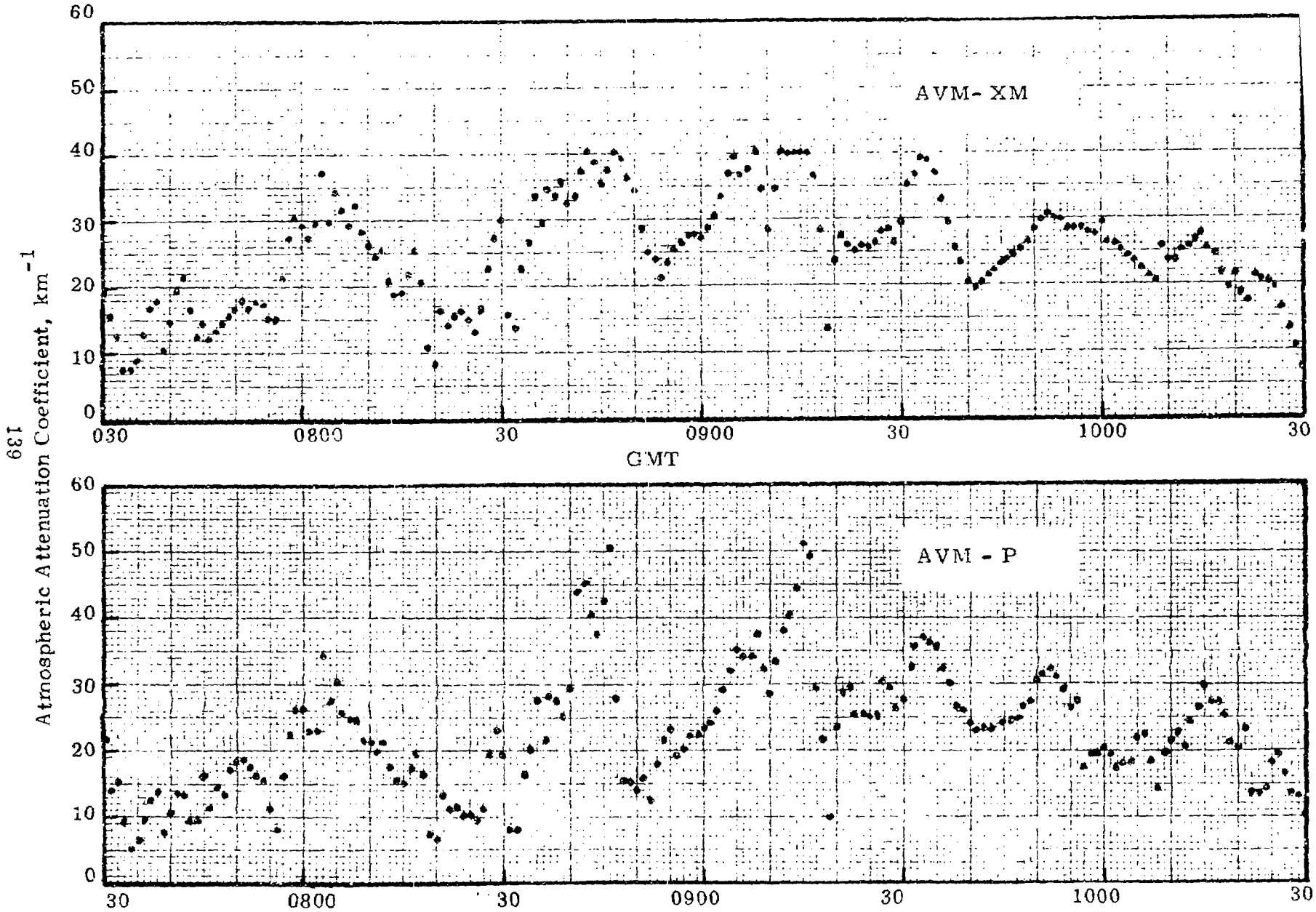

Figure 10.8. Thick Fog Event, 19 August 1982, Otis AFB.

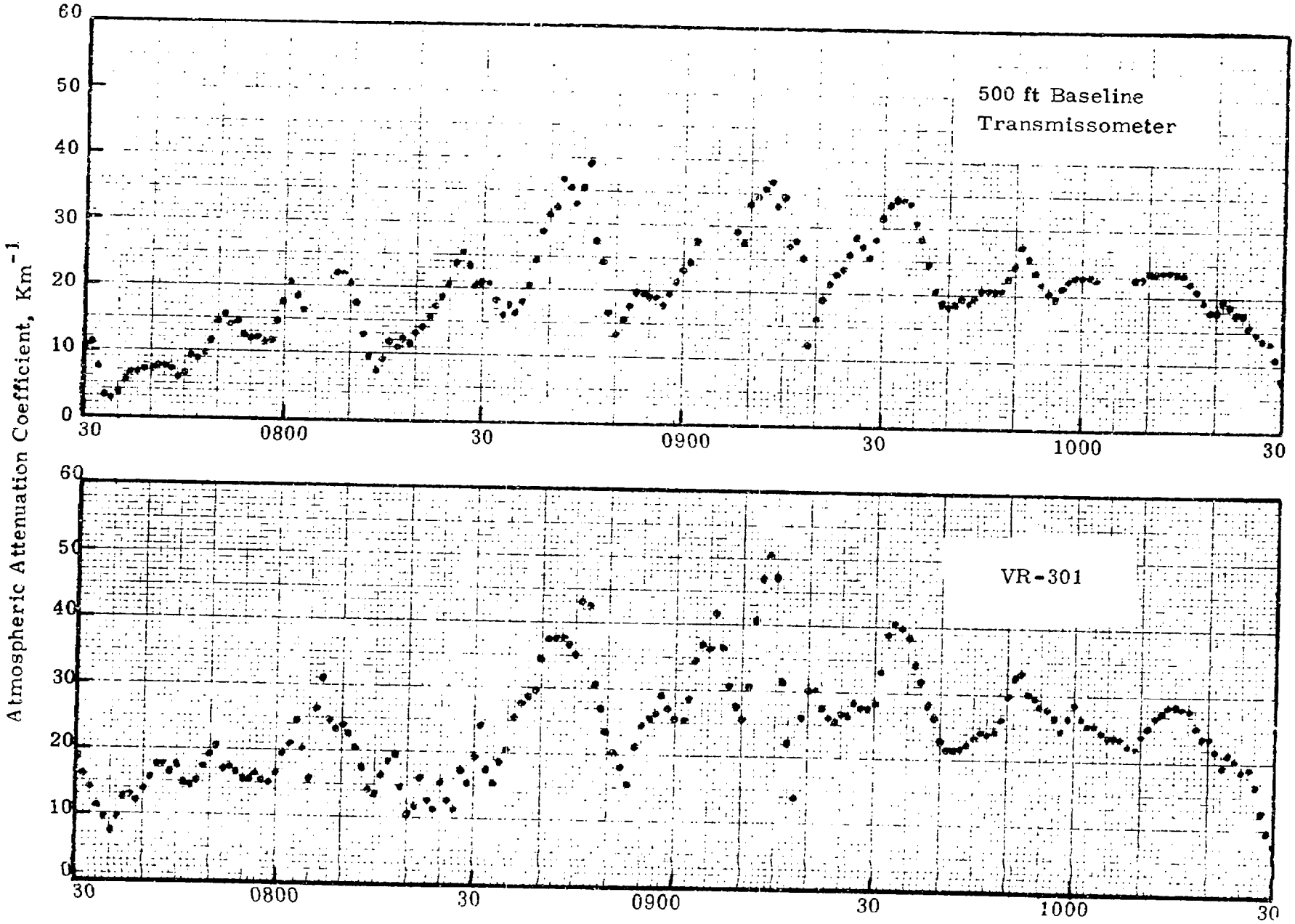

Figure 10.9. Thick Fog Event, 19 August 1982, Otis AFB.

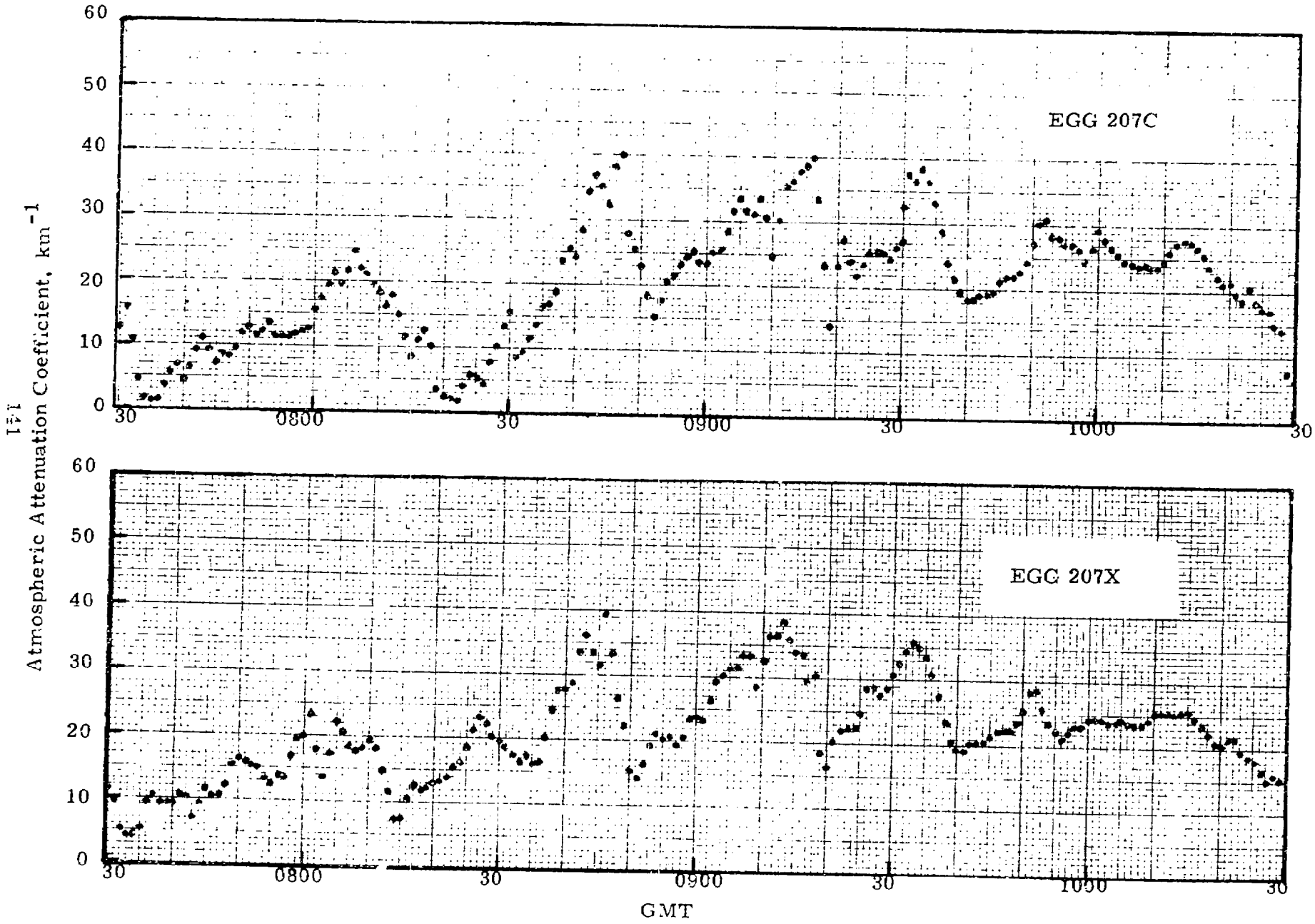

Figure 10.10. Thick Fog Event, 19 August 1982, Otis AFB.

missometer than in the case of the previously cited episodes. This is particularly true for the prototype AVM. Undoubtedly, this is somehow related to the fact that the sample volume is below the instrument, but the actual cause of this phenomena is not readily apparent. Given the high variability of this thick fog episode, the degree of correlation between readings of all sensors is quite remarkable.

Precipitation Episode:

An episode which started with drizzle and turned to light rain began at 2130 GMT on 20 July. Readings of the two AVM sensors are shown in Figure 10.11. Readings of the 500 foot baseline transmissometer and two other visibility meters are shown in Figure 10.12.

The small sample volume of the AVM leads to noticeably greater fluctuations in the measurement during this precipitation event as is evident in the readings of the experimental model AVM. The readings of the prototype AVM (whose sample volume is shielded from precipitation) demonstrate markedly less fluctuations. A comparison of the prototype AVM readings with those of the transmissometer, the VR-301, and the EG&G-207 indicates that fog made a significant contribution to the extinction coefficient during this episode.

The measurements displayed in this episode illustrate a paradoxical situation of great relevance to the determination of visual range during precipitation and around which much discussion is presently concerned. The situation is as follows: In hazes, fogs, mist and drizzle the measurements of transmissometers and forward scatter meters are in good agreement. In rain, forward scatter meters record noticeably higher values of extinction coefficient. There is a tendency to attribute this divergence during rainfall to an inherent error in forward scatter meters. Such is not the case! The error, if it may be called one, is inherent to transmissometers. (See for example Reference 14). Forward scatter meters provide more correct values of extinction coefficient in rain than do transmissometers if their measurements have not been corrected for radiation diffracted from raindrops which enter the receiver. The diffracted component of scattered light is so strongly forward scattered by raindrops that it is not distinguishable from the direct radiation proceeding from the transmitter to the receiver.

The paradoxical question in this situation is which of the two measured values of extinction coefficient, that of the transmissometer or that of the forward scatter meter, best relates to the perception of the human eye. This fundamental

question remains unanswered. The correct answer must, however, lie somewhere between the two extremes; i.e. the low visual range assigned by forward scatter meters or the higher visual range assigned by transmissometers. There may not be a single correct answer. Visual range during rainfall may depend upon observation parameters such as the angular size of an object and whether it is self-luminous or not. Until this matter is clarified it would appear that forward scatter meters provide safer visual range estimates during precipitation than do transmissometers.

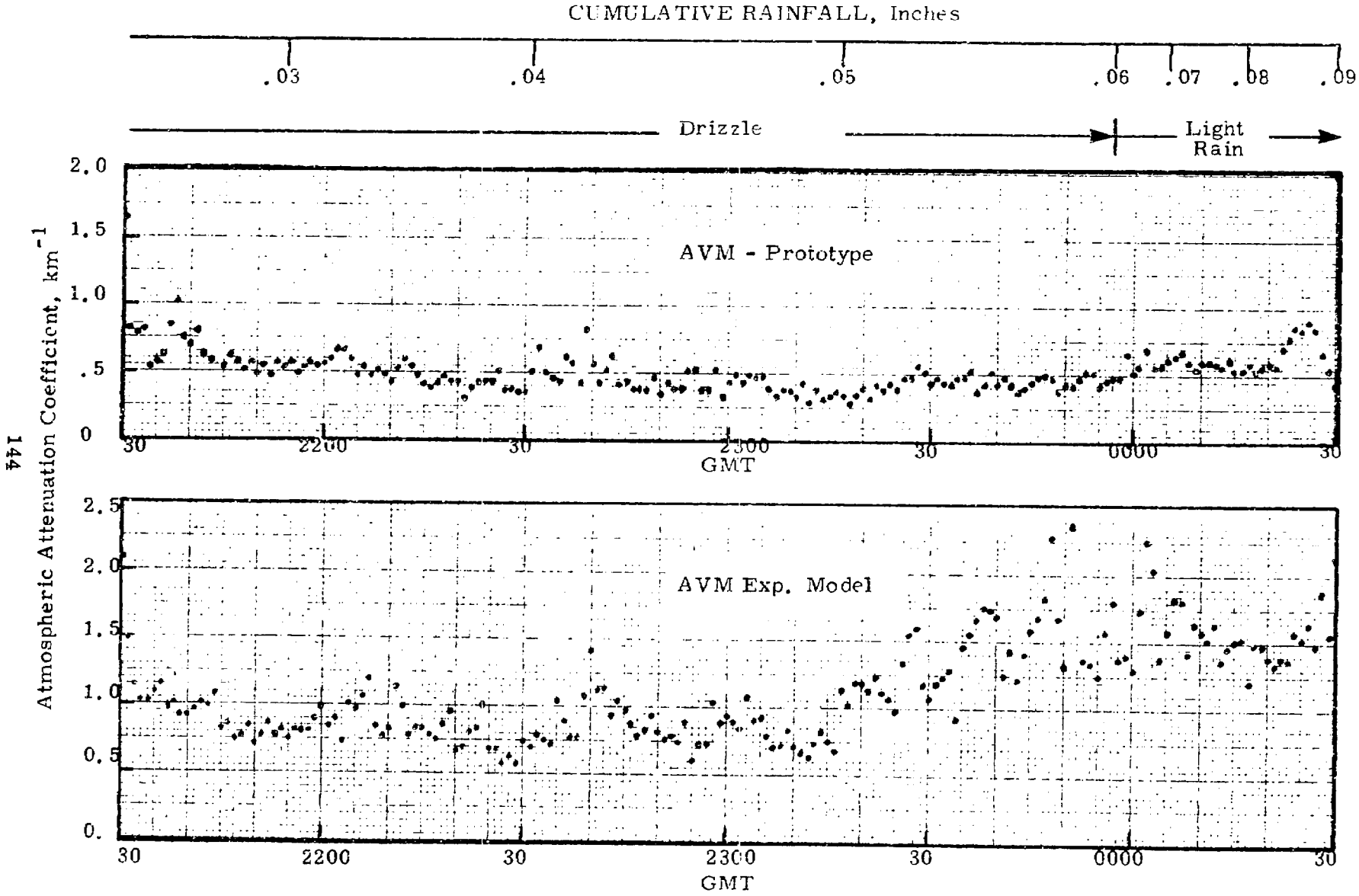

Figure 10.11. Precipitation Episode, 20 July 1982, Otis AFB.

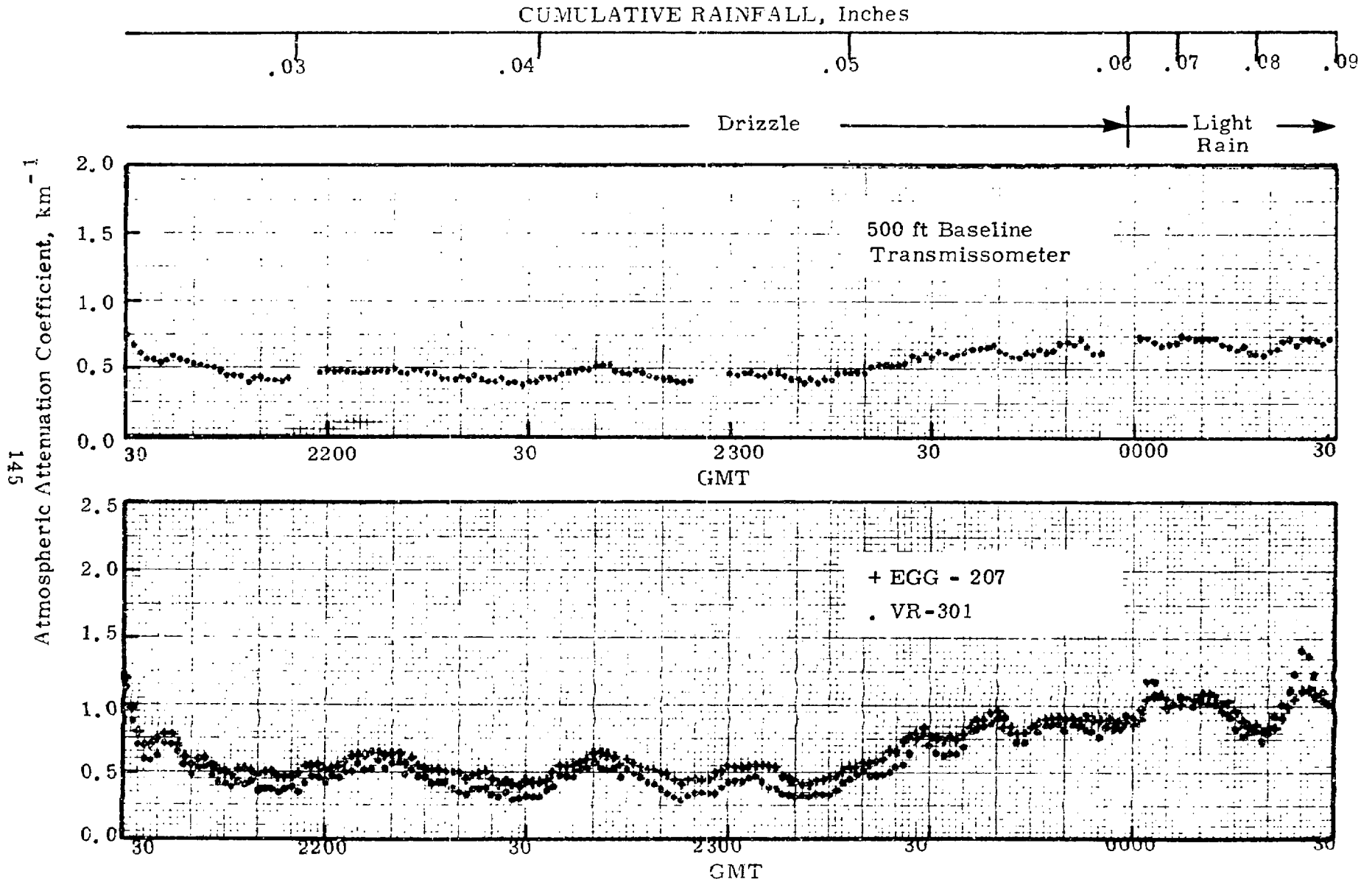

Figure 10.12. Precipitation Episode, 20 July 1982, Otis AFB.

10.4 Measurement Accuracy

The accuracy of measurement of the AVM is dependent on three components of error: (1) calibration errors, (2) instrumental errors, and (3) sampling errors. These are, statistically, independent error components, thus the total error is found by taking the square root of the sum of the squares of the individual contributions.

We shall define sampling error, in the case of forward scatter meters, as the error which is introduced into the determination of the mean value of extinction coefficient because of the size of the sampling volume and the fact that the environment (particularly fogs) may not be spatially uniform. Defined in this manner, we can hope to establish the sampling error with some degree of confidence by comparison with the measurements of a long path transmissometer. Obviously, differences in locations of sensors and the integration time of their measurements strongly influence the sampling error.

The accuracy of the calibration of the AVM is determined, primarily, by the measurement accuracy of the instruments from which the calibration was established; this was by a comparison of measurements in the same environment in the CALSPAN environmental chamber. CALSPAN assigns a measurement accuracy of 3 to 5 percent to their measuring instruments in the appropriate range of measurement; i.e., transmissometers in fogs and on an MRI integrating nephelometer in hazes. To be conservative, we shall adopt a calibration error of 5 percent for the AVM.

In the previous section of this report we have made comparisons of the AVM measurements with those of a 500 ft baseline transmissometer. We found that the correlation was extremely good in fogs and hazes but not during precipitation. This good correlation is due, in part, to the fact that the mean values are one minute averages of the measurements of both instruments and because the AVM s have 15 second time constants. The small differences in measurements between the AVM s and the transmissometer are readily explained by spatial variability in the fog which presented a somewhat different

environment to each of the instruments because they were so widely separated in the MAWS array. Thus, we find the sampling error to be indeterminate, but small; small enough that we shall take it to be negligible for purposes of an error analysis of the AVM.

While it is certainly true that the AVM s in actual operation on RPV s will not have long time constants, and also will not have the benefit of one minute averaging of readings, there will be a compensating factor tending to minimize the sampling error. That factor will be the motion of the RPV which will enable the small geometric sample volume to measure a large integrated sample volume.

To determine the instrumental error of the AVM we have performed a statistical error analysis of data from two haze situations, one a daytime episode, the other a nighttime episode. Table 10.3 is a one-hour excerpt from the MAWS print-out beginning 150° (GMT) on 26 September. Extinction coefficients measured by the two AVM instruments, two transmissometers and two EG&G forward scatter meters are tabulated. A similar tabulation for the nighttime episode is presented in Table 10.4

Mean values of extinction coefficient and the standard deviations of the measurements for each instrument are given in Table 10.5 for the daytime episode and in Table 10.6 for the nighttime episode.

One striking fact is evident from Tables 10.5 and 10.6; that is, there are large differences in the mean values of the extinction coefficient from instrument to instrument. The transmissometer measurements are suspect in this haze environment because the visual range is much greater than 10 to 20 times the baseline of the transmissometer (i.e. beyond the limit where they are intended to provide accurate measurements. Similarly, the EG&G forward scatter meters are said to have error problems in light haze situations. The differences between the mean value extinction coefficient measured by the AVM-P and the AVM-XM can be attributed to calibration errors.

Table 10.3. Atmospheric Attenuation Coefficient Measured at Otis AFB Beginning 1500, 26 September 1982.

Min.	AVM-XM	KL 500	MN 300	C10	X	AVM P
	km^{-1}	$km^{-1} \times 10$				km^{-1}
	.30	2.75	3.75	1.50	1.25	.26
	.19	2.73	3.70	1.50	1.50	.28
	.21	2.75	3.70	1.50	1.50	.27
	.22	2.79	3.64	1.50	1.50	.27
	.22	++++	++++	1.50	1.50	.31
	.30	++++	++++	1.50	1.50	.27
	.27	++++	++++	1.50	1.50	.27
	.25	++++	++++	1.50	1.50	.27
	.31	++++	++++	1.50	1.50	.27
9	.34	2.96	4.37	1.50	1.50	.27
10	.27	2.88	4.15	1.50	1.50	.27
11	.36	2.89	4.15	1.50	1.25	.27
12	.24	2.86	4.20	1.50	1.50	.27
13	.24	2.86	4.09	1.50	1.25	.26
14	.33	2.89	4.03	1.50	1.25	.27
15	.33	2.88	4.09	1.50	1.50	.27
16	.27	2.83	4.03	1.50	1.50	.27
17	.27	2.86	4.03	1.50	1.50	.27
18	.24	2.82	4.03	1.50	1.25	.28
19	.25	2.83	3.98	1.50	1.25	.28
20	.27	2.82	3.92	1.50	1.25	.28
21	.22	2.86	3.86	1.50	1.50	.26
22	.24	2.89	3.81	1.50	1.25	.25
23	.17	2.84	3.81	1.75	1.25	.25
24	.27	2.83	3.75	1.50	1.50	.27
25	.24	2.82	3.70	1.50	1.50	.31
26	.34	2.89	3.64	1.50	1.50	.26
27	.27	2.86	3.70	1.50	1.50	.27
28	.25	2.86	3.70	1.50	1.25	.27
29	.22	2.86	3.75	1.50	1.25	.28
30	.28	2.92	3.86	1.50	1.25	.26
31	.27	2.92	4.03	1.50	1.50	.27
32	.33	2.92	4.09	1.75	1.50	.27
33	.34	2.92	4.09	1.50	1.75	.26
34	.34	2.96	4.15	1.50	1.50	.26
35	.27	2.96	4.09	1.50	1.50	.26
36	.20	2.96	4.09	1.75	1.75	.26
37	.25	2.96	4.03	1.75	1.75	.28
38	.25	2.96	4.03	1.75	1.75	.28
39	.22	2.99	3.92	1.50	1.50	.27
40	.27	2.99	3.98	1.75	1.50	.27
41	.28	3.03	3.92	1.75	1.50	.27
42	.30	3.03	3.86	1.75	1.75	.26
43	.22	3.03	3.86	1.75	2.00	.26
44	.31	2.99	3.86	1.50	1.75	.26
45	.30	2.99	3.81	1.50	1.50	.26
46	.22	2.99	3.75	1.75	1.50	.28
47	.24	2.99	3.75	1.75	1.50	.26
48	.28	2.96	3.86	1.75	1.50	.27
49	.25	2.96	3.92	1.50	1.50	.24
50	.28	2.99	4.09	1.75	1.50	.26
51	.21	2.99	4.15	1.75	1.50	.31
52	.26	2.99	4.22	1.75	1.50	.31
53	.27	2.99	4.03	1.75	1.75	.23
54	.30	2.86	4.09	1.75	1.75	.26
55	.31	2.96	3.98	1.75	1.50	.23
56	.24	2.96	3.98	1.50	1.25	.26
57	.19	2.89	3.92	1.50	1.50	.26
58	.28	2.89	3.92	1.50	1.50	.31
59	.24	2.82	3.86	1.50	1.75	.18

Table 10.4. Atmospheric Attenuation Coefficient Measured at Otis AFB Beginning 0200, 10 September 1982.

MIN.	AVM XM	KL 500	MN 300	C10	X	AVM P
	km^{-1}	$km^{-1} \times 10$				km^{-1}
	.42	******	******	2.50	2.00	.33
	.46	******	******	2.25	2.00	.33
2	.39	******	******	2.25	2.00	.33
	.37	4.03	4.94	2.50	2.00	.33
	.40	3.96	4.71	2.50	2.00	.33
5	.40	3.93	4.54	2.25	2.00	.36
	.40	3.86	4.48	2.50	2.00	.36
7	.39	3.89	4.37	2.50	1.75	.33
8	.39	3.89	4.37	2.25	1.75	.31
	.34	3.73	4.37	2.00	1.75	.31
10	.34	3.89	4.37	2.00	2.00	.33
11	.36	3.89	4.32	2.25	2.00	.31
12	.37	3.89	4.32	2.25	1.75	.33
13	.37	3.93	4.32	2.00	2.00	.33
14	.34	3.89	4.37	2.00	1.75	.33
15	.36	3.89	4.32	2.00	1.75	.31
16	.36	3.89	4.32	2.00	1.75	.33
17	.37	3.82	4.32	2.25	2.00	.31
18	.33	3.89	4.32	2.00	1.75	.33
19	.37	3.93	4.32	2.00	1.75	.31
20	.30	3.93	4.37	2.25	1.75	.33
21	.34	3.82	4.32	2.25	1.75	.31
22	.37	3.89	4.32	2.25	2.00	.31
23	.36	3.93	4.37	2.25	2.00	.31
24	.39	3.89	4.32	2.25	1.75	.33
25	.36	3.89	4.32	2.00	2.00	.33
26	.37	3.86	4.37	2.25	1.75	.33
27	.37	3.93	4.37	2.25	1.75	.31
28	.34	3.82	4.37	2.00	1.75	.31
29	.36	3.86	4.37	2.25	1.75	.31
30	.37	3.93	4.43	2.25	2.00	.33
31	.37	4.00	4.43	2.25	2.00	.33
32	.40	3.89	4.43	2.50	2.00	.33
33	.39	3.96	4.43	2.50	2.00	.36
34	.39	3.82	4.43	2.25	2.00	.33
35	.37	3.89	4.48	2.25	2.25	.33
36	.39	3.93	4.43	2.50	2.00	.33
37	.37	3.96	4.48	2.25	2.00	.31
38	.37	4.00	4.43	2.25	2.00	.33
39	.37	3.96	4.43	2.25	2.00	.33
40	.40	3.96	4.43	2.50	2.00	.33
41	.39	3.89	4.48	2.25	2.00	.33
42	.37	3.93	4.43	2.50	2.00	.33
43	.42	3.93	4.43	2.25	2.00	.33
44	.39	4.00	4.43	2.50	2.00	.36
45	.37	4.03	4.48	2.25	2.00	.33
46	.34	3.96	4.43	2.50	2.00	.31
47	.34	4.00	4.43	2.25	2.00	.33
48	.39	3.96	4.43	2.25	2.00	.33
49	.37	4.00	4.48	2.25	2.00	.31
50	.37	4.00	4.43	2.25	2.00	.33
51	.39	4.00	4.43	2.25	2.00	.33
52	.39	3.86	4.43	2.25	2.00	.33
53	.40	3.82	4.43	2.25	1.75	.33
54	.37	3.93	4.48	2.25	1.75	.36
55	.40	4.03	4.48	2.25	2.00	.33
56	.33	4.07	4.48	2.25	2.00	.33
57	.37	******	******	2.25	2.00	.31
58	.40	******	******	2.25	2.00	.36
59	.39	******	******	2.50	2.25	.33

Table 10.5 . Mean Value and Standard Deviation of Daytime One-Hour Data Sets Measured at Otis AFB, 1982.

INSTRUMENT	START TIME		EXTINCT. COEFF (km^{-1})	
	GMT	EDT	Mean	Std. Dev.
AVM-P	1500: 26 Sept	1100: 26 Sept	.259	.0308
AVM-XM	1500: 26 Sept	1100: 26 Sept	.265	.0405
KL-500	1500: 26 Sept	1100: 26 Sept	.292	.00676
MN-300	1500: 26 Sept	1100: 26 Sept	.394	.0167
207-C10	1500: 26 Sept	1100: 26 Sept	.158	.0116
207-X	1500: 26 Sept	1100: 26 Sept	.149	.0169

Table 10.6 . Mean Value and Standard Deviation of Nighttime One-Hour Data Sets Measured at Otis AFB, 1982.

INSTRUMENT	START TIME		EXTINCT. COEFF. (km^{-1})	
	GMT	EDT	Mean	Std. Dev.
AVM-P	0200:10 Sept	2200: 9 Sept	.327	.0154
AVM-XM	0200:10 Sept	2200: 9 Sept	.376	.0203
KL-500	0200:10 Sept	2200: 9 Sept	.392	.00603
MN-300	0200:10 Sept	2200: 9 Sept	.442	.0103
207-C10	0200:10 Sept	2200: 9 Sept	.226	.0152
207-X	0200:10 Sept	2200: 9 Sept	.194	.0127

The instrumental errors for the six instruments, in day and night situations, are given in Table 10.7 in the form of relative standard deviations; i.e. the standard deviation divided by the mean value.

The prototype AVM has design improvements which we believe may explain a lower instrumental error in daytime when compared with the error of the experimental model AVM. We shall therefore adopt the instrumental errors of the AVM-P as the basis of establishing the measurement accuracy of the AVM in the treatment which follows.

The relative errors given in Tables 10.7 and 10.8 are for visual ranges different than 10 kilometers. A method of scaling those errors to other visual ranges is required.

Since the S/N ratio is proportional to β we might expect that the instrumental errors would decrease inversely with an increase in β. However, to allow for sampling errors in fog environments we shall assume the very pessimistic case that S/N is proportional to $\sqrt{\beta}$ when the visual range is less than 10 kilometers. (If we were to examine cases where the visual range were greater than 10 kilometers we would adopt the pessimistic posture that the error was related to the inverse of β, not the inverse of $\sqrt{\beta}$).

In Table 10.8 the relative error of the AVM is given for various time constants and at a visual range of 10 kilometers. Similarly the relative errors at a visual range of 100 meters and for various time constants are given in Table 10.9.

The relative errors were scaled to visual ranges of 10 kilometers and 100 meters based on the argument outlined above. Since these errors are based on the one minute averages of MAWS system it was necessary to assume that the errors were for a one minute time constant. The errors for other time constants were derived using the square root relationship between signal-to-noise and time constant.

Table 10.7. Relative Errors in the Measured Values of Extinction Coefficient Shown in Tables 10.5 and 10.6.

INSTRUMENT	RELATIVE STANDARD DEVIATION	
	Daytime	Nighttime
AVM-P	± 0.119	± 0.047
AVM-XM	± 0.153	± 0.054
KL-500	± 0.023	± 0.016
MN-300	± 0.042	± 0.023
207-C10	± 0.073	± 0.067
207-X	± 0.113	± 0.065

Table 10.8. Relative Instrumental Error of the AVM for Various Time Constants of Integration at a Visual Range of 10 kilometers.

TIME CONSTANT (sec)	RELATIVE STANDARD DEVIATION	
	Daytime	Nighttime
τ = 60	± 0.110	± 0.049
τ = 15	± 0.22	± 0.098
τ = 5	± 0.38	± 0.170
τ = 3	± 0.49	± 0.219
τ = 1	± 0.85	± 0.380

Table 10.9. Relative Instrumental Error of the AVM for Various Time Constants of Integration at a Visual Range of 100 Meters.

TIME CONSTANT (sec)	RELATIVE STANDARD DEVIATION	
	Daytime	Nighttime
τ = 60	$\pm$ 0.011	$\pm$ 0.0049
τ = 15	$\pm$ 0.022	$\pm$ 0.0098
τ = 5	$\pm$ 0.038	$\pm$ 0.017
τ = 3	$\pm$ 0.049	$\pm$ 0.022
τ = 1	$\pm$ 0.085	$\pm$ 0.038
τ = 0.5	$\pm$ 0.120	$\pm$ 0.054

11. CONCLUSIONS AND RECOMMENDATIONS

11.1 Operational Objectives

The AVM development program was one of a number of programs being conducted under the aegis of the PRESSURES program. Many of these programs are ongoing and their investigations, which will impact the AVM design, are yet to be completed. The physical characteristics and measurement performance of the AVM will, ultimately, be dependent upon the findings and determinations arrived at in these other programs. For example, the selection of a specific RPV will determine where the AVM can be mounted, thus influencing its size, shape and weight. The flight performance characteristics of the RPV, along with studies which will determine the optimum mission flight profiles, will influence the performance requirements (i.e. mainly the signal-to-noise ratio and the electronic time constant of the AVM).

In July 1982 the PRESSURS program adopted a "strawman" position regarding weather observable requirements (Reference 15) from that list of requirements we have extracted those requirements which are pertinent to the AVM development:

Weather Observable	Measurement Accuracy
Cloud Cover (Lowest Deck)	$\pm$ 1/8
Cloud Base	$\pm$ 100 ft. (surf. to 1000 ft)
Cloud Tops	$\pm$ 500 ft. (tops $\leq$ 2500 ft)
	$\pm$ 20% (above 2500 ft)
Slant Range Visibility (eye)	$\pm$ 20% (0.1 km to 10 km)

From the standpoint of influencing the performance requirements of the AVM the two weather observables which place the greatest demands on the instrument are: (1) the measurement of the cloud

bases to an accuracy of ± 100 ft., and (2) the measurement of a 10 kilometer slant visual range to an accuracy of ± 20 percent.

To examine the demands these requirements place on the AVM we must make an assumption about the vertical rate of ascent or descent of the carrier vehicle, i.e. the RPV. For purposes of reaching some preliminary conclusions we shall adopt a vertical rate of ascent or descent of 5000 feet per minute (83.3 ft. per second).

11.2 Measurement of Cloud Base Height

Assume that the RPV is ascending into the base of a cloud at the rate of 5000 ft/min. The extinction coefficient measured by the AVM will change from some value $\beta \leq 1\ km^{-1}$ to a value anywhere from $2\ km^{-1}$ to $100\ km^{-1}$. If we were to require that the instrument readings approach their final value to within 5 percent (three e-foldings at a time constant τ) at, or before, the time the RPV had penetrated the cloud base by more than 100 feet we would find that a time constant of $\tau = 0.4$ seconds is required.

This time constant requirement is, perhaps, too stringent. Let us assume that once the attenuation has reached $\beta = 2\ km^{-1}$ we affirm that a cloud layer has been penetrated. The time to reach a value of $\beta = 2\ km^{-1}$ will depend upon the actual extinction coefficient within the cloud as shown in Figure 11.1 and, of course, on the time constant of the instrument. Again, we adopt conservative assumptions, that the cloud extinction coefficient is only $\beta = 2.5\ km^{-1}$ and the extinction coefficient outside the cloud is zero. The instrument must then have a time constant $\tau = 0.75$ sec to determine the cloud base height within 100 feet.

When the RPV is descending through the base of a cloud the situation is somewhat different. Now we must define a value of β to be reached that signifies that the RPV has definitely exited the cloud.

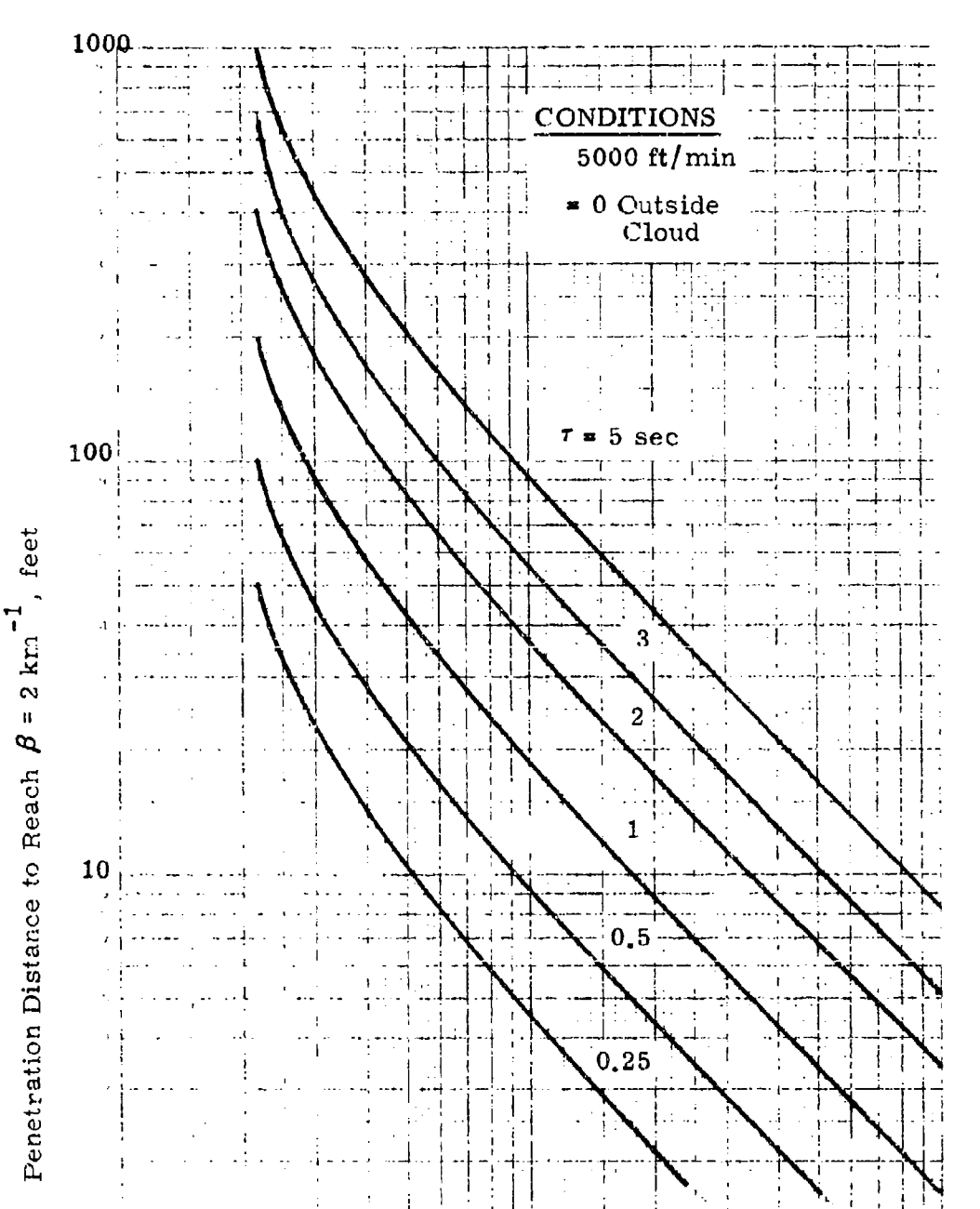

Figure 11.1 . Penetration distance for ascending RPV to certify presence of a cloud base; certification criteria is a value $\beta = 2\ km^{-1}$.

If we make the conservative assumption that $\beta = 10\ km^{-1}$ inside the cloud and $\beta = 0.3\ km^{-1}$ outside the cloud and require that the value of β decrease to $\beta = 1.0\ km^{-1}$ to assert that the cloud layer has been exited we will find that a time constant of $\tau = 0.5$ seconds is required to measure the base height to an accuracy of 100 feet.

The time constant of the AVM can be set to allow the measurement of cloud base heights to the accuracy required, i.e. a time constant of approximately $\tau = 0.5$ seconds. The analysis given in Section 10 indicates that adequate S/N ratio could still be maintained for purposes of defining the cloud base height. However, the S/N ratio reduction would then be too severe to maintain the required visual range measurement accuracy in haze situations.

11.3 Visual Range Measurements in Haze

It is required that the AVM be capable of determining slant visual ranges up to 10 kilometers to an accuracy of $\pm$ 20 per cent. If that accuracy can be achieved at 10 kilometers slant range then in all probability a better accuracy is achieved at all slant ranges less than 10 kilometers.

If an RPV bearing an AVM could fly level for many seconds at a series of heights above the ground a long time constant could be used and a high measurement accuracy could be achieved. But we will base our considerations on an RPV ascent or descent velocity of about 5000 ft/min.

To achieve the required accuracy in the measurement of visual range it is essential to make the measurement time constant as long as can be tolerated consistent with the errors introduced by the changes in extinction coefficient as the RPV climbs or descends. We shall examine two cases to ascertain the maximum allowable time constant.

Elterman Model Atmosphere - We shall assume an atmospheric situation such as shown in Case 3 of Figure 3.5; i.e. an

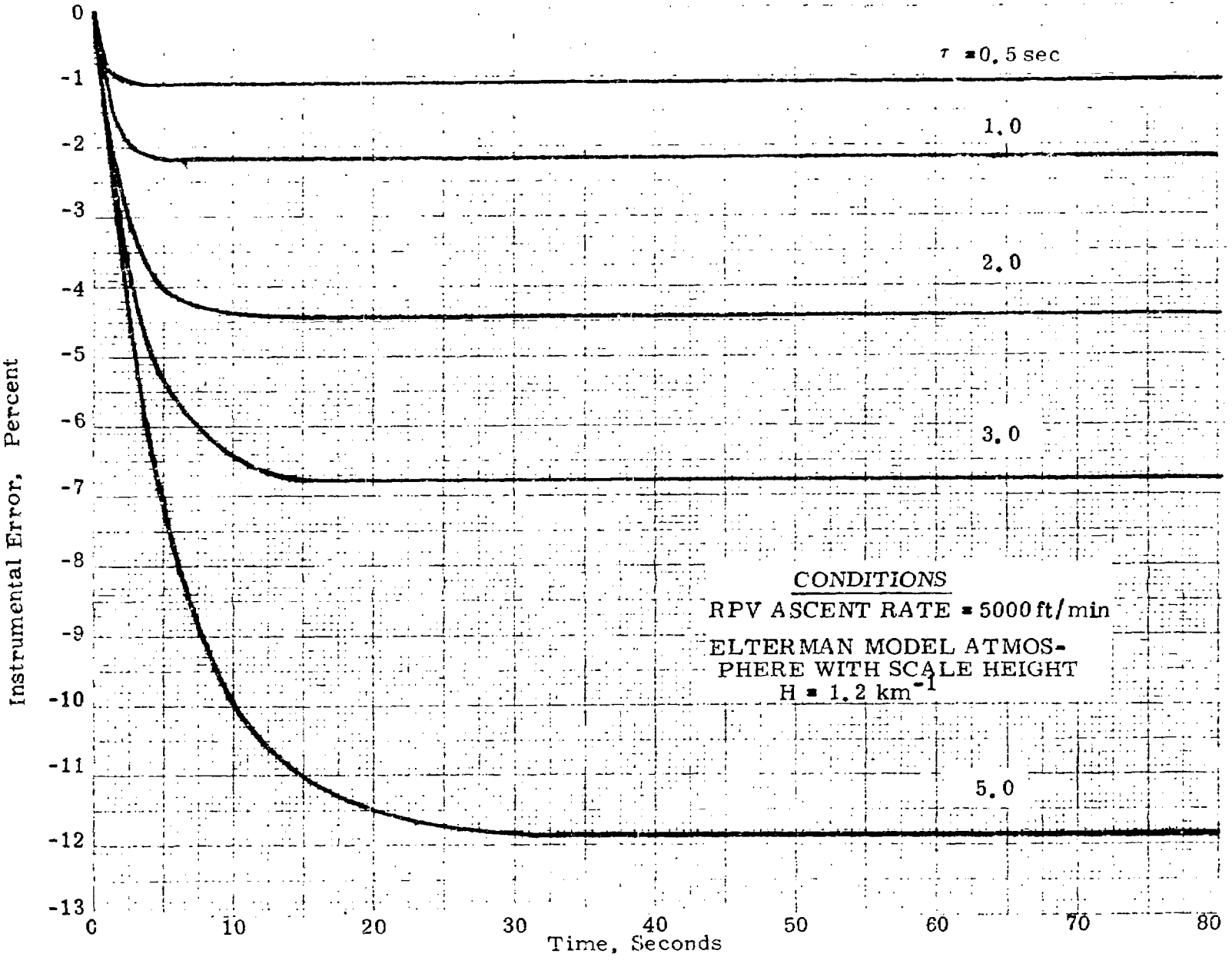

Figure 11.2. Relative measurement error due to sensor time lag for an RPV ascending from ground level at a rate of 5000 ft/min.

Elterman Model Atmosphere with a scale height H = 1.2 km^{-1} for the aerosol distributions. Because the extinction coefficient varies exponentially with altitude, and because the AVM has a finite time constant, there will be a sensor lag time as the RPV ascends or descends. The equation for calculating this lag time may be found in Reference 16. Using that equation we have determined the instrumental error introduced by the lag time for several values of sensor time constant as shown in Figure 11.2.

An acceptable error due to lag time might be 5 to 7 percent in which case we find from Figure 11.2 that a time constant in the range of τ = 2 to τ = 3 seconds can be tolerated.

Atmospheric Boundary Layer - The most probable haze situation is described by a boundary layer where the aerosol distribution is fairly constant below the layer and decreases exponentially above it. Such a situation is depicted in Case 2 of Figure 3.5.

After much reflection we believe that the simplest way of arriving at an acceptable time constant for this case is to assume: (1) that the RPV is descending through the boundary layer and that it must provide a reading which is within 5 percent (three e-foldings) of its final value before the RPV has dropped a distance equal to 20 percent of the altitude of the boundary layer.

If we assume a boundary layer altitude, say of 1 kilometer (3278 ft), and a negligible extinction coefficient above it, then the RPV must descend 656 ft before the AVM sensor reading reaches 95 percent of its final value. Under these circumstances a time constant of τ = 2.6 seconds is permissible. Obviously, this is a pessimistic situation.

11.4 Recommendations

11.4.1 Measurement Accuracy

The two most challenging tasks assigned to the AVM sensor

are: (1) the measurement of cloud base heights to an accuracy of ± 100 feet and,(2) the measurement of 10 km slant visual ranges to an accuracy of ± 20 percent. We have seen that these two requirements place conflicting constraints on the measuring time constant of the instrument.

Cloud base height measurements from an RPV ascending or descending at a rate of 5000 ft/min. require the time constant to be as short as $\tau = 0.5$ seconds if the desired accuracy in base height is to be achieved. The analysis in Chapter 10 indicates that the time constant in the present AVM design can be decreased to 0.5 seconds and the instrument will still have sufficient signal-to-noise ratio to perform the cloud attenuation coefficient measurements necessary to establish the base height to an accuracy of ± 100 feet.(See Table 10.9)

On the other hand, it has been shown that the present AVM design requires a time constant of approximately $\tau = 15$ seconds to measure a daytime visual range of 10 km to an accuracy of ± 20 percent. A 15 second time constant is too long to provide accurate measurements when the instrument is ascending to descending at a rate of 5000 ft/min. At such a rate of ascent or descent the instrument time constant must be shortened to approximately 2 seconds to prevent the introduction of a serious error due to sensor lag time. But if the AVM time constant is reduced to 2 seconds, the S/N ratio, hence the visual range measurement accuracy, would be reduced by a unacceptable amount. Table 10.8 implies that a factor of three increase in signal strength would be required to offset the loss of S/N ratio caused by a reduction of the time constant from 15 seconds to 2 seconds.

One should also note that if the time constant were reduced from 15 seconds to 0.5 seconds a factor of six improvement in signal flux would be required to maintain the ± 20 percent accuracy in

a 10 km slant visual range measurement.

There is every reason to believe that an increase of a factor of three in signal flux can be achieved without great difficulty. A factor of six improvement is within the realm of possibility at this time, but not without a drastic physical reconfiguration of the instrument.

The factor of three increase in signal flux can be achieved by a combination of two changes in the present instrument design: (1) by substituting an IRED source of higher radiant power, which is now commercially available but was not at the time the prototype AVM was fabricated, and (2) by decreasing the central scattering angle a small amount, say from 55 to 45 degrees.

Assuming a factor of three additional signal flux could be gained in the manner outlined above, then the dilemma posed by two conflicting objectives could be resolved by having two output channels for the instrument, one with a time constant of 0.5 seconds the other with a time constant of 2 seconds.

11.4.2 Physical Characteristics

The size, shape and weight of the AVM are not firmly established. The power requirements are so minimal that they will undoubtedly be compatible with any carrier vehicle. When an RPV has been chosen and a mounting location on the RPV is assigned it may be necessary to reconfigure the AVM.

Considerable leeway for reconfiguration of the AVM exists. Only two physical parameters must remain unchanged if S/N ratio is not to be lost: (1) the distances from the transmitter and receiver assemblier to the sample volume must not increase (Note: even this rule can be violated if a larger silicon detector is employed), and (2) the central scattering angle may decrease, but it cannot be in-

creased. Other than these constraints, any reconfiguration for purposes of adapting the AVM to an RPV are admissible.

11.4.3 Measurement of Precipitation

At the outset of the AVM development program there was no requirement that the AVM measure parameters related to precipitation. Should that requirement change we believe that with the addition of a modest amount of circuitry and an additional output channel the AVM could perform the following additional tasks: (1) determine if precipitation were occurring over a target area, (2) determine the type of precipitation, and (3) determine the rate of precipitation. Laboratory experiments described earlier in this report form the basis for this belief.

11.4.4 Flight Tests of the AVM

Flight testing of the prototype AVM is a very desirable step prior to any physical reconfiguration in the design of the AVM. Testing could be performed with the prototype mounted on an RPV or on a small commercial aircraft.

Two important goals can be realized by flight testing of the prototype AVM. First, the optimum aerodynamic shape can be found by experimenting with attachments to the body of the present instrument (actually wind tunnel testing might be a better approach to achieving this goal). Second, the measurement performance in clouds and haze can be verified. This verification can be achieved by flying the AVM at a location where the AFGL Baxicon nephelometer (Reference 17) can also be flown to determine the "air truth" (i.e. the true atmospheric extinction profile over altitude ranges from 0 to 10,000 feet).

REFERENCES

1. Kit G. Cottrell, Maj USAF; Paul D. Try, Lt Col USAF, Donald B. Hodges, Lt Col, USAF, Ronald F. Wachtmann, Lt Col, USAF; "Electro-Optical Handbook, Volume 1 Weather Support for Precision Guided Munitions"; AWS/TR-79/002, May 1979.

2. W.E. Knowles Middleton, "Vision Through the Atmosphere"; University of Toronto Press, 1968.

3. L. Elterman, "UV, Visible, and IR Attenuation for Altitudes to 50 km, 1968", AFCRL-68-0153, April 1968. AD 671933

4. Eric P. Shettle, Robert W. Fenn, "Models for the Aerosols of the Lower Atmosphere and the Effects of Humidity Variations on Their Optical Properties", AFGL-TR-79-0214, 20 Sept 1979. AD A085951

5. AGARD Advisory Group for Aerospace Research and Development, NATO; "AGARD Conference Proceedings No. 183 on Optical Propagation in the Atmosphere"; AGARD-CP-183, October 1979.

6. L. Elterman, "UV, Visible and IR Attenuation for Altitudes to 50 km, 1968", AFCRL-68-0153, April 1968. AD 671933

7. O. D. Barteneva; Bull. Acad. Sci; USSR Geophys. Ser. 12; 1237; 1960.

8. O. D. Barteneva and G. Ya. Bashilov; Bull. Acad. Sci.; USSR Geophys. Ser. 4; 395; 1961.

9. J. V. Winstanley and M. J. Adams; "Point Visibility Meter: A Forward Scatter Instrument for the Measurement of Aerosol Extinction Coefficient"; Appl. Opt.; Vol 14, No. 9; 2151; September 1975.

10. E. P. Shettle and R. W. Fenn, Private Communication.

11. D. Deirmendjian; "Electromagnetic Scattering on Spherical Polydispersions; The RAND Corporation, Santa Monica, California; American Elsevier Publishing Company, Inc., New York, 1969.

12. William L. Wolfe and George J. Zissis, Ed., "The Infrared Handbook", The Infrared Information and Analysis Center, Environmental Research Institute of Michigan for the Office of Naval Research, Wash., D.C., 1978.

13. E.J. Mack; "Collection and Reduction of Drop Size Distribution Data in Simulated and Natural Fogs"; Interim Technical Report, May 1980.

14. Adarsh Deepak and Michael A. Box, "Forwardscattering Corrections for Optical Extinction Measurements in Aerosol Media. 1: Monodispersions", Applied Optics Vol. 17, No. 18, 15 September 1978.

15. Frederick J. Brousaides, "Meteorological Sensors for the PRESSURS Program and an Assessment of the AN/GMQ-13 Cloud Height Set", Final Report, Air Force Geophysics Laboratory, September 1981 (To be published).

16. B. R. Bean and E. J. Dutton, "Radio Meteorology", Dover Publications, New York, 1968.

17. Harold S. Stewart, Willem Brouwer, Marion P. Shuler, "Baxicon: An Efficient Fixed-Angle Nephelometer", HSS Inc Final Report on Contract F19628-73-C-0257, AFCRL-TR-74-0199, April 1974. AD 921479

APPENDIX A

The most general expression for the law of contrast reduction by the atmosphere as stated by Duntley is

$$C = C_o(B'_o / B')e^{-\int_o^R \gamma(r)\, dr} \qquad (A.1)$$

where:

C_o = the inherent contrast of an object seen against a background.

C = the apparent contrast of the same object seen against the same background as viewed along a slant path of length R

$\gamma(r)$ = atmospheric extinction coefficient, km^{-1}

R = slant range from the object to the observer, km

B'_o = inherent brightness of the background (in arbitrary units)

B' = apparent brightness of the background (arbitrary units).

We wish to define a set of observational conditions for the downward viewing situation such that a Slant Visual Range R_s can be determined solely from the measurements of the atmospheric extinction coefficient in a manner similar to that in which horizontal visual range V is determined from Koschmieder's Law, $V = 3.912/\gamma$. The set of conditions we shall define may be overly restrictive and there may be many other sets of equally valid conditions. Our purpose here is to show that there is at least one set of physically realizable conditions in which the slant visual range can be determined solely from measurements of the extinction coefficient.

A first condition, which is not very restrictive, is that aerosol scattering be the dominant attenuator of optical radiation, and that the aerosols be horizontally stratified.

A second condition is that the object be perfectly black, and the background against which it is viewed be a white or gray Lambertian surface. We also restrict the illumination conditions to be dominated by direct sunlight along the slant path from the observer to the object.

When these conditions are fulfilled, the apparent brightness of the object B is given by

$$B = \Phi H \left(1 - e^{-\int_0^R \sigma(r)\, dr} \right) \qquad (A.2)$$

where $\sigma(r)$ is the aerosol scattering coefficient, Φ is the phase function for aerosol scattering and H is the sunlight illumination along the slant path R. Since the object is considered to be black, Equation A.2 represents the "air light" generated by atmospheric scattering along the slant observational path.

The apparent brightness of the background B' under these same set of conditions is

$$B' = \Phi H \left(1 - e^{-\int_0^R \sigma(r)\, dr} \right) + \frac{H}{\pi} \rho \cos Z\, e^{-\int_0^R \sigma(r)\, dr} \qquad (A.3)$$

where Z is the zenith angle of the sun, ρ is the diffuse reflectivity of the Lambertian background and

$$B'_o = \frac{H}{\pi} \rho \cos Z \qquad (A.4)$$

is the inherent brightness of the background.

We now make a further restrictive condition that the angle of solar illumination of the background, and the downward angle of observation of the object and background be such that

$$\Phi H = \frac{H}{\pi} \rho \cos Z \qquad (A.5)$$

Then, under this final condition of pseudo "optical equilibrium", we may set

$$B' = B'_o = \Phi H \qquad (A.6)$$

Referring to Equation A.1 we see that when $B' = B'_o$ then

$$C = C_o e^{-\int_o^R \sigma(r)\, dr} \qquad (A.7)$$

We define the Slant Visual Range R_s to be that range where the contrast transmittance of a **black** target through the atmosphere has been reduced to a value of 0.05, i.e.

$$.05 = e^{-\int_o^{R_s} \sigma(r)\, dr} \qquad (A.8)$$

We have now reached the desired goal which was to define a set of conditions under which slant visual range is determined only by measurements of the scattering coefficients along the slant path of observation.

The first two conditions which must be met for Equation (A.8) to hold were not very restrictive. The third condition defines a specific geometric situation wherein

$$\Phi(0) = \rho \frac{\cos Z}{\pi} \qquad (A.9)$$

A physical situation in which Equation A.9 is realized is achieved when $Z = 60°$, $\rho = 1.0$ and the downward look angle from the horizontal toward the target and its background is 10 degrees. Then the forward scatter angle, assuming the sun, the object and the observer are coplanar, is $\theta = (30° + 10°) = 40°$ and

$$\Phi(40°) = .158 \text{ ster}^{-1} \qquad \text{(A.10)}$$

The phase function for rural aerosols at a scattering angle of 40° is approximately 0.16 which is nicely in agreement with Equation A.10.

We have not performed an analysis of geometric conditions which must apply when the sky is overcast with clouds. Intuitively, it would seem that, because the light which is scattered from each volume element along the observational path comes from the whole sky, the geometric conditions to be imposed on the observation angle may be more relaxed than for the situation which was analyzed in this appendix.